



# Clean Air Journal

ISSN 1017 - 1703

Vol 30 No 2

November / December 2020

Official publication of the  
National Association for Clean Air

# CLEAN AIR JOURNAL

ISSN 1017-1703  
November / December 2020  
Volume 30, No. 2

Published twice yearly by the National Association for Clean Air, Republic of South Africa

## Editors

**Dr Gregor Feig**  
South African Environmental Observation Network

**Prof Rebecca Garland**  
Council for Scientific and Industrial Research

**Dr Kristy Langerman**  
University of Johannesburg

## Editorial Advisory Board

**Prof Harold Annegarn**  
North-West University, South Africa

**Prof Paul Beukes**  
North West University, South Africa

**Prof Michael J. Gatari Gichuru**  
University of Nairobi, Kenya

**Dr Patience Gwaze**  
Department of Environmental Affairs, South Africa

**Dr Enda Hayes**  
University of West of England, United Kingdom

**Dr Gerrit Kornelius**  
University of Pretoria, South Africa

**Prof Hannes Rautenbach**  
South African Weather Service, South Africa

**Prof Siva Venkataraman**  
University of KwaZulu-Natal, South Africa

**Prof Kuku Vuyi**  
School of Health Systems and Public Health, University of Pretoria, South Africa

**Prof Noureddine Yassaa**  
Centre de Développement des Energies Renouvelables, Algeria

## Website and archive copies

[www.cleanairjournal.org.za](http://www.cleanairjournal.org.za)

## Contact

[info@cleanairjournal.org.za](mailto:info@cleanairjournal.org.za)

# Contents

## News

- 3 Air Pollution and its impacts on health in Africa - insights from the State of Global Air 2020

## Commentary

- 6 Low-cost sensors, an interesting alternative for air quality monitoring in Africa

## Research brief

- 9 A summary of the paper "Natural archives of long-range transported contamination at the remote lake Letšeng-la Letsie, Maloti Mountains, Lesotho"

## Erratum

- 10 The need for open data on air quality monitoring in logistically difficult environments

## Research articles

- 12 Air pollution in Kigali, Rwanda: spatial and temporal variability, source contributions, and the impact of car-free Sundays
- 28 The impacts of commissioning coal-fired power stations on air quality in South Africa: insights from ambient monitoring stations
- 40 Chemical characterization of fine particulate matter, source apportionment and long-range transport clusters in Thohoyandou, South Africa
- 53 Morphology and elemental analysis of freshly emitted particles from packed-bed domestic coal combustion

## Technical article

- 64 An exploratory characterisation of the carbon and stable isotope composition of atmospheric particulate matter from opencast coal mining activities and adjacent communities



## INTELLIGENT, ROBUST, EASY-TO-USE

### Air Dispersion Modeling

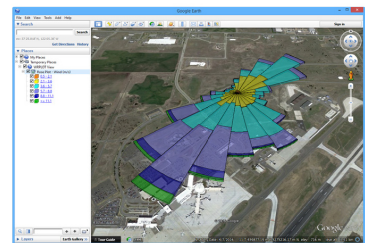
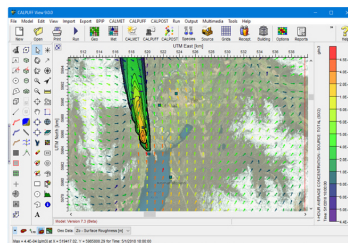
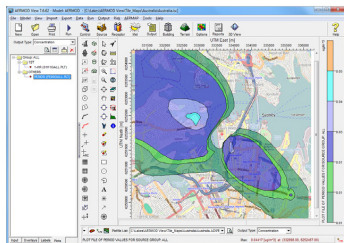
AERMOD View | CALPUFF View

- Powerful 2D and 3D Visualization
- Parallel Versions for Faster Runs
- Easy Automated Download of:
  - Satellite Maps
  - Worldwide Terrain
  - Landuse Data Files

### Met Data

WRF | MM5 | Station

- CALMET-Ready WRF Met Data
- AERMET-Ready WRF Met Data
- Ideal for Locations Without Met Stations
- Custom WRF Runs Available
- AERMOD-Ready Station Data (USA Only)
- Data Available in as Little as One Day



[www.webLakes.com](http://www.webLakes.com) | [info@webLakes.com](mailto:info@webLakes.com)

## Air Pollution and its impacts on health in Africa - insights from the State of Global Air 2020

Joanna Keel, Katherine Walker, Pallavi Pant \*

Health Effects Institute, 75 Federal Street, Suite 1400, Boston, MA, 02110 USA

\*Corresponding Author E-mail: ppant@healtheffects.org

<https://doi.org/10.17159/caj/2020/30/2.9270>

According to the State of Global Air 2020<sup>1</sup>, total air pollution (including ambient PM<sub>2.5</sub> and ozone as well as household air pollution) emerged as the 3rd leading risk factor for death and disability in sub-Saharan Africa in 2019, surpassed only by malnutrition and unsafe water, sanitation and hygiene. Exposure to air pollution was linked to more than 900,000 premature deaths (95% uncertainty interval [UI]: 760,000-1.1 million) in sub-Saharan Africa, equal to about 12% (UI: 10%-13%) of all deaths in the region. Globally, air pollution was linked to 6.67 million deaths (UI: 5.90-7.49 million) in 2019.

Countries in Africa continue to experience some of the highest exposures to ambient PM<sub>2.5</sub> in the world, along with countries in the Middle East and Asia. In both the sub-Saharan Africa and the North Africa and Middle East regions (as defined by the GBD project), the PM<sub>2.5</sub> exposure was ~44 µg/m<sup>3</sup> (UI: 36-54 µg/m<sup>3</sup>, 38-50 µg/m<sup>3</sup>) in 2019, severalfold higher than the PM<sub>2.5</sub> Air Quality Guideline set at 10 µg/m<sup>3</sup> by the World Health Organization. Within the region, Egypt, Niger, Nigeria, Mauritania, and Cameroon experienced even higher PM<sub>2.5</sub> concentrations in 2019, ranging from 65 µg/m<sup>3</sup> to 80 µg/m<sup>3</sup>. These countries all rank among the top 10 countries in the world with the highest levels of PM<sub>2.5</sub>. Note that higher PM<sub>2.5</sub> exposures in some North African countries include contributions from local dust sources as well as wind-blown dust from the Sahara Desert.

Across Sub-Saharan Africa, PM<sub>2.5</sub> exposures have increased by 3% since 2010, even as other regions including Southeast Asia, East Asia, and Oceania have seen reductions. Nigeria saw a 12% increase (7.5 µg/m<sup>3</sup>) over the same time period, from 63 µg/m<sup>3</sup> (UI: 41-92 µg/m<sup>3</sup>) to 70 µg/m<sup>3</sup> (UI: 45-105 µg/m<sup>3</sup>).

A major source of exposure and health impact in much of Africa continues to be linked to lack of access to clean energy. Without it, a large percentage of people rely on burning of various solid fuels (coal, charcoal, wood, agricultural residue) as well as kerosene for heating or for cooking using open fires or

cookstoves with limited ventilation resulting in high exposures to particulate matter in their homes, referred to as household air pollution. In fact, more than 97% of the populations in Central African Republic, South Sudan, Rwanda, Burundi, Niger, Mali, Madagascar, Tanzania, Uganda, and Guinea-Bissau all relied on solid fuels for cooking in 2019.

Progress toward cleaner fuels has been slow in the region on average. However, some countries have made great strides in reducing reliance on solid fuels for cooking in the last decade. In Equatorial Guinea, the percentage of the population relying on solid fuels decreased from 50% (UI: 45-55%) to 25% (UI: 18-33%) between 2010 and 2019. In the same time period, Cabo Verde saw a decrease from 30% (UI: 26-34%) to 19% (UI: 15-24%), and Botswana from 48% (UI: 45-52%) to 39% (UI: 30-48%).

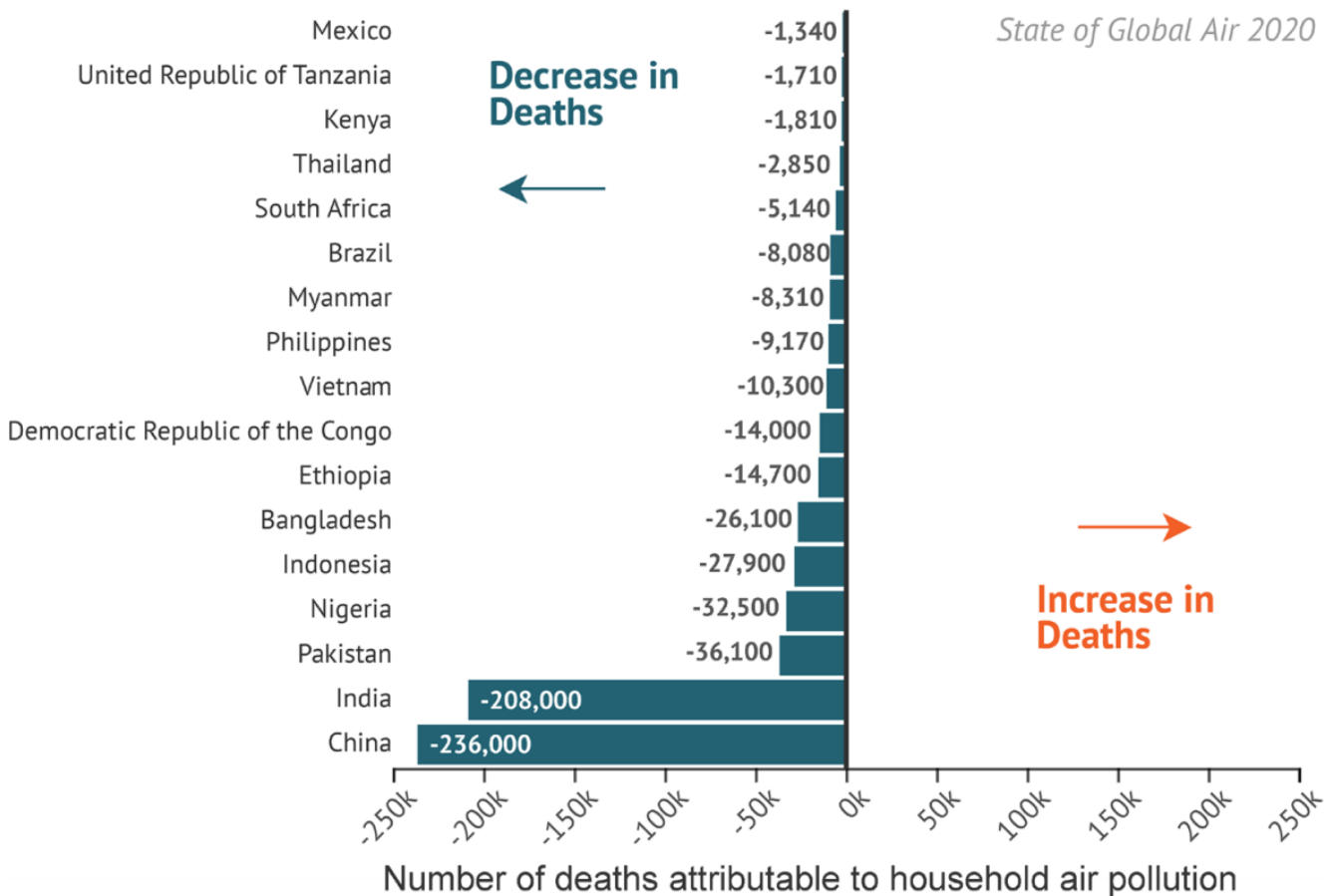
Exposure to both outdoor and indoor air pollution can each place a heavy burden on health, although the burden they impose is not equal. In Sub-Saharan Africa, exposure to household air pollution contributes to more than three times the number of deaths (684,000 deaths; UI: 516,000-863,000 deaths, 9%; UI: 7-11% of all deaths in 2019) as exposure to ambient PM<sub>2.5</sub> (216,000 deaths; UI: 142,000-311,000 deaths, about 3%; UI: 2-4% of all deaths). 43% of air pollution deaths in sub-Saharan Africa result from non-communicable diseases that are linked with exposure to air pollution, including chronic obstructive pulmonary disease (COPD), diabetes, ischemic heart disease, lung cancer and stroke. Air pollution is also linked to lower respiratory infections, which pose a particular risk of illness and death to children under 5 years of age.

For the first time, State of Global Air also presented results on the impacts of air pollution on the health of infants in their first month of life. Babies born to mothers exposed to air pollution during pregnancy may be born too early or too small, which may result in a variety of additional complications including lower-respiratory infections, diarrheal diseases, brain damage

<sup>1</sup>The State of Global Air is a collaboration between the Health Effects Institute and the Institute for Health Metrics and Evaluation, based on annual data from the Global Burden of Disease (GBD) Study. Each year, the GBD study produces estimates of current and yearly trends in exposures and burden of disease from key risk factors in countries and territories around the world, making use of state-of-the-art comparative risk assessment methods.

<sup>2</sup>The amount of uncertainty differs from place to place given differences in the quantity and quality of the underlying data for the estimates.

<sup>3</sup>In much of Africa, data on air quality from ground-based monitors are limited. The numbers presented represent the best estimate of annual average exposures based on a combination of ground-based monitoring data, satellite data and modelled estimates.



Change in the number of deaths attributable to household air pollution in the 17 countries with over 50 million people and at least 10% of their population cooking with solid fuels, 2010–2019.

**Figure 1:** Several countries in Africa have seen reductions in the number of deaths attributable to household air pollution in the last decade. Household air pollution has historically been and remains a challenge in other regions of the world as well.

and inflammation, blood disorders, and jaundice and in some cases, death. Sub-Saharan Africa has carried a particularly heavy burden for infants. In 2019, 23% (UI: 21-25%) or more than 235,000 (UI: 191,000-291,000) infant deaths were attributable to air pollution in this age group, almost half the global total. Household air pollution is the major culprit in the region – accounting for about 80% of these infant deaths.

Air pollution continues to impose a heavy and increasing burden on health in many countries in Africa. Millions of people every year have borne an avoidable burden from air pollution-related disease and premature mortality; the impacts on newborns and on children under five are particularly harsh. While exposures to PM<sub>2.5</sub> and household air pollution remain high across the continent, some countries are beginning to undertake policy measures to improve air quality. A silver lining is the increasing adoption of cleaner cooking technologies in some countries across Africa, which is contributing to declines in the number of people exposed to household air pollution. By publishing these trends each year, we seek to focus public attention on the progress, but also on the major problems that have yet to be

addressed. Our objective is to inform actions to reduce pollution in ways that have the greatest potential to benefit health.

The State of Global Air is a source of open-access, objective, high-quality, and comparable air quality and health data and information. Learn more at our website: <https://www.stateofglobalair.org> and contact us with any questions or opportunities for collaboration ([contactsga@healtheffects.org](mailto:contactsga@healtheffects.org)). Health Effects Institute released the fourth edition of its State of Global Air 2020 annual report and interactive website on the levels and trends of air quality and health in countries around the world on October 21, 2020.



## Air Pollution is Breathtaking!!!

Proud Sole Distributors Of:



Joint Distributors Of:



**DURAG GROUP**



And more...

For all your Air Pollution Monitoring requirements contact us on:

[www.airpolguys.com](http://www.airpolguys.com) [info@airpolguys.com](mailto:info@airpolguys.com)

012 803 5124 / 012 803 5126

# Commentary

## Low-cost sensors, an interesting alternative for air quality monitoring in Africa

Farid Rahal 

Laboratory of Sciences, Technology and Process Engineering, University of Sciences and Technology of Oran, Mohamed Boudiaf, BP 1505 El M'Naouer, Oran, Algeria, farid.rahaldz@gmail.com

<https://doi.org/10.17159/caj/2020/30/2.9223>

In Algeria, the lack of continuous measurement of air pollution is a real problem that hinders studies, strategies and decision-making to fight against this phenomenon. Indeed, the pollution measurement networks installed by the public authorities in the main urban centers of the country (Rahal et al., 2014) are no longer operational. This situation in Algeria is just one example among many in developing countries where the monitoring of air quality is in a deplorable state (Kumar et al., 2019), because this monitoring is a costly policy, which requires sufficient and sustainable financial means. Furthermore, the technical skills to maintain and operate the instrumentation of measuring equipment are scarce.

In Africa, the ground based air quality monitoring is often sparse, short term, piecemeal and where most of these campaigns are to test new technologies, and thus the scarce resources are not often targeted towards the local problems but rather at the external project priorities (Mbandi, 2020). Despite the investments made by several African countries to acquire conventional air quality monitoring networks, these infrastructure are often inoperative after few years because their maintenance is expensive.

Indeed, an economic barrier prevents the establishment of air pollution-monitoring networks in many African countries. An alternative (or supplement) to the traditional air quality monitoring infrastructure can potentially come from the recent development in electrochemical sensor technologies for air quality monitoring. These sensors are generally small, consume little energy, cost between 10 and 1,000 US Dollars, and measure concentrations of all major air pollutants. Compared to large, high-end solutions costing more than 100,000 US Dollars, low-cost sensors are particularly useful for large-scale static and mobile deployments (Maag et al., 2018; Rai et al., 2017; Baron et al., 2017).

Furthermore, low-cost air pollution sensors have been successfully integrated into various long-term deployments to provide detailed information on air pollution for quantitative studies and utilities (Yi et al., 2015).

Electrochemical air quality sensors have the potential to fill the gap left by conventional monitoring of air pollution. The cost and size of air pollution sensors is decreasing, which means that

it is now possible to use portable and inexpensive air pollution analyzers (Gunawan et al., 2018).

The low costs of these components make it possible to deploy several copies to assess air pollution at a finer spatial resolution than could be possible with traditional monitoring setups. This solution is interesting for developing countries, which do not have air quality monitoring networks and the necessary budgets for the acquisition of conventional analyzers.

Several implementations have been done in this area in Africa, for example in Senegal (Ngom et al., 2018), Mauritius (Khedo et al., 2017), and Algeria (Rahal et al., 2020).

However, we should no longer stay at the experimental stage but move to an operational level with a dense network of sensors where the continuously measured pollutants concentrations would be shared on an African portal dedicated to air quality. Air pollution can travel long distances depending on the nature of the pollutants and their lifespan in the atmosphere. Pollutant emissions in one country can move to another neighboring country. Therefore, it is essential that air quality data was shared and accessible to all stakeholders in the field of air pollution in Africa.

The pooling of African resources in terms of measurement means, data and scientific skills in the field of air quality could lead to a synergy in line with one of the ideals of Pan-Africanism, which encourages the practice of solidarity between African peoples (Kassabo, 2009).

Africa's industrialization is moving rapidly (Pezzini et al., 2019). The development potential of the African continent is enormous. However, if this development follows the same path of Western countries, our continent will suffer many of the same adverse environmental impacts. In particular, a poor air quality.

It is necessary to do not repeat the same mistakes as the Western countries where industrialization and changing lifestyles have generated a lasting air pollution problem with major impacts on national budgets, through increased health impacts, decreased productivity and adverse impacts on the provision of ecosystem services. In Europe, it has been estimated that complying with WHO (World Health Organization) air quality guidelines can

save 31 billion euros per year which 19 million euros due to hospitalizations. This estimate includes direct and/or indirect costs (Conti et al., 2020).

The recent COVID-19 pandemic has shown that health risks are accentuated by poor air quality. Indeed, there has been a close correlation between regions with worse air pollution and diffusion of the virus (Sterpetti, 2020). The combination between air pollution and meteorological conditions with high relative humidity, low wind speed and fog, trigger a take-off of viral infectivity (Coccia, 2020a).

The related risks with air pollution are becoming larger, it becomes urgent to reduce the gap of Africa in air quality monitoring.

Low-cost electrochemical sensors can effectively contribute to this, provided that a comprehensive strategy to fight atmospheric pollution in Africa is put in place by mobilizing all African resources in this area.

The other aspects of this strategy would be to establish pollutant emissions inventories in Africa, to develop air quality modeling in order to establish forecasts and carry out scenario studies aimed at facilitating the choice of the best policies to protect the environment and the health of African citizens against poor air quality.

## References

- Baron, R. and Saffell, J., 2017. 'Amperometric gas sensors as a low cost emerging technology platform for air quality monitoring applications: A review'. *ACS sensors*, 2(11):1553-66. <https://doi.org/10.1021/acssensors.7b00620>
- Coccia, M., 2020. 'The effects of atmospheric stability with low wind speed and of air pollution on the accelerated transmission dynamics of COVID-19'. *International Journal of Environmental Studies*, 16:1-27. <https://doi.org/10.1080/00207233.2020.1802937>
- Conti, S., Ferrara, P., D'Angiolella, L.S., Lorelli, S.C., Agazzi, G., Fornari, C., Cesana, G. and Mantovani, L.G., 2020. 'The economic impact of air pollution: a European assessment'. *European Journal of Public Health*, 30. <https://doi.org/10.1093/eurpub/ckaa165.084>
- Gunawan, T.S., Munir, Y.M.S., Kartiwi, M. and Mansor, H., 2018. 'Design and implementation of portable outdoor air quality measurement system using arduino'. *International Journal of Electrical and Computer Engineering*, 8(1):280. <https://doi.org/10.11591/ijece.v8i1.pp280-290>
- Kassabo, L.D., 2009. 'Le système africain de sécurité collective régionale à l'ère de l'Union Africaine'. Ph.D. thesis. University of Padova, Italy.
- Kumar, A. and Gurjar, B.R., 2019. 'Low-Cost Sensors for Air Quality Monitoring in Developing Countries—A Critical View'. *Asian Journal of Water, Environment and Pollution*, 16(2):65-70. <https://doi.org/10.3233/AJW190021>
- Khedo, K.K. and Chikhooreeah, V., 2017. 'Low-cost energy-efficient air quality monitoring system using wireless sensor network'. *Wireless Sensor Networks-Insights and Innovations*. IntechOpen. <https://doi.org/10.5772/intechopen.70138>
- Maag, B., Zhou, Z. and Thiele, L., 2018. 'A survey on sensor calibration in air pollution monitoring deployments'. *IEEE Internet of Things Journal*, 5(6):4857-70. <https://doi.org/10.1109/JIOT.2018.2853660>
- Mbandi, A.M., 2020. 'Air Pollution in Africa in the time of COVID-19: the air we breathe indoors and outdoors'. *Clean Air Journal*, 30(1):1-3. <https://doi.org/10.17159/caj/2020/30/1.8227>
- Ngom, B., Seye, M.R., Diallo, M., Gueye, B. and Drame, M.S., 2018, July. 'A Hybrid Measurement Kit for Real-time Air Quality Monitoring Across Senegal Cities'. *2018 1st International Conference on Smart Cities and Communities (SCCIC)* (pp. 1-6). IEEE. <https://doi.org/10.1109/SCCIC.2018.8584551>
- Pezzini, M. and Minsat, A., 2019. 'L'industrialisation de l'Afrique nécessite une approche continentale en association avec les entrepreneurs locaux'. *Annales des Mines-Realites industrielles* (No. 3, pp. 8-12). FFE. <https://doi.org/10.3917/rindu1.193.0008>
- Rahal, F., Benharrats, N., Blond, N., Clappier, A. and Ponche, J.L., 2014. Modelling of air pollution in the area of Algiers City, Algeria. *International Journal of Environment and Pollution*, 54(1):32-58. <https://doi.org/10.1504/IJEP.2014.064049>
- Rahal, F., Rezak, S. and Benabadji N., 2020: In press. 'Evaluation of the impact of the COVID-19 pandemic on photochemical pollution in urban areas'. *Environmental Health Engineering and Management Journal*. 7(4).
- Rai, A.C., Kumar, P., Pilla, F., Skouloudis, A.N., Di Sabatino, S., Ratti, C., Yasar, A. and Rickerby, D., 2017. 'End-user perspective of low-cost sensors for outdoor air pollution monitoring'. *Science of The Total Environment*, 607:691-705. <https://doi.org/10.1016/j.scitotenv.2017.06.266>
- Sterpetti, A.V., 2020. 'Lessons learned during the COVID-19 virus pandemic'. *Journal of the American College of Surgeons*, 230(6):1092-3. <https://doi.org/10.1016/j.jamcollsurg.2020.03.018>
- Yi, W.Y., Lo, K.M., Mak, T., Leung, K.S., Leung, Y. and Meng, M.L., 2015. 'A survey of wireless sensor network based air pollution monitoring systems'. *Sensors*, 15(12):31392-427. <https://doi.org/10.3390/s151229859>

# BE PART OF THE REVOLUTION



AQMesh is a **wireless, battery-powered** monitor designed to offer a robust and easy-to-use **air quality monitoring** system. It delivers accurate, near **real-time data** of all major priority pollutants including dust and noise which in turn supports initiatives to reduce air pollution and its risk to human health.

With over **65 successfully operating units** throughout the sub-Saharan region, isn't it time to join the revolution?



[info@sianalytics.co.za](mailto:info@sianalytics.co.za)  
[www.sianalytics.co.za](http://www.sianalytics.co.za)



# Research brief

## A summary of the paper “Natural archives of long-range transported contamination at the remote lake Letšeng-la Letsie, Maloti Mountains, Lesotho”

Neil L. Rose<sup>1\*</sup>, Alice M. Milner<sup>2</sup>, Jennifer M. Fitchett<sup>3</sup>, Kristy E. Langerman<sup>4</sup>  
Handong Yang<sup>1</sup>, Simon D. Turner<sup>1</sup>, Anne-Lise Jourdan<sup>5</sup>, James Shilland<sup>1</sup>,  
César C. Martins<sup>6</sup>, Amanda Câmara de Souza<sup>6</sup>, Christopher J. Curtis<sup>4</sup>

<sup>1</sup>Environmental Change Research Centre, Department of Geography, University College London, Gower Street, London WC1E 6BT, UK \*n.rose@ucl.ac.uk

<sup>2</sup>Department of Geography, Royal Holloway University of London, Egham, Surrey TW20 0EX, UK

<sup>3</sup>School of Geography, Archaeology and Environmental Studies, University of the Witwatersrand, 1 Jan Smuts Avenue, Braamfontein, 2050, South Africa

<sup>4</sup>Department of Geography, Environmental Management and Energy Studies, University of Johannesburg, Corner Ditton and University Avenue, Auckland Park, Johannesburg, South Africa

<sup>5</sup>Bloomsbury Environmental Isotope Facility, Department of Earth Sciences, University College London, Gower Street, London WC1E 6BS, UK

<sup>6</sup>Centro de Estudos do Mar da Universidade Federal do Paraná, Caixa Postal 61, 83255-976 Pontal do Paraná, PR, Brazil

<https://doi.org/10.17159/caj/2020/30/2.9273>

Lake sediments and wetland peats provide valuable archives of changes in anthropogenic inputs into natural ecosystems. Sediments of remote mountain lakes are particularly useful because contaminants in these settings are solely derived from atmospheric deposition. This study presents the first historical record of contamination for Lesotho, a hydrologically important region in southern Africa, exporting about 35% of the water used in the Gauteng/Mpumalanga urban-industrial complex in South Africa.

Lake sediment and wetland cores were collected from Letšeng-la Letsie, a remote mountain lake in the Maloti Mountains of Lesotho, impounded in 1968. The lake and wetland cores provide records extending back  $85 \pm 16$  and  $119 \pm 23$  years respectively. These were analysed for atmospheric contaminants, including trace metals and metalloids (Hg, Pb, Cu, Ni, Zn, As), spheroidal

carbonaceous fly-ash particles (SCPs), stable nitrogen isotopes and organic pollutants including polycyclic aromatic hydrocarbons (PAHs) and persistent organic pollutants (POPs).

Contaminant levels were found to be low (Figure 1). Most trace metal and organic contaminant concentrations were below the consensus threshold effect concentration for effects on sediment-dwelling organisms. SCP fluxes were similar to fluxes in remote mountain lakes of Europe and North America. Peak Hg concentrations in Letšeng-la Letsie sediments were equivalent to those reported from remote lakes on the Tibetan Plateau and lower than Hg concentrations in lake sediments in the Rwenzori Mountains in Uganda, the Rocky Mountains in the United States and in central Alaska.

There were increasing trends in mercury, fly-ash particles, high molecular weight PAHs and total PCBs levels since the 1970s

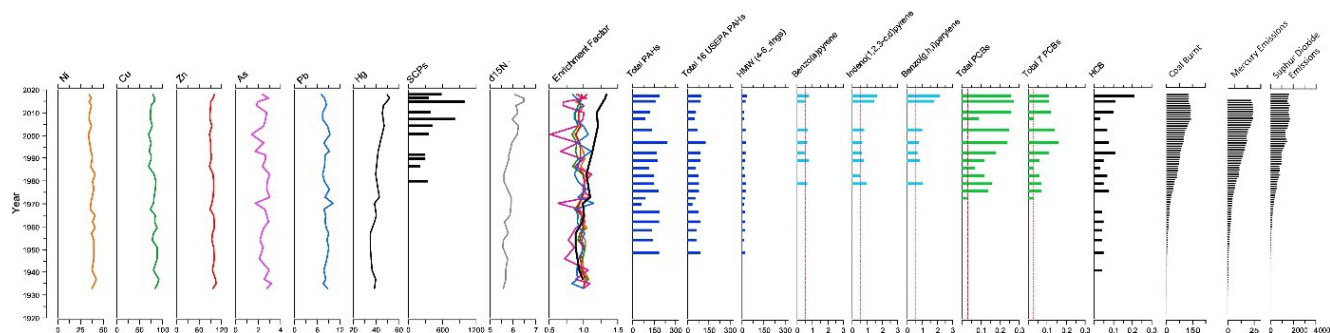


**Figure 1:** Trace metal, SCP and  $\delta^{15}\text{N}$  concentrations, trace metal enrichment factors, total PAHs, total 16 USEPA PAHs, total high molecular weight (HMW) PAHs, selected individual HMW PAH concentrations, total PCBs, total PCB7 concentrations, and total HCBs for the lake sediment cores for Letšeng-la Letsie. Trace metal concentrations are  $\mu\text{g g}^{-1}$  except for Hg which is in  $\text{ng g}^{-1}$ . SCP concentrations are ‘per g dry mass of sediment’ ( $\text{g DM}^{-1}$ ).  $\delta^{15}\text{N}$  concentrations are per mil (‰). PAH, PCB and HCB concentrations are in  $\text{ng g}^{-1}$ . Vertical red dotted lines are analytical limits of detection. Adapted from Rose et al. (2020).

(Figure 1). The contaminants showing some recent enrichment are likely derived from long-range transport of products of coal combustion for power generation and other industrial processes on the South African Highveld. Back trajectory analysis showed that long-range transport to southern Lesotho from the industrialised Highveld occurs in association with anticyclonic conditions, evidence of which was also found by Piketh et al. (2002) at Ben Macdhui in the Eastern Cape. Transport from industrialised regions is infrequent, accounting for the low contaminant levels.

This evidence of atmospheric deposition of contaminants from sources over 400 km away in a remote mountain ecosystem suggests that further research is required into transport pathways and fate of Highveld pollutants, and the potential impacts on Afromontane systems.

## References

Piketh, S.J., Swap, R.J., Maenhaut, W., Annegarn, H.J., Formenti, P. (2002). Chemical evidence of long-range transport over southern Africa. *Journal of Geophysical Research Atmospheres*, 107, D24, ACH 7-1-ACH 7-3.

Rose, N.L., Milner, A.M., Fitchett, J.M., Langerman, K.E., Yang, H., Turner, S.D., Jourdan, A.-L., Shilland, J., Martins, C.C., Souza, A.C., Curtis, C.J. (2020). Natural archives of long-range transported contamination at the remote lake Letšeng-la Letsie, Maloti Mountains, Lesotho. *Science of The Total Environment*, 737, 139642. <https://doi.org/10.1016/j.scitotenv.2020.139642>.

## Erratum

# The need for open data on air quality monitoring in logistically difficult environments

Published in *Clean Air Journal*, 28(2), 2018 - <http://dx.doi.org/10.17159/2410-972X/2018/v28n2a13>

**Collins Gameli Hodoli<sup>1</sup>, Aidatu Abubakari<sup>2</sup>, Gameli Adzaho<sup>3</sup>,  
Frederic Coulon<sup>1</sup>, Mohammed I Mead<sup>1\*</sup>**

<sup>1</sup>Cranfield University, School of Water, Energy and Environment, Cranfield, MK43 0AL, UK

<sup>2</sup>University of Ghana Business School, Department of Marketing and Entrepreneurship, University of Ghana, Legon, Accra-Ghana

<sup>3</sup>Global Lab Network, Accra, Ghana

\*Corresponding author: [Iq.Mead@cranfield.ac.uk](mailto:Iq.Mead@cranfield.ac.uk)

<http://dx.doi.org/10.17159/2410-972X/2018/v28n2a13E>

The lead author (C.G.H.) wishes to add two authors to the published commentary; Frederic Coulon and Mohammed I Mead have been added to the author list, and Mohammed I Mead is now the corresponding author. The above author list and affiliations are correct.

## Finding an environmental equilibrium



**We provide a full range of environmental legal services across all environmental media, including air, water, waste, contamination and biodiversity.**

**With respect to air quality law, we advise on:**

- AEL applications appeals • Reviews and prosecutions • Compliance notices and directives
- Noise and odour • GHG compliance • Carbon Tax.

**Contact information:**

**Durban: +27 31 575 7000**

**Johannesburg: +27 11 290 2540**

**Ian Sampson: sampson@wylie.co.za**

**Siya Mkhize: smkhize@wylie.co.za**

**Shepstone**  **Wylie**  
ATTORNEYS

[www.wylie.co.za](http://www.wylie.co.za)

## Research article

# Air pollution in Kigali, Rwanda: spatial and temporal variability, source contributions, and the impact of car-free Sundays

R Subramanian<sup>1,2,7,\*</sup>, Abdou Safari Kagabo<sup>3</sup>, Valérien Baharane<sup>3</sup>, Sandrine Guhirwa<sup>3</sup>, Claver Sindayigaya<sup>3</sup>, Carl Malings<sup>1,2,8</sup>, Nathan J Williams<sup>4,7</sup>, Egide Kalisa<sup>5</sup>, Haofan Li<sup>1</sup>, Peter Adams<sup>1</sup>, Allen L Robinson<sup>1</sup>, H. Langley DeWitt<sup>6</sup>, Jimmy Gasore<sup>3,7</sup>, and Paulina Jaramillo<sup>4,7</sup>

<sup>1</sup>Center for Atmospheric Particle Studies, Carnegie Mellon University, Pittsburgh, PA 15218, USA

<sup>2</sup>Observatoire Sciences de l'Univers-Enveloppes Fluides de la Ville à l'Exobiologie, CNRS UMS3563, France

<sup>3</sup>Department of Physics, University of Rwanda, Kigali, Rwanda

<sup>4</sup>Department of Engineering and Public Policy, Carnegie Mellon University, Pittsburgh, PA, USA

<sup>5</sup>Institute for Applied Ecology New Zealand, School of Science, Auckland University of Technology, Auckland 1142, New Zealand

<sup>6</sup>Center for Global Change Science, Massachusetts Institute of Technology, Cambridge, MA, USA

<sup>7</sup>Kigali Collaborative Research Center, Kigali, Rwanda

<sup>8</sup>NASA Postdoctoral Program Fellow, Goddard Space Flight Center, Greenbelt, Maryland, MD 20771, USA

\*Corresponding author, E-mail: subu@cmu.edu subu@lisa.u-pec.fr

Received: 3 March 2020 - Reviewed: 8 April 2020 - Accepted: 17 August 2020

<https://doi.org/10.17159/caj/2020/30/2.8023>

## Abstract

Ambient air pollution, particularly fine particulate mass ( $PM_{2.5}$ ) and ozone ( $O_3$ ), is associated with premature human mortality and other health effects, but monitoring is scarce to non-existent in large parts of Africa. Lower-cost real-time affordable multi-pollutant (RAMP) monitors and a black carbon (BC) monitor were deployed in Kigali, Rwanda to fill the air quality data gap here.  $PM_{2.5}$  data were corrected using data from a coincident, short-term campaign that used standard filter-based gravimetry, while gas data were verified by collocation with reference carbon monoxide (CO) and  $O_3$  monitors at the Rwanda Climate Observatory at Mt Mugogo, Rwanda. Over March 2017–July 2018, the ambient average  $PM_{2.5}$  in Kigali was  $52 \mu\text{g}/\text{m}^3$ , significantly higher than World Health Organization (WHO) Interim Target 1. Study average BC was  $4 \mu\text{g}/\text{m}^3$ , comparable to mid-sized urban areas in India and China and significantly higher than BC in cities in developed countries. Spatial variability across various urban background sites in Kigali appears to be limited, while  $PM_{2.5}$  at Mt Mugogo is moderately correlated with  $PM_{2.5}$  in Kigali. A sharp diurnal profile is observed in both  $PM_{2.5}$  and BC, with the Absorption Angstrom Exponent (AAE) indicating that the morning peak is associated with rush-hour traffic-related air pollution (TRAP) while the late evening peak can be attributed to both traffic and domestic biofuel use.  $PM_{2.5}$  in the dry seasons is about two times  $PM_{2.5}$  during the following wet seasons while BC is 40–60% higher. Local sources contribute at least half the ambient  $PM_{2.5}$  during wet seasons and one-fourth during dry seasons. Traffic restrictions on some Sundays appear to reduce  $PM_{2.5}$  and BC by  $10\text{--}12 \mu\text{g}/\text{m}^3$  and  $1 \mu\text{g}/\text{m}^3$  respectively, but this needs further investigation. Dry season ozone in Kigali can exceed WHO guidelines. These lower-cost monitors can play an important role in the continued monitoring essential to track the effectiveness of pollution-control policies recently implemented in Rwanda.

## Keywords

fine particulate matter, ozone, black carbon, sub-Saharan Africa, urban air pollution, vehicular emissions, biofuel emissions, low-cost sensors

## Introduction

Ambient air pollution, especially fine particulate mass ( $PM_{2.5}$ ) and ozone ( $O_3$ ), has been associated with premature human mortality (Dockery et al., 1993; Jerrett et al., 2009; Laden et al., 2006). The World Health Organization (WHO) estimates that

in 2016, ambient air pollution caused about three thousand deaths in Rwanda (Brauer et al., 2012; WHO, 2018). However, such estimates can be uncertain because exposure is inferred from satellite estimates. There has been no long-term ground-based monitoring in major cities like Kigali to validate estimated

exposures. The situation is similar in many other sub-Saharan African countries (Kalisa et al., 2019; Petkova et al., 2013). This lack of monitoring due to resource limitations also hampers scientific understanding of the sources contributing to air pollution in these countries, which is essential to formulating effective environmental management policies.

In Rwanda, biomass use accounts for 85% of energy consumption, in the form of wood and charcoal (MININFRA, 2018). Wood is used in rural households and charcoal in urban households. Petroleum in the form of transportation fuel, liquified petroleum gas (LPG) for household cooking, and electricity generation accounts for 13% of national energy consumption (MININFRA, 2018). As of 2018, 77% of on-road vehicles (excluding motorcycles) were manufactured before 2005 (Duhuze, 2018). As a result, air pollution in Kigali can be significantly higher at roadside locations than at urban background locations (Kalisa et al., 2018). Rwandan air quality is also influenced by regional forest fires and seasonal weather patterns (DeWitt et al., 2019). Rwanda’s electricity generation (218 MW) is composed of 45% hydropower, diesel and heavy fuel oil at 27%, methane (14%), peat (7%), and solar (6%). Diesel is used to fuel peaking power stations and for backup generation during power outages, which can be significant contributors to ambient air pollution (Farquharson et al., 2018; Subramanian et al., 2018). Some of these sources were identified by Henninger (2013) using scanning electron microscopy of filter samples.

To more accurately quantify source contributions (a requirement for effective air quality management), source apportionment is often conducted with chemical mass balance (CMB) or receptor modeling (e.g. positive matrix factorization) using organic molecular markers (Shrivastava et al., 2007; Subramanian et al., 2007) or aerosol mass spectrometry (AMS) (Zhang et al., 2011). However, such studies require extensive sample collection and offline analysis or long-term deployment of expensive equipment, especially if sources can vary between seasons. Pikridas et al. (2013) find that an observation-based method (OBM), which uses the temporal pattern of pollution measured with even a low-cost PM monitor, closely replicates the regional/urban divide based on PM<sub>2.5</sub> composition measurements inside and upwind of Patras, Greece. Diamantopoulou et al. (2016) use regional air quality modeling to simulate observations and find

the OBM analysis of the pseudo-observations comparable to the model-computed regional/local divide.

Traffic restrictions such as car-free days, low-emission zones (LEZ), and “odd/even” policies have been used in cities worldwide to reduce air pollution. The evidence that such policies reduce human exposure is mixed. No effect was observed on air quality in Mestre-Venice (Masiol et al., 2014). London’s LEZ saw decreases in nitrogen dioxide (NO<sub>2</sub>), but no significant changes in PM<sub>2.5</sub> or PM<sub>10</sub> (Mudway et al., 2019). Extensive traffic control measures in Beijing during the 2008 Olympics reduced median black carbon (BC) concentrations by as much as 50% (Wang et al., 2009). The Rwandan government, to promote social welfare, has recently implemented “car-free” Sundays, wherein major roads are blocked off and people take part in group exercises on car-free streets starting at 7 AM and ending either at 10 AM or at noon. In 2017, the first Sunday of each month was designated “car-free”, while in 2018 that was expanded to the first and third Sundays of each month. Additionally, to curb the use of older imported cars and harmonize duty structures with other East African countries, in 2017 the Rwandan government increased duties on cars, with the increase depending on the vehicle age (RRA, 2017). The vehicle import rate dropped by 20% in the first half of 2017, likely connected to the higher import duties (Ngabonziza, 2017). Monitoring is required to quantify the impact of these policies on air quality in Kigali.

Here, we show how low-cost sensors can improve scientific understanding of air quality in resource-challenged countries. The high time resolution of the RAMPs and BC monitor enables an examination of diurnal patterns in each season, which is not possible with integrated daily filter samples. We apply OBM to the RAMP and BC datasets to get a preliminary estimate of the regional and local contribution to Kigali air pollution in each season. Measurements at multiple “urban background” sites within Kigali allow us to examine intra-urban variability in air pollution at non-roadside locations across Kigali, unlike the urban background/roadside comparison by Kalisa et al. (2018). Long-term monitoring with RAMP monitors allows examination of the seasonal variability in ambient air pollution across multiple dry and wet seasons. Furthermore, we evaluate the impact of the “car-free Sunday” policy on air pollution. The multi-wavelength aerosol light absorption from the BC monitor helps

**Table 1:** Site descriptions and deployment periods for the measurements reported in this study.

Site	UR-CST	CMU-Africa	Gacuriro	Belle Vue	RCO
Type	Urban	Urban	Urban	Urban	Rural
Latitude	-1.96279	-1.94455	-1.9219	-1.92563	-1.58625
Longitude	30.06473	30.08961	30.09389	30.0924	29.56568
Instrument and deployment period					
RAMP #140			March-June 2017		July-Dec 2017
RAMP #145		March-June 2017		July-Dec 2017	
RAMP #152	July 17-July 18				
BC-1054	July 17-April 18				

us qualitatively identify contributions from biomass burning and fossil fuel combustion. Comparison of urban and rural air pollution provides insight into the impact of urbanization on air quality. We end with recommendations on ways to implement and improve such studies in Rwanda and other countries in the Global South.



**Figure 1:** Measurement sites in Rwanda (a) and specifically in Kigali (b) where RAMPs were deployed for varying periods over 2017–2018. Maps generated using Google Earth Pro.

## Methodology

### Sampling locations

Starting in March 2017, RAMP monitors were deployed in Kigali at multiple locations (Figure 1) as summarized in Table 1. Kigali terrain is composed of hills and valleys; the RAMPs in this study were all located at hilltop sites. The Gacuriro and Belle Vue Estate locations are both residential neighborhoods about 0.5 km apart. The Carnegie Mellon University (CMU-Africa) site is about 2.5 km from Gacuriro, located in a commercial building complex near a major road and six stories above ground (this was the campus till late 2019). RAMP #152 and a Met-One 10-wavelength BC monitor (BC-1054) were deployed in July 2017 on the roof of the University of Rwanda’s five-story College of Science & Technology building (UR-CST), where Kalisa et al. (2018) had collected filter-based samples for their urban background location over April–June 2017. This manuscript focuses on RAMP data collected at UR-CST between July 2017–July 2018. The BC data ends in April 2018 as the pump malfunctioned, which made

the instrument inoperable. The Gacuriro and Belle Vue sites are about 5 km from the UR-CST site.

### The RAMPs and gas sensor calibration

The RAMPs (Figure S1) were manufactured by Sensever (now owned by Sensit Technologies, Valparaiso, IN, USA) and cost about US\$ 3,000 each at the time of purchase (base unit without an external PM sensor). The RAMP monitors and calibration methodologies are described in previous work (Malings et al., 2019, 2020; Subramanian et al., 2018; Zimmerman et al., 2018). Briefly, the RAMP uses passive Alphasense (UK) electrochemical sensors to measure CO, nitrogen dioxide (NO<sub>2</sub>), O<sub>3</sub>, and other gases. The raw signals of the RAMP electrochemical gas sensors (collected at 4 times per minute) are processed and averaged to provide hourly ambient concentrations using generalized RAMP (gRAMP) calibration models (Malings et al., 2019) developed in Pittsburgh, Pennsylvania, USA. The gRAMP calibration models are based on data from several RAMP monitors collocated with reference gas monitors at the CMU campus in Pittsburgh in 2017 and were shown to transfer better to other locations in Pittsburgh than calibration models developed for individual RAMPs. For CO, a quadratic regression (QR) gRAMP model is used and for O<sub>3</sub>, a hybrid random forest/linear regression (“hybrid-RF”) gRAMP model is used.

For local verification of CO and O<sub>3</sub>, RAMP #140 was collocated with reference monitors for CO and CO<sub>2</sub> (Picarro G2401) and O<sub>3</sub> (Teledyne T400) at the Rwanda Climate Observatory (RCO) on the summit of Mt Mugogo (about 70 km from Kigali and 2590 m above sea level, DeWitt et al. (2019)) over July–December 2017. Due to instrument malfunctions, collocated measurements are available for only 60 days of this six-month period. “Mugogo” linear regression, QR, and hybrid-RF models are developed using a subset (four weeks) of the collocation data; as shown in Zimmerman et al. (2018), a four week period is sufficient to develop calibration models for these electrochemical sensors. The remaining collocation data (32 days) are set aside to provide an independent or unseen data set for testing model performance, a practice previously established by our group in Zimmerman et al. (2018) and Malings et al. (2019). The performance of the Mugogo and the Pittsburgh gRAMP models is shown in Table 2. For CO, the gRAMP models showed slightly worse correlation (Pearson *r*) and normalized mean absolute error (CvMAE) than the Mugogo-based calibration models. For O<sub>3</sub>, the gRAMP model is comparable to the better-performing Mugogo QR and hybrid-RF models for *r* and CvMAE. RAMP-specific Mugogo models show lower bias than the gRAMP models. During the dry season, most of the data from the gRAMP ozone model are within ±30% of the reference monitor data at RCO (Figure S2).

RAMP-specific models trained on one RAMP may not transfer as well to other RAMPs as the gRAMP models (Malings et al., 2019). As most of the Kigali O<sub>3</sub> data is from RAMPs not collocated at Mugogo, the results presented here for ambient CO and O<sub>3</sub> are based on the gRAMP models. As we do not have local verification for NO, NO<sub>2</sub>, or SO<sub>2</sub>, these data are not presented here.

**Table 2:** Summary statistics showing the performance of Pittsburgh-based gRAMP and RAMP-specific Mugogo calibration models, both tested on 32 days of collocation at the Mugogo site. (These testing data were not used to build the Mugogo calibration models.)

Model	CO			Ozone		
	Pearson r	CvMAE	Bias (ppb)	Pearson r	CvMAE	Bias (ppb)
Pittsburgh gRAMP	0.82	0.19	15.7	0.57	0.24	6.02
Mugogo linear	0.87	0.16	-4.22	0.16	0.24	1.10
Mugogo QR	0.92	0.13	-1.83	0.63	0.20	0.30
Mugogo hybrid-RF	0.90	0.16	-6.28	0.56	0.22	0.32

## PM<sub>2.5</sub> measurements

PM<sub>2.5</sub> is measured using a Met-One neighborhood PM monitor (NPM) paired with each RAMP. The NPM is a nephelometer with a PM<sub>2.5</sub> cyclone, an inlet heater to reduce humidity effects, and a pump (flow rate 2 lpm). The PM<sub>2.5</sub> data are processed using methods developed based on collocations of over two dozen NPMs with US Environmental Protection Agency (EPA) federal equivalent method (FEM) beta attenuation monitors (BAM) at an urban background location and a source-impacted location in Pittsburgh (Malings et al., 2020). Either a physical (assumed composition and hygroscopic growth with scaling to BAM values) or an empirical approach (a quadratic regression with raw data, temperature, and RH as the variables) is used to convert as-reported NPM readings to “BAM-equivalent” PM<sub>2.5</sub> mass concentration (reported at 35% RH and 22 °C); both methods performed similarly in Pittsburgh. For Rwanda, we use the Pittsburgh-based physical approach, then apply a further localized correction to account for differences in aerosol size distribution and composition between Kigali and Pittsburgh. This localized correction of the “BAM-equivalent” PM<sub>2.5</sub> data is based on a comparison of the Gacuriro RAMP with 24-hour integrated filter-based measurements in April 2017 collected by Kalisa et al. (2018) at UR-CST about 5 km away (described in the SI). Briefly, the “BAM-equivalent” PM<sub>2.5</sub> data (corrected for hygroscopic growth but not for aerosol differences between Kigali and Pittsburgh) are strongly correlated (correlation coefficient,  $r^2 = 0.77$ ) with the filter-based PM<sub>2.5</sub> for non-working days (weekends, holidays, and car-free Sundays). However, the comparison is more scattered for working days (weekdays that are not holidays), which might indicate some intraurban variability related to local activities such as traffic and industrial emissions that may be more prominent on working days. Overall, the working day “BAM-equivalent” RAMP PM<sub>2.5</sub> values are scaled up by 1.69 and the non-workday “BAM-equivalent” RAMP PM<sub>2.5</sub> data are scaled up by 1.39 (Figure S3).

## BC mass and AAE measurements

The BC-1054 monitor (Met One Instruments, Inc.) deployed at the UR-CST site measures light attenuation by a filter sample at ten wavelengths between 370-950 nm. The as-reported BC mass concentrations from this monitor were processed using manufacturer-provided software (BC Load Correction 1.3.1), which corrects for known filter-loading artifacts (Kirchstetter and Novakov, 2007) using the algorithm developed by Virkkula et al. (2007). However, no correction is made for potential light

absorption enhancement due to BC mixing state (Bond et al., 2006), which means the BC mass concentrations reported here may be overestimates. The Absorption Angstrom Exponent (AAE) was calculated based on all ten wavelengths as the negative slope of the relationship between the wavelength-dependent attenuation and the wavelength in a log-log space (Moosmüller et al., 2011). For fresh combustion aerosol mainly composed of black carbon and for particles small relative to the wavelength, AAE is expected to be near unity. A compilation of studies (Lack and Langridge, 2013) on fossil fuel emissions and urban pollution with BC as the dominant absorber yielded an average AAE of  $1.1 \pm 0.3$  ( $\pm$  one standard deviation). The AAE for light-absorbing organic compounds (brown carbon or BrC) associated with biomass burning or humic-like substances is higher, with estimates ranging from 2 to 6 (Kirchstetter et al., 2004; Sun et al., 2007). Hence, higher values of AAE can be used to qualitatively identify periods when non-BC aerosol components such as light-absorbing dust or biomass burning containing BrC are significant contributors to aerosol light absorption. We do not attempt to quantify the contributions of fossil fuel and biomass burning emissions here as there can be significant uncertainty associated with such methods, as described in DeWitt et al. (2019) and references therein.

## Results and discussion

### Intra-urban variability across Kigali

The UR-CST and Belle Vue Estate sites are about 5 km apart and have the largest paired data set across both dry (July-September) and wet (October-November) seasons. An orthogonal distance regression (ODR) fit of the paired hourly average PM<sub>2.5</sub> concentrations yields a slope  $0.996 \pm 0.012$  and effectively zero-intercept. An ordinary least-squares fit (not forced through zero) has a correlation ( $r^2$ ) of 0.61. The UR-CST and Belle Vue Estate sites in Kigali are typical of urban background hilltop locations (Figure 1), unlike the urban background/roadside comparison where Kalisa et al. (2018) found significant differences. The much smaller dataset of 337 paired hourly average PM<sub>2.5</sub> measurements at the Gacuriro and CMU-Africa sites yields a slope of  $0.967 \pm 0.03$  (and an effectively zero intercept) with the ODR fit. For the sake of simplicity (as the succeeding analysis focuses on longer-term comparisons), the measurements at all four sites are averaged into a single time series providing hourly average PM<sub>2.5</sub> values from March 2017 to July 2018.

A comparison of the  $O_3$  measured at the matched residential and university locations (Gacuriro and CMU-Africa; Belle Vue Estate and UR-CST) shows that most paired values are in reasonable agreement around the 1:1 line (Figure S4). An ODR fit of the 1-hour  $O_3$  values measured at Gacuriro and CMU-Africa yields a slope of  $0.97 \pm 0.01$  with negligible intercept. A comparison of the UR-CST and Belle Vue estate  $O_3$  measurements is complicated by the significantly higher  $O_3$  apparently measured at the UR-CST site during the mid-July to mid-September period. The reason for these differences is unclear, as temperature and relative humidity (two variables likely to affect sensor performance) measured at the two urban background locations are identical. This issue of potentially high  $O_3$  at UR-CST needs to be investigated further; here, we take a conservative approach and present the data set as a unified  $O_3$  time-series (as we do for  $PM_{2.5}$ ), except the UR-CST measurements are excluded from the current analysis. This restricts our analysis to the March–November 2017 period (as there is only a week of data for December 2017 from the Belle Vue estate site), which are the two 2017 wet seasons (March–April–May or MAM and ON) and the long dry season (June–July–August–September, JJAS).

Unlike  $O_3$  and  $PM_{2.5}$ , differences in CO concentrations were sometimes observed at the residential locations and the campus sites in Kigali (Figure S5 of the SI). The highest concentrations were observed usually at the campus sites, which might reflect the greater traffic seen by these sites compared to residential neighborhoods. However, the Gacuriro neighborhood did experience two hours when CO exceeded 3 ppm. Overall, the study average CO concentrations were similar at UR-CST and Belle Vue Estate at  $0.446 \pm 0.322$  ppm and  $0.447 \pm 0.283$  ppm (average and standard deviation) respectively. CO was  $0.504 \pm 0.499$  ppm at CMU-Africa and  $0.404 \pm 0.320$  ppm at Gacuriro. Concentrations at rural Mugogo were even lower, at  $0.225 \pm 0.097$  ppm. However, the measured CO concentrations at all locations were low and far below US EPA standards (35 ppm for 1 hour). The WHO has not set guideline values for CO. The higher standard deviations at the urban sites compared to the rural site suggests that the urban areas are more likely to see large spikes of CO.

## Average monthly patterns of $PM_{2.5}$ and changes from 2017 to 2018

The unified Kigali time series for ambient  $PM_{2.5}$  is summarized as monthly average  $PM_{2.5}$  values, covering the period between March 2017 and July 2018 (Figure 2). The least data were collected in June–July 2018 (100 and 64 hours) due to maintenance issues. For all other months, between 298–744 hours of data are available, averaging 634 hourly values per month (88% of a 30-day period). The monthly average  $PM_{2.5}$  values range from  $25 \mu\text{g}/\text{m}^3$  in May 2018 to  $102 \mu\text{g}/\text{m}^3$  in July 2017, all higher than the WHO annual guideline of  $10 \mu\text{g}/\text{m}^3$ ; most months also exceed the WHO's first interim target (WHO IT 1) of  $35 \mu\text{g}/\text{m}^3$ . The study average hourly  $PM_{2.5}$  in Kigali is  $52.4 \pm 33.7 \mu\text{g}/\text{m}^3$ ; the large standard deviation suggests significant temporal variability that will be explored further in later sections.

A comparison of the overlapping months shows a reduction of almost 40% from 2017 to 2018 for March, April, and May, and 51% for July, while the June monthly average is practically unchanged. However, June and July 2018 had the least data coverage (as noted in the preceding paragraph), and fewer than 300 hours of data are available for June 2017. The March–May comparisons are more robust with 1,683 and 1,942 hours of data available in 2017 and 2018 respectively. April 2017 had a larger fraction of non-working day data (43%) compared to the other five months (30–34%), but similar reductions are seen when the comparison is restricted to working days. An examination of spatially-resolved reanalysis data (Siebert et al., 2019) for rainfall (Rwanda Meteorology Agency, 2019) in Kigali (Figure S6) shows that the UR-CST site during MAM 2018 experienced 38 rainy days ( $\geq 5$  mm/day), compared to 16 such rainy days in MAM 2017 at Gacuriro. Total rainfall was also substantially higher in 2018; 612 mm at UR-CST in MAM 2018 compared to just 180 mm at Gacuriro in MAM 2017. The more frequent and heavier rainfall in MAM 2018 could at least partly explain the significantly lower  $PM_{2.5}$  in MAM 2018 compared to MAM 2017.

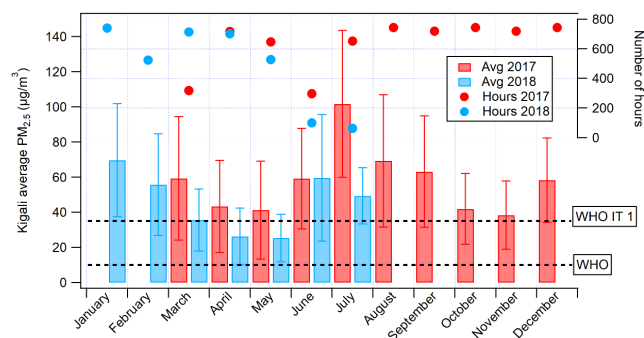


**Figure 2:** Monthly average  $PM_{2.5}$  measured in Kigali over the course of this study. Red bars indicate 2017 and blue bars indicate 2018 data. Error bars are one standard deviation of the hourly measurements in that month. Solid round markers show the number of hourly data points collected in that month. Horizontal dashed lines indicate WHO annual guideline and the WHO's first interim target (IT 1).

## Working day/non-Working day and seasonal differences in $PM_{2.5}$

Figure 3 shows the distribution of hourly  $PM_{2.5}$  values measured in Kigali across each of the four seasons: long wet season (MAM 2017 and MAM 2018), long dry season (JJAS 2017, henceforth JJAS), short wet season (ON 2017, henceforth ON), and short dry season (December 2017 and January–February 2018, henceforth DJF.) Note that August and September are both considered “dry” here. As Figure 2 showed, the monthly average  $PM_{2.5}$  value for September is closer to that of August and June, and noticeably higher than the average  $PM_{2.5}$  for October and November. Additionally, September 2017 saw just 17 mm of rainfall, compared to 104 mm of rainfall in October–November 2017 (Figure S6). This suggests that our classification is appropriate for 2017.

Figure 3 shows that ambient  $PM_{2.5}$  levels are higher in the dry seasons than in the wet seasons. The hourly data collected with the RAMPs on non-working days (nWD) in MAM 2018 and ON

shows a pear-shaped pattern, in contrast to the hourglass shape of MAM 2017 nWD data; this is also seen in the working day (WD) data. This suggests that there are fewer high-concentration periods in the later wet season months. WD  $PM_{2.5}$  values are higher than the nWD concentrations for all seasons by 19-27%. However, as discussed earlier, WD  $PM_{2.5}$  values are scaled upwards by 1.69 based on a comparison with the Kalisa et al. (2018) wet season filter measurements while nWD  $PM_{2.5}$  values are similarly upscaled by 1.39 - a difference of 22%. Thus, this weekday-weekend effect could reflect Kalisa et al.'s results for April 2017 and needs to be investigated further for other months of the year.

Table 3 summarizes the seasonal averages for working days. The dry season average  $PM_{2.5}$  concentrations are about two times the following wet season average; to be exact, JJAS/ON is 1.89 (95% confidence intervals 1.82-1.97) and DJF/MAM 2018 is 2.11 (95% CI 2.03-2.19). This was also observed for non-working days. Higher pollution in the dry season was also observed by Kalisa et al. (2018) for  $PM_{2.5}$  in Kigali (though in campaigns of 2-4 weeks in each season) and by DeWitt et al. (2019) for BC at Mt Mugogo, who attribute the higher dry season concentrations to regional biomass burning. Kalisa et al. measured a median daily  $PM_{2.5}$  of 126  $\mu\text{g}/\text{m}^3$  (IQR 113-141  $\mu\text{g}/\text{m}^3$ ) over June 15-30, 2017. The median for our JJAS hourly measurements (which does not include data for the June 15-28 period) was 66.2  $\mu\text{g}/\text{m}^3$  (IQR 45.4-95.4  $\mu\text{g}/\text{m}^3$ ). It seems that the June 15-28 period saw higher pollution based on Kalisa et al.'s results, but other parts of the same dry season were relatively cleaner based on our results, showing the importance of long-term monitoring.

### BC and AAE in Kigali

A total of 6,850 hours of BC data were collected at UR-CST between July 6, 2017-April 24, 2018. The equivalent BC mass concentration (as measured at 880 nm) hourly averages ranged from 0.14  $\mu\text{g}/\text{m}^3$  to 49.6  $\mu\text{g}/\text{m}^3$ , with a study average of  $4.04 \pm 2.86 \mu\text{g}/\text{m}^3$ . This value is significantly higher than the values observed in urban areas of developed countries; e.g. in the early 2000s, urban ambient BC was 2 and 1  $\mu\text{g}/\text{m}^3$  respectively in the states of New Jersey and California in the USA after decades of reductions (Kirchstetter et al., 2017). The Kigali BC values are comparable to mid-sized urban areas in China and India. In Hefei (central China), annual average BC in 2012-2013 was 3.5  $\mu\text{g}/\text{m}^3$  (Zhang et al., 2015). In Pune (western India), the average BC over 2015-2016 was 3.9  $\mu\text{g}/\text{m}^3$  (Kolhe et al., 2018).

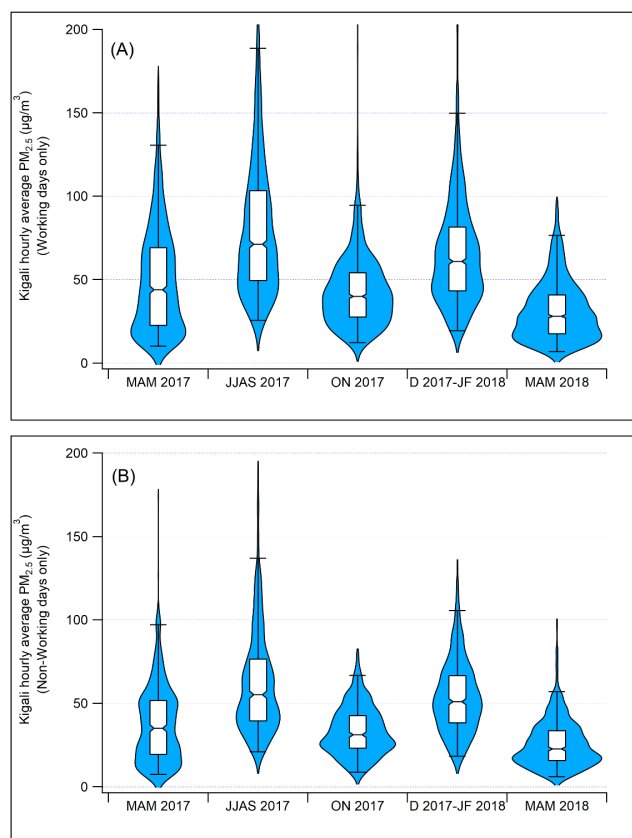


**Figure 3:** Distribution of 1-hour average  $PM_{2.5}$  in each of the seasons over the course of this study, grouped into (A) working day and (B) non-working day measurements. March-May (MAM) and October-November (ON) are the wet seasons; June-September (JJAS) and December-February (DJF) are the dry seasons. The boxes show the interquartile range (IQR), i.e. the 25th and 75th percentiles of data; the notch in each box shows the median value; and the whiskers mark the 2nd and 98th percentile of all data. The violin plot shows the relative distribution of all data. Y-axis truncated at 200  $\mu\text{g}/\text{m}^3$  for visual clarity.

BC working day seasonal averages are summarized in Table 3. Non-working day seasonal averages were 0.2-0.9  $\mu\text{g}/\text{m}^3$  lower. The difference between the wet and dry seasons (dry season BC 40-60% higher) in Kigali is lower than the factor-of-four difference observed in similarly-tropical Pune (Kolhe et al., 2018) or even at the rural Mt Mugogo site in Rwanda, where DeWitt et al. (2019) found dry and wet season BC different by almost a factor-of-three.

The study average AAE was 1.53, with most values between 0.9-2.1 (Figure S7). As shown in Table 3, AAE was slightly lower in

**Table 3:** Seasonal  $PM_{2.5}$  and BC statistics for this study in Kigali, Rwanda

Season	WD $PM_{2.5}$ average $\pm$ SD ( $\mu\text{g}/\text{m}^3$ ) (A)	Average diurnal minimum WD $PM_{2.5}$ ( $\mu\text{g}/\text{m}^3$ ) (B)	Regional WD $PM_{2.5}$ (%) C = B/A	WD BC average $\pm$ SD ( $\mu\text{g}/\text{m}^3$ )	AAE
MAM 2017	49.9 $\pm$ 31.7	21.3	42.7	N/A	N/A
JJAS	81.2 $\pm$ 42.3	57.3	70.6	5.20 $\pm$ 3.56	1.47 $\pm$ 0.15
ON	42.9 $\pm$ 21.0	22.8	53.2	3.20 $\pm$ 2.24	1.57 $\pm$ 0.16
DJF	66.0 $\pm$ 31.6	50.7	76.8	4.52 $\pm$ 2.96	1.52 $\pm$ 0.16
MAM 2018	31.3 $\pm$ 17.7	22.8	73.0	3.30 $\pm$ 2.40	1.59 $\pm$ 0.19

the dry seasons than in the wet seasons. Monthly average AAE values ranged from 1.39-1.59, lower than the 1.5-1.9 range seen at rural Mt Mugogo (DeWitt et al., 2019); this could indicate a greater contribution from vehicular sources to ambient BC in urban Kigali. Higher AAE (>1.8) values were almost always only seen at BC concentrations below  $5 \mu\text{g}/\text{m}^3$  (Figure S7), while higher BC concentrations showed AAE values around 1.4 or less, which suggests that fossil fuel combustion is associated with higher BC levels, but the background BC is dominated by biomass burning.

### Diurnal profiles of $\text{PM}_{2.5}$ and BC

Figure 4 shows the average diurnal pattern of  $\text{PM}_{2.5}$  and BC for the five seasons (four for BC) during the study period for which we have a large number of measurements. Only working day data are shown for visual clarity; a similar pattern is observed for the non-working day measurements. As noted earlier,  $\text{PM}_{2.5}$  concentrations are substantially higher in the dry seasons than in the wet seasons. A morning peak (likely related to traffic) is observed between 8 AM-10 AM local time for all seasons except MAM 2017. Concentrations then fall during the day (as the boundary layer height increases) before rising back up in the evening, likely a combination of evening emissions and lower boundary layer heights. The MAM 2017 night-time highs (and to some extent the JJAS night-time highs) remain at that level until the morning traffic peak. For the other three seasons, the morning traffic peak is higher than the night-time high values. While the BC concentrations follow a similar diurnal profile, in all seasons the maxima occur during the morning rush hours, with concentrations lowest in the afternoon. In further contrast to the  $\text{PM}_{2.5}$  dry/wet seasonal differences, the wet and dry season BC concentrations are much closer to each other, though dry season BC is still higher.

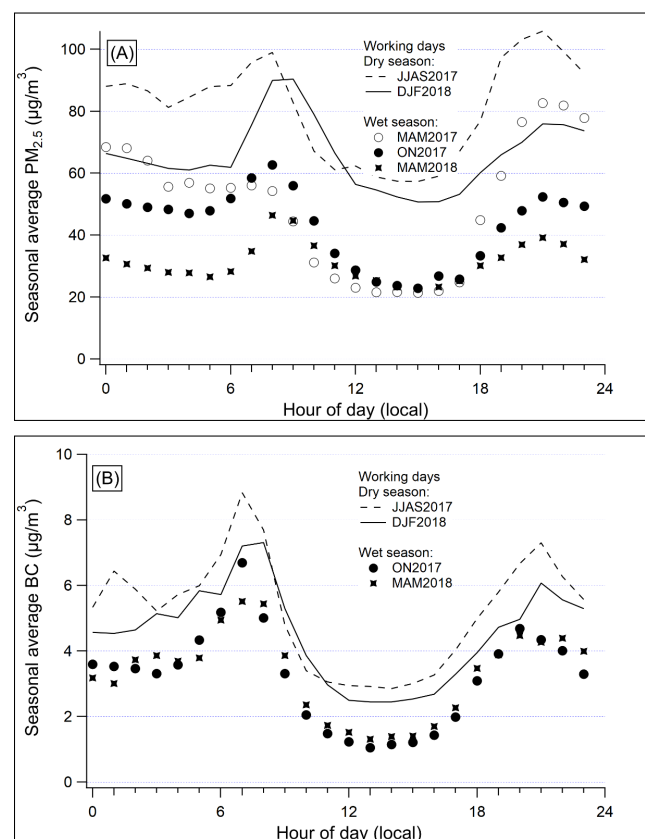
The highest  $\text{PM}_{2.5}$  concentrations are observed at night-time during MAM 2017 and JJAS, with average  $\text{PM}_{2.5}$  around  $80 \mu\text{g}/\text{m}^3$  between 8 PM-12 AM in the wet season (MAM 2017) and around  $100 \mu\text{g}/\text{m}^3$  between 7 PM-11 PM in the dry season (JJAS). In contrast, the highest average  $\text{PM}_{2.5}$  levels in other seasons were observed during the morning rush hour - around  $60 \mu\text{g}/\text{m}^3$  between 7 AM-10 AM in ON, around  $90 \mu\text{g}/\text{m}^3$  between 8 AM-10 AM in DJF, and around  $45 \mu\text{g}/\text{m}^3$  between 8 AM-10 AM in MAM 2018. The BC maxima all occur during the morning rush hour between 7 AM-8 AM except for DJF, when levels are marginally higher between 8 AM-9 AM than during the preceding hour.

The morning and evening peaks at similar times for  $\text{PM}_{2.5}$  and BC indicate that these PM peaks are related to combustion emissions. Figure 5 shows the diurnal variation in AAE during the dry and wet seasons. In both cases, AAE is lower between 6 AM to 9 AM, when BC mass concentrations are higher; the lowest median AAE is 1.4 between 7 AM-8 AM during the dry season. However, the night-time peaks in  $\text{PM}_{2.5}$  and BC are associated with higher AAE values, when hourly medians approach 1.6-1.7. These differences suggest that while the morning BC and  $\text{PM}_{2.5}$  peaks are mostly associated with fossil-fuel vehicular emissions, the night-time BC and  $\text{PM}_{2.5}$  peaks are additionally

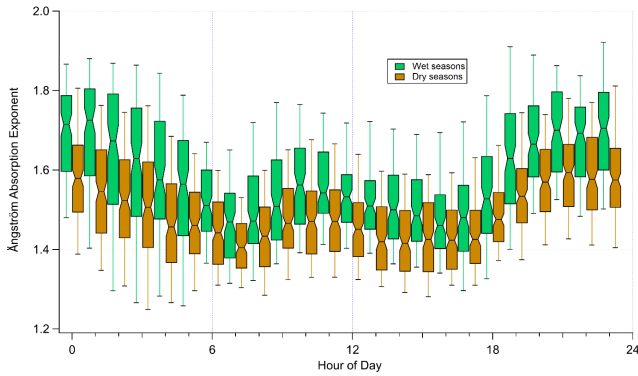
influenced by domestic biofuel use. However, compared to previous studies showing AAE values of  $\sim 1.1 \pm 0.3$  for fossil fuel BC-dominated pollution, the AAE values observed in Kigali are often higher, suggesting that there is always some biomass burning influence (associated with BrC).

### Local and regional contributions to $\text{PM}_{2.5}$ and BC in Kigali

We use OBM (Diamantopoulou et al., 2016; Pikridas et al., 2013) to estimate the regional and local contributions to ambient  $\text{PM}_{2.5}$  in Kigali. During the dry season, a higher regional background is likely, as transported pollution may not be rained out. The background can include regional biomass burning, dust, and other upwind emissions as well as secondary  $\text{PM}_{2.5}$ . The OBM assumes that the minimum value of a seasonal diurnal profile based on hourly measurements is the seasonal average regional contribution. Then, the seasonal average local contribution is the difference between the seasonal average ambient  $\text{PM}_{2.5}$  and the seasonal average regional contribution. These estimates of regional contribution assume the ambient concentrations at the minima are entirely regional, but there may be local vehicular and domestic biofuel emissions all day. Thus, the results are the upper bound of the regional contribution and the lower bound for the local contribution.



**Figure 4:** Average diurnal patterns of (A)  $\text{PM}_{2.5}$  and (B) BC for each season over the course of this study. Data restricted to working days, with similar patterns observed for non-working days.



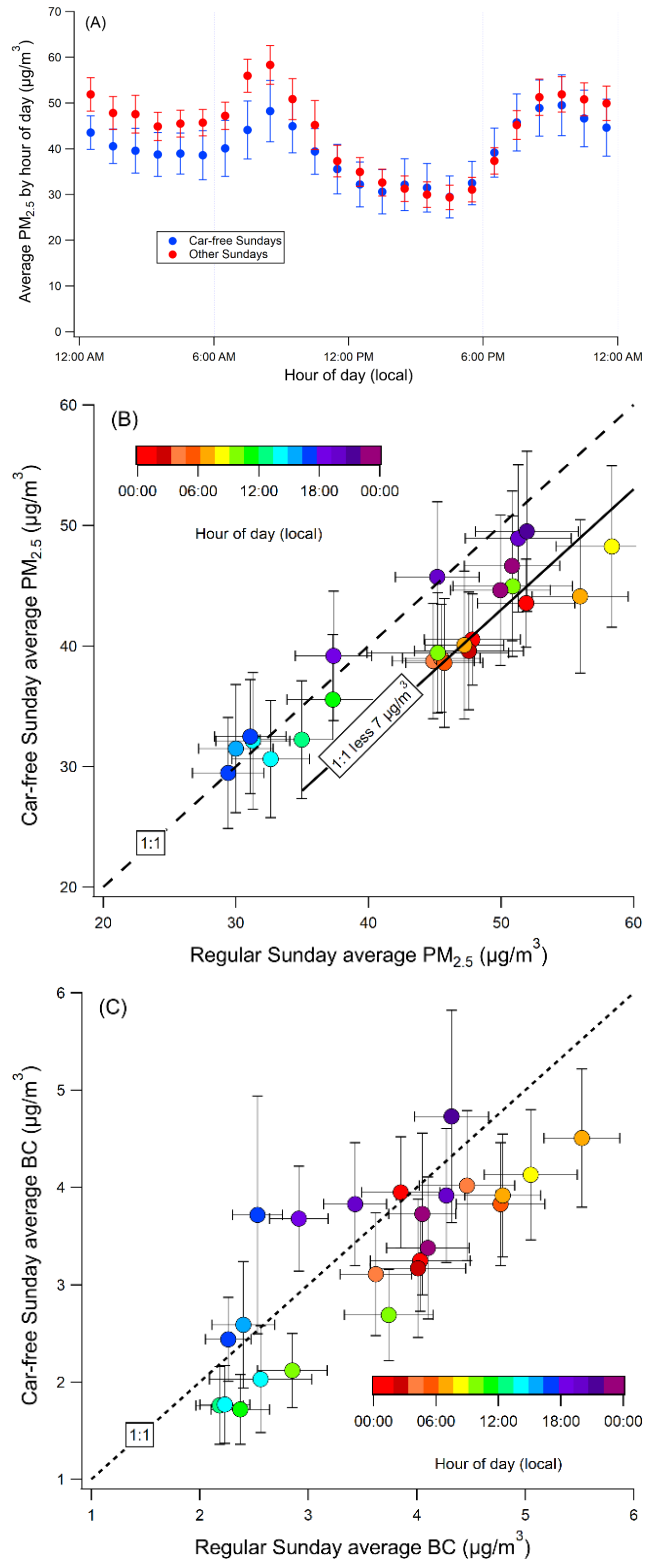
**Figure 5:** Diurnal variations in Angstrom Absorption Exponent (AAE) during the dry and wet seasons suggest vehicular emissions and domestic biofuel use contribute to ambient air pollution at different times of the day. The boxes show the IQR (25th and 75th percentiles of data); the notch shows the median; whiskers indicate the 9th and 91st percentiles. The corresponding hourly boxes for the two types of seasons are offset for visual clarity.

Table 3 summarizes the seasonal statistics required to calculate the average regional contribution to Kigali ambient  $PM_{2.5}$  for each season. The minimum average  $PM_{2.5}$  values were observed between 3-4 PM local time in all seasons. About half the ambient  $PM_{2.5}$  in Kigali appears to be from regional sources in the wet season, and the regional share rises to over 70% in the dry seasons. Put another way, local sources contribute at least half the observed  $PM_{2.5}$  during the 2017 wet seasons, and one-fourth of ambient  $PM_{2.5}$  during the two dry seasons. The MAM 2018 wet season appears to be an anomaly compared to the two other wet seasons, but in terms of absolute  $PM_{2.5}$  concentrations, the regional component is about the same in MAM 2018 as during the 2017 wet seasons.

Following a similar procedure for BC, the regional contribution on working days is 54-55% in the JJAS and DJF dry seasons, but only 33% and 40% in the wet MAM 2018 and ON seasons. The regional contribution to Kigali BC on non-working days is 7-8% higher during JJAS, ON, and MAM 2018, which likely reflects lower local emissions (including car-free Sundays). Overall, local sources are larger contributors to ambient BC than to  $PM_{2.5}$  in Kigali, ranging from about half in the dry season to two-thirds in the wet seasons.

### The impact of Sunday car-free hours on urban background air pollution

An estimate of the impact of traffic-related air pollution (TRAP) at non-roadside, urban background locations can be obtained by comparing the RAMP and BC measurements on “car-free” Sundays with the measurements on all other Sundays. In this study period,  $PM_{2.5}$  (BC) measurements were made on 16 (11) “car-free” Sundays that can be compared to data from 42 (30) regular Sundays. However, in Rwanda, the car-free policy is only in effect on Sunday mornings. The time-resolved data from the RAMPs and BC monitor allows investigation of the benefits of this policy for the specific periods when such policies are in effect.



**Figure 6:** Impact of limiting vehicular traffic on Sunday mornings in Kigali, Rwanda. Panel (A) shows the average hourly  $PM_{2.5}$  measured over 16 car-free Sundays and 42 regular Sundays between April 2017-May 2018. Panel (B) shows the same  $PM_{2.5}$  data as a scatter plot. Panel (C) shows a scatter plot of the corresponding BC concentrations. Error bars are the standard error.

Figure 6 shows a comparison of the hourly average  $PM_{2.5}$  between regular Sundays and car-free Sundays. The average hourly  $PM_{2.5}$  concentration is lower in the morning period by an average of  $7 \mu\text{g}/\text{m}^3$ . In the afternoon and evening periods, the diurnal patterns converge, indicating no significant difference in pollution. The reduction in ambient  $PM_{2.5}$  is highest between 7 AM-9 AM, when  $PM_{2.5}$  on regular Sundays is highest; during these hours the average  $PM_{2.5}$  is reduced by 10-12  $\mu\text{g}/\text{m}^3$  on car-free Sundays or 20% of  $PM_{2.5}$  at the same time on regular Sundays. BC concentrations are lower by about  $1 \mu\text{g}/\text{m}^3$  between 7 AM-10 AM on car-free Sundays, which is 18%-28% of the corresponding concentrations on regular Sundays. However, there are also similar differences for pre-7 AM “business-as-usual” times on these Sundays, and so the observed reductions during the morning car-free periods may not be directly attributable to the car-free policy.

## Ozone in Kigali and Mugogo

Only 942 hours of RAMP data are available from rural Mt Mugogo for JJAS (dry season) and 881 hours for ON (wet season), compared to the 2,400 and 1,464 hours of  $O_3$  measurements in Kigali for the same seasons. The maximum 8-hour average  $O_3$  value at rural Mugogo as measured by the RAMP using the gRAMP calibration models were 34.4 ppb in dry JJAS and 33.0 ppb in wet ON – similar, unlike the significantly higher  $O_3$  observed in urban Kigali during the dry season (JJAS) compared to the wet season (MAM and ON). However, as discussed previously, the gRAMP model (hybrid-RF) is positively biased at Mt Mugogo during ON. The RCO reference monitor at this site shows a seasonal difference, with maximum 8-hour  $O_3$  concentrations of 40.6 ppb in JJAS and 30.6 ppb in ON (restricting the comparison to common periods with the RAMP data.) This is consistent with previous findings at this site (DeWitt et al., 2019). The RAMP-specific Mugogo QR model, which is not seasonally biased, shows maximum 8-hour  $O_3$  concentrations of 33.9 ppb in JJAS and 26.5 ppb in ON – below the reference values but capturing the seasonality. A closer examination of the data (for common periods) indicates that both the reference monitor and the gRAMP model show the maximum 8-hour  $O_3$  on the same day of the dry season - September 2, 2017. The RAMP  $O_3$  maximum (34.4 ppb) occurs between 8 AM-4 PM, during which time the reference monitor average was 40.3 ppb.

The average 1-hour  $O_3$  concentrations in Kigali during March-November 2017 were 16 ppb in the wet season (MAM 2017 and ON) compared to 22 ppb in the dry season (JJAS). The maximum  $O_3$  values, 66 ppb (1-hour average) and 57 ppb (8-hour average), were observed in the dry season. Previous measurements over Kigali during aircraft takeoff and landings in the MOZAIK campaign (Sauvage et al., 2005) over 1997-2003 also showed significantly higher  $O_3$  concentrations in the dry season in the lower troposphere.

The current US EPA standard for 8-hour average  $O_3$  is 65 ppb and the WHO guideline value for 8-hour average  $O_3$  is 50 ppb.  $O_3$  in Kigali is higher than the WHO guideline on 10 days over our sampling period, of which six are in July. However, the highest

8-hour average occurs on August 30, 2017 between 10 AM-6 PM. All 8-hour averages over 50 ppb occur during the daytime, for 8-hour periods beginning usually at 10 AM or 11 AM.

## Conclusions and recommendations for future work

We have presented the results of a long-term ground-based monitoring campaign, the first of its kind in Kigali, Rwanda. Lower-cost and relatively low maintenance RAMP monitors were used for this study, with local verification and correction of sensor calibrations by collocation with reference monitoring during an overlapping campaign and at RCO.

$O_3$  pollution in Kigali was usually below WHO guidelines, but the 50-ppb threshold could be exceeded in the dry season. Periods of high ozone can be identified using low-cost sensors and a general calibration, though local calibrations improve sensor performance. The RAMP  $PM_{2.5}$  (before filter-based correction) correlates strongly with filter-based  $PM_{2.5}$  on non-working days when TRAP and other working-day contributions are lower, but the RAMP  $PM_{2.5}$  values were still a significant underestimate. These differences suggest that the size distribution of  $PM_{2.5}$  in Kigali is quite different from that in Pittsburgh, with substantial contributions from sub-300 nm particles (where low-cost optical sensors are less sensitive). Future studies with lower-cost monitors should include collocated filter-based measurements or short-term intensive studies with aerosol sizing instruments (e.g. a scanning mobility particle sizer, SMPS) to account for such differences.

The Health Effects Institute (2019) (HEI) using data from the Global Burden of Disease Study 2017 estimates that the population-weighted annual average  $PM_{2.5}$  in Rwanda was  $43 \mu\text{g}/\text{m}^3$  in 2017 (and the same for 2015-2016). Our study found that the study average  $PM_{2.5}$  in Kigali is  $52 \pm 34 \mu\text{g}/\text{m}^3$  at residential or university locations, which can be considered as “urban background” sites. Kalisa et al. (2018) show that pollution levels can be significantly higher at the roadside in Kigali than at the urban background locations where our measurements were made. Air pollution in the low-lying valleys of Kigali can also be higher (Henninger, 2013). RAMP measurements at Musanze in late 2017 showed  $PM_{2.5}$  concentrations at this rural site were moderately correlated ( $r^2 = 0.54$ ) with Kigali  $PM_{2.5}$  and about 20% lower (not shown). These results suggest that the HEI population-weighted average for Rwanda and other similar satellite-based estimates could be underestimates that need to be updated with ground-based monitoring, like the campaign presented here.

Three recent studies – this paper, DeWitt et al. (2019), and Kalisa et al. (2018) – have found that air pollution is significant in urban and rural Rwanda, with considerable spatial variability due to local conditions and sources. Hence, future studies with low-cost monitors should include a variety of locations, such as low-lying areas and roadside locations. Our results should be

considered a lower estimate of the  $PM_{2.5}$  pollution that Kigali residents are exposed to – which is concerning since the average monthly concentrations in our 16+ month study were above the WHO annual guideline and often over WHO's first interim target.

Long-term monitoring over five seasons shows that differences in  $PM_{2.5}$  between working days and non-working days are smaller than the differences between the dry and wet seasons. The average dry season  $PM_{2.5}$  levels are about two times the succeeding wet season  $PM_{2.5}$  while the comparable seasonal differences in BC are about 40–60%, indicating that transported non-BC (e.g. dust) or low-BC (e.g. forest fires) pollution is important in the dry season. Particulate pollution in Kigali has a distinct diurnal profile, as the morning rush-hour usually results in the maximum BC and  $PM_{2.5}$  due to traffic pollution, and minima occur in the afternoons. The higher AAE values associated with the overnight BC and  $PM_{2.5}$  peaks suggest that domestic biofuel use could also be a significant contributor to overnight air pollution.

Overall, local sources could contribute half the  $PM_{2.5}$  and two-thirds of the BC in the wet seasons in Kigali, which means that local pollution control policies can significantly improve Kigali's air quality. In MAM 2018, heavier local rainfall may have helped reduce ambient  $PM_{2.5}$  levels, though the January–July 2018 average  $PM_{2.5}$  was  $43.7 \mu\text{g}/\text{m}^3$ , still above the WHO's first interim target for annual average  $PM_{2.5}$ . New pollution control policies are being implemented in Rwanda, including doubling the number of car-free Sundays and increased duties on older imported used cars. Continued monitoring is essential to evaluate the impact of these policies.

Air pollution in Kigali is also influenced by substantial regional contributions especially in the dry season; for example, the dry season daily minimum  $PM_{2.5}$  was over  $50 \mu\text{g}/\text{m}^3$ , or over 70% of average  $PM_{2.5}$ . About half the BC during the dry season also appears to be regional, which suggests a significant biomass burning influence in the regional/background contribution in line with DeWitt et al. (2019). Hence, controls on regional biomass burning are essential to reducing  $PM_{2.5}$  concentrations in Kigali. Studies with more advanced instrumentation (such as an AMS) would help better quantify the time-resolved contribution of different local and regional sources to air pollution in Rwanda, which in turn would help identify additional air quality interventions.

This study was carried out in collaboration with the University of Rwanda and RCO (co-authors on this paper) and with the support of local residents who hosted the RAMPs. Towards the end of this study, the Rwanda Environmental Management Authority (REMA) acquired a reference monitoring station as well as eight RAMPs to establish their own air quality monitoring network. Low-cost monitors can significantly reduce the costs of air quality monitoring for developing countries, but local support and buy-in are keys to success.

## Acknowledgments

This research was supported by the College of Engineering, the Department of Engineering and Public Policy, and the Department of Mechanical Engineering at Carnegie Mellon University via discretionary funding support for Paulina Jaramillo and Allen Robinson. This work also benefited from State assistance managed by the National Research Agency under the “Programme d'Investissements d'Avenir” under the reference “ANR-18-MPGA-0011” (“Make our planet great again” initiative). The results and conclusions of this paper are the sole responsibility of the authors and do not represent the views of the funding sources.

## Author contributions

Conceptualisation: RS, ALR, PJ; methodology: RS, JG, HLD; data collection: ASK, VB, SG, CS, NJW, EK; data analysis and validation: RS, CM, ASK, SG, HL, EK; writing/initial draft: RS; writing/revisions: all authors; student supervision: JG, RS, PJ, PA; project leadership and management: RS; funding acquisition: ALR, PJ, RS

## Data availability

The RAMP data (gRAMP-based gas concentrations and “BAM-equivalent”  $PM_{2.5}$  mass concentrations, without filter-based correction) and BC data are available at <https://doi.org/10.6084/m9.figshare.8074436.v1>

## References

- Bond, T.C., Habib, G., Bergstrom, R.W., 2006. Limitations in the enhancement of visible light absorption due to mixing state. *Journal of Geophysical Research: Atmospheres* 111. <https://doi.org/10.1029/2006JD007315>
- Brauer, M., Amann, M., Burnett, R.T., Cohen, A., Dentener, F., Ezzati, M., Henderson, S.B., Krzyzanowski, M., Martin, R.V., Van Dingenen, R., van Donkelaar, A., Thurston, G.D., 2012. Exposure Assessment for Estimation of the Global Burden of Disease Attributable to Outdoor Air Pollution. *Environ. Sci. Technol.* 46, 652–660. <https://doi.org/10.1021/es2025752>
- DeWitt, H.L., Gasore, J., Rupakheti, M., Potter, K.E., Prinn, R.G., Ndikubwimana, J. de D., Nkusi, J., Safari, B., 2019. Seasonal and diurnal variability in  $O_3$ , black carbon, and CO measured at the Rwanda Climate Observatory. *Atmospheric Chemistry and Physics* 19, 2063–2078. <https://doi.org/10.5194/acp-19-2063-2019>
- Diamantopoulou, M., Skyllakou, K., Pandis, S.N., 2016. Estimation of the local and long-range contributions to particulate matter levels using continuous measurements in a single urban background site. *Atmospheric Environment* 134, 1–9. <https://doi.org/10.1016/j.atmosenv.2016.03.015>

- Dockery, D.W., Pope, C.A., Xu, X., Spengler, J.D., Ware, J.H., Fay, M.E., Ferris, B.G., Speizer, F.E., 1993. An association between air pollution and mortality in six U.S. cities. *N. Engl. J. Med.* 329, 1753–1759. <https://doi.org/10.1056/NEJM199312093292401>
- Duhuze, R.N., 2018. Fuel and Vehicle Standards: Vehicle Inspection, compliance and enforcement - case of Rwanda. Presented at the UNEP “Africa Clean Mobility Week” conference, Nairobi, Kenya.
- Farquharson, D., Jaramillo, P., Samaras, C., 2018. Sustainability implications of electricity outages in sub-Saharan Africa. *Nature Sustainability* 1, 589. <https://doi.org/10.1038/s41893-018-0151-8>
- Health Effects Institute, 2019. State of Global Air 2019 [WWW Document]. URL <https://www.stateofglobalair.org/data/#/air/plot> (accessed 5.1.19).
- Henninger, S.M., 2013. When Air Quality Becomes Deleterious—A Case Study for Kigali, Rwanda. *Journal of Environmental Protection* 04, 1. <https://doi.org/10.4236/jep.2013.48A1001>
- Jerrett, M., Burnett, R.T., Pope, C.A., Ito, K., Thurston, G., Krewski, D., Shi, Y., Calle, E., Thun, M., 2009. Long-Term Ozone Exposure and Mortality. *New England Journal of Medicine* 360, 1085–1095. <https://doi.org/10.1056/NEJMoa0803894>
- Kalisa, E., Archer, S., Nagato, E., Bizuru, E., Lee, K., Tang, N., Pointing, S., Hayakawa, K., Lacap-Bugler, D., 2019. Chemical and Biological Components of Urban Aerosols in Africa: Current Status and Knowledge Gaps. *International Journal of Environmental Research and Public Health* 16, 941. <https://doi.org/10.3390/ijerph16060941>
- Kalisa, E., Nagato, E.G., Bizuru, E., Lee, K.C., Tang, N., Pointing, S.B., Hayakawa, K., Archer, S.D.J., Lacap-Bugler, D.C., 2018. Characterization and Risk Assessment of Atmospheric PM<sub>2.5</sub> and PM<sub>10</sub> Particulate-Bound PAHs and NPAHs in Rwanda, Central-East Africa. *Environ. Sci. Technol.* 52, 12179–12187. <https://doi.org/10.1021/acs.est.8b03219>
- Kirchstetter, T.W., Novakov, T., 2007. Controlled generation of black carbon particles from a diffusion flame and applications in evaluating black carbon measurement methods. *Atmospheric Environment* 41, 1874–1888. <https://doi.org/10.1016/j.atmosenv.2006.10.067>
- Kirchstetter, T.W., Novakov, T., Hobbs, P.V., 2004. Evidence that the spectral dependence of light absorption by aerosols is affected by organic carbon. *Journal of Geophysical Research: Atmospheres* 109. <https://doi.org/10.1029/2004JD004999>
- Kirchstetter, T.W., Preble, C.V., Hadley, O.L., Bond, T.C., Apte, J.S., 2017. Large reductions in urban black carbon concentrations in the United States between 1965 and 2000. *Atmospheric Environment* 151, 17–23. <https://doi.org/10.1016/j.atmosenv.2016.11.001>
- Kolhe, A.R., Aher, G.R., Ralegankar, S.D., Safai, P.D., 2018. Investigation of aerosol black carbon over semi-urban and urban locations in south-western India. *Atmospheric Pollution Research* 9, 1111–1130. <https://doi.org/10.1016/j.apr.2018.04.010>
- Lack, D.A., Langridge, J.M., 2013. On the attribution of black and brown carbon light absorption using the Ångström exponent. *Atmospheric Chemistry and Physics* 13, 10535–10543. <https://doi.org/10.5194/acp-13-10535-2013>
- Laden, F., Schwartz, J., Speizer, F.E., Dockery, D.W., 2006. Reduction in fine particulate air pollution and mortality: Extended follow-up of the Harvard Six Cities study. *Am. J. Respir. Crit. Care Med.* 173, 667–672. <https://doi.org/10.1164/rccm.200503-443OC>
- Malings, C., Tanzer, R., Haurlyliuk, A., Kumar, S.P.N., Zimmerman, N., Kara, L.B., Presto, A.A., R. Subramanian, 2019. Development of a general calibration model and long-term performance evaluation of low-cost sensors for air pollutant gas monitoring. *Atmospheric Measurement Techniques* 12, 903–920. <https://doi.org/10.5194/amt-12-903-2019>
- Malings, C., Tanzer, R., Haurlyliuk, A., Saha, P.K., Robinson, A.L., Presto, A.A., Subramanian, R., 2020. Fine particle mass monitoring with low-cost sensors: Corrections and long-term performance evaluation. *Aerosol Science and Technology*, 54:2, 160–174, <https://doi.org/10.1080/02786826.2019.1623863>
- Masiol, M., Agostinelli, C., Formenton, G., Tarabotti, E., Pavoni, B., 2014. Thirteen years of air pollution hourly monitoring in a large city: Potential sources, trends, cycles and effects of car-free days. *Science of The Total Environment* 494–495, 84–96. <https://doi.org/10.1016/j.scitotenv.2014.06.122>
- MININFRA, 2018. Energy Sector Strategic Plan, 2018/19-2023/24.
- Moosmüller, H., Chakrabarty, R.K., Ehlers, K.M., Arnott, W.P., 2011. Absorption Ångström coefficient, brown carbon, and aerosols: basic concepts, bulk matter, and spherical particles. *Atmospheric Chemistry and Physics* 11, 1217–1225. <https://doi.org/10.5194/acp-11-1217-2011>
- Mudway, I.S., Dundas, I., Wood, H.E., Marlin, N., Jamaludin, J.B., Bremner, S.A., Cross, L., Grieve, A., Nanzer, A., Barratt, B.M., Beevers, S., Dajnak, D., Fuller, G.W., Font, A., Colligan, G., Sheikh, A., Walton, R., Grigg, J., Kelly, F.J., Lee, T.H., Griffiths, C.J., 2019. Impact of London’s low emission zone on air quality and children’s respiratory health: a sequential annual cross-sectional study. *The Lancet Public Health* 4, e28–e40. [https://doi.org/10.1016/S2468-2667\(18\)30202-0](https://doi.org/10.1016/S2468-2667(18)30202-0)
- Ngabonziza, D., 2017. Car Imports to Rwanda Drop by 20% As High Taxes Bite – KT PRESS [WWW Document]. URL <https://ktpress.rw/2017/05/car-imports-to-rwanda-drop-by-20-as-high-taxes-bite/> (accessed 5.1.19).

- Petkova, E.P., Jack, D.W., Volavka-Close, N.H., Kinney, P.L., 2013. Particulate matter pollution in African cities. *Air Qual Atmos Health* 6, 603–614. <https://doi.org/10.1007/s11869-013-0199-6>
- Pikridas, M., Tasoglou, A., Florou, K., Pandis, S.N., 2013. Characterization of the origin of fine particulate matter in a medium size urban area in the Mediterranean. *Atmospheric Environment* 80, 264–274. <https://doi.org/10.1016/j.atmosenv.2013.07.070>
- RRA, 2017. EAC Proposed Depreciation Schedule [WWW Document]. URL <https://www.rra.gov.rw/index.php?id=219> (accessed 5.1.19).
- Rwanda Meteorology Agency, 2019. Reanalysis data [WWW Document]. URL <https://meteorwanda.gov.rw/index.php?id=2> (accessed 5.1.19).
- Sauvage, B., Thouret, V., Cammas, J.-P., Gheusi, F., Athier, G., Nédélec, P., 2005. Tropospheric ozone over Equatorial Africa: regional aspects from the MOZAIC data. *Atmospheric Chemistry and Physics* 5, 311–335. <https://doi.org/10.5194/acp-5-311-2005>
- Shrivastava, M.K., Subramanian, R., Rogge, W.F., Robinson, A.L., 2007. Sources of organic aerosol: Positive matrix factorization of molecular marker data and comparison of results from different source apportionment models. *Atmospheric Environment* 41, 9353–9369. <https://doi.org/10.1016/j.atmosenv.2007.09.016>
- Siebert, A., Dinku, T., Vuguziga, F., Twahirwa, A., Kagabo, D.M., delCorral, J., Robertson, A.W., 2019. Evaluation of ENACTS-Rwanda: A new multi-decade, high-resolution rainfall and temperature data set—Climatology. *International Journal of Climatology* 0. <https://doi.org/10.1002/joc.6010>
- Subramanian, R., Donahue, N.M., Bernardo-Bricker, A., Rogge, W.F., Robinson, A.L., 2007. Insights into the primary–secondary and regional–local contributions to organic aerosol and PM<sub>2.5</sub> mass in Pittsburgh, Pennsylvania. *Atmospheric Environment* 41, 7414–7433. <https://doi.org/10.1016/j.atmosenv.2007.05.058>
- Subramanian, R., Ellis, A., Torres-Delgado, E., Tanzer, R., Malings, C., Rivera, F., Morales, M., Baumgardner, D., Presto, A., Mayol-Bracero, O.L., 2018. Air Quality in Puerto Rico in the Aftermath of Hurricane Maria: A Case Study on the Use of Lower Cost Air Quality Monitors. *ACS Earth Space Chem.* 2, 1179–1186. <https://doi.org/10.1021/acsearthspacechem.8b00079>
- Sun, H., Biedermann, L., Bond, T.C., 2007. Color of brown carbon: A model for ultraviolet and visible light absorption by organic carbon aerosol. *Geophysical Research Letters* 34. <https://doi.org/10.1029/2007GL029797>
- Virkkula, A., Mäkelä, T., Hillamo, R., Yli-Tuomi, T., Hirsikko, A., Hämeri, K., Koponen, I.K., 2007. A Simple Procedure for Correcting Loading Effects of Aethalometer Data. *Journal of the Air & Waste Management Association* 57, 1214–1222. <https://doi.org/10.3155/1047-3289.57.10.1214>
- Wang, X., Westerdahl, D., Chen, L.C., Wu, Y., Hao, J., Pan, X., Guo, X., Zhang, K.M., 2009. Evaluating the air quality impacts of the 2008 Beijing Olympic Games: On-road emission factors and black carbon profiles. *Atmospheric Environment* 43, 4535–4543. <https://doi.org/10.1016/j.atmosenv.2009.06.054>
- WHO, 2018. Global Health Observatory: Deaths - by country [WWW Document]. WHO. URL <http://apps.who.int/gho/data/node.main.BODAMBIENTAIRDTHS?lang=en> (accessed 5.1.19).
- Zhang, Q., Jimenez, J.L., Canagaratna, M.R., Ulbrich, I.M., Ng, N.L., Worsnop, D.R., Sun, Y., 2011. Understanding atmospheric organic aerosols via factor analysis of aerosol mass spectrometry: a review. *Anal Bioanal Chem* 401, 3045–3067. <https://doi.org/10.1007/s00216-011-5355-y>
- Zhang, X., Rao, R., Huang, Y., Mao, M., Berg, M.J., Sun, W., 2015. Black carbon aerosols in urban central China. *Journal of Quantitative Spectroscopy and Radiative Transfer, Topical issue on optical particle characterization and remote sensing of the atmosphere: Part I* 150, 3–11. <https://doi.org/10.1016/j.jqsrt.2014.03.006>
- Zimmerman, N., Presto, A.A., Kumar, S.P.N., Gu, J., Haurlyliuk, A., Robinson, E.S., Robinson, A.L., R. Subramanian, 2018. A machine learning calibration model using random forests to improve sensor performance for lower-cost air quality monitoring. *Atmospheric Measurement Techniques* 11, 291–313. <https://doi.org/10.5194/amt-11-291-2018>

## Appendix

### Further investigation of the performance of Pittsburgh gRAMP calibration models and comparison with local “Mugogo” models

We further explore the performance of the Pittsburgh hybrid RF gRAMP model by comparing it with the Mugogo QR model, which had the best overall performance for O<sub>3</sub> among the Mugogo models. Figure S2 shows scatter plots of the RAMP-reported concentrations (as 8-hour running averages) for the two calibration approaches against the reference monitor, separated into the dry (June–July–August–September, JJAS) and wet (October–November, ON) seasons. However, the gRAMP model is positively biased in ON, with most of the data above the 1:1 line and clustered around the +30% line. In other words, the gRAMP model overpredicts O<sub>3</sub> during the wet season. The Mugogo model (panels B and D) performs better (expected since it was trained on just under half of the underlying 15-minute dataset), yielding O<sub>3</sub> concentrations clustered around the 1:1 line.

## RAMP $PM_{2.5}$ data compared to filter-based 24-hour “reference” concentrations

For local calibration verification, we compare data from RAMP #140 (deployed in Gacuriro) with the filter-based 24-hour  $PM_{2.5}$  concentrations reported by Kalisa et al. (2018) for the UR-CST site (about 5 km from Gacuriro) in April 2017 (wet season). Kalisa et al. (2018) reported that in Kigali, workday  $PM_{2.5}$  was almost 50% higher than non-workday  $PM_{2.5}$ . The RAMP and filter-based  $PM_{2.5}$  are strongly correlated (Figure S3) on eight out of ten non-workdays, with a correlation coefficient ( $r^2$ ) of 0.77 and a slope of  $1.39 \pm 0.06$  (forced through the origin). On April 2 (Sunday), there was construction activity on the CST site close to the filter sampler, which could explain high PM levels that would not be seen in Gacuriro. It is not clear what was different about April 15 (Saturday), when the filter-based  $PM_{2.5}$  was comparable to or higher than the highest workday PM levels. In this paper, all weekend RAMP  $PM_{2.5}$  values are scaled upwards by 1.39. The

comparison of working day data between filter-based  $PM_{2.5}$  and the RAMP  $PM_{2.5}$  is worse ( $r^2$  of 0.08); this could reflect local variations on specific days as the sites are 5 km apart. We use the slope ( $1.69 \pm 0.18$ ) of a fit forced through zero to scale up all weekday RAMP  $PM_{2.5}$  data. Due to RAMP malfunctions, no RAMP data were collected for the dry season days (June 15–29) when Kalisa and co-workers collected filter-based measurements, so the wet season scaling factors are used for all RAMP data.

## Reference

Kalisa, E., Nagato, E.G., Bizuru, E., Lee, K.C., Tang, N., Pointing, S.B., Hayakawa, K., Archer, S.D.J., Lacap-Bugler, D.C., 2018. Characterization and Risk Assessment of Atmospheric  $PM_{2.5}$  and  $PM_{10}$  Particulate-Bound PAHs and NPAHs in Rwanda, Central-East Africa. *Environ. Sci. Technol.* 52, 12179–12187. <https://doi.org/10.1021/acs.est.8b03219>



**Figure S1:** The RAMPs and the external Met-One NPMs in the lab (left) and a unit deployed in Kigali, Rwanda (right).

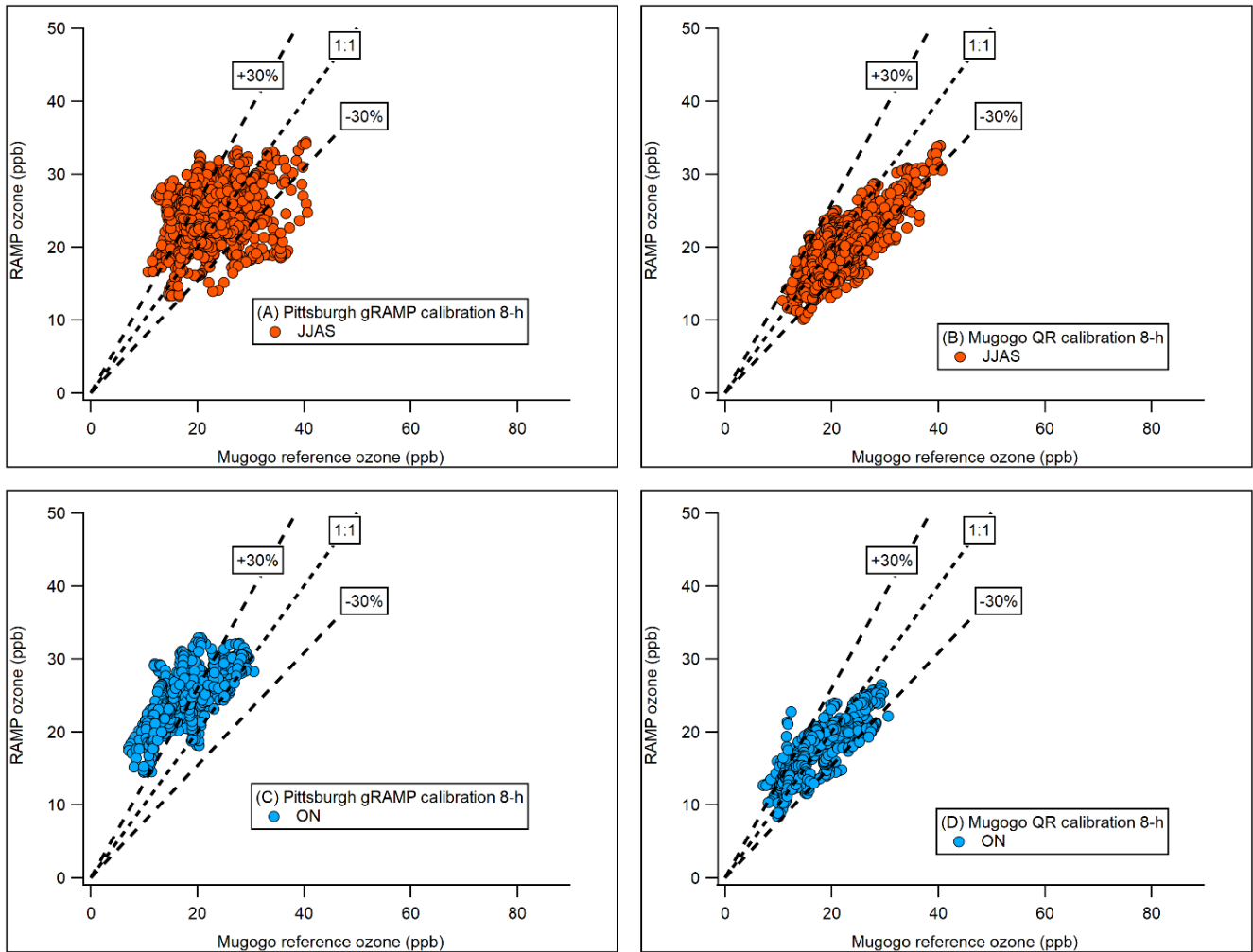


**Figure S2:** Comparison of RAMP calibration models for ozone with reference monitor data at the Mt Mugogo Climate Observatory. The “Pittsburgh gRAMP” model (A,C) is developed on collocations in Pittsburgh, PA, USA. The “Mugogo QR” model (B,D) is based on a collocation with the reference monitor at Mugogo; the data shown here includes both training (28 days) and testing (32 days) data. JJAS (A,B) is the dry season and ON (C,D) is the wet season.

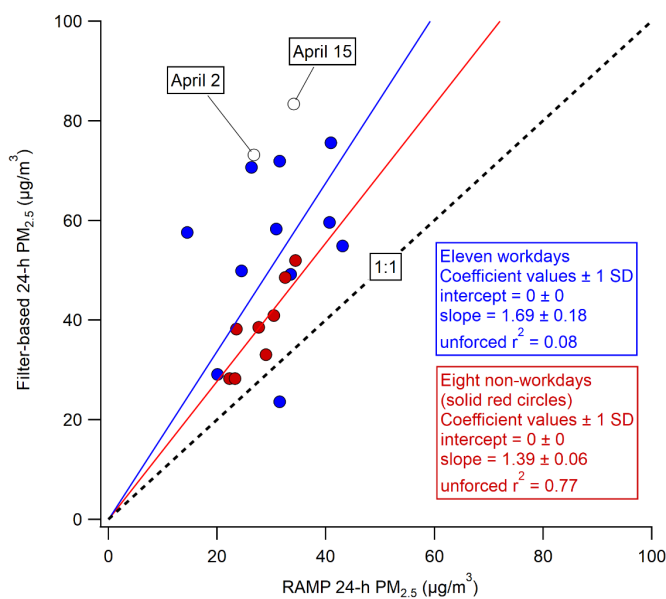


**Figure S3:** Developing scaling factors for optical RAMP  $PM_{2.5}$  measurements by comparison with filter-based 24-hour  $PM_{2.5}$  measurements (reported by Kalisa et al. 2018). Solid blue circles indicate workdays. Solid red circles show eight non-workdays that are used to develop the non-workday scaling factor, which excludes two non-workdays that experienced significantly higher filter-based  $PM_{2.5}$  than even workdays (shown by the open circles.) The filter measurements were conducted at the University of Rwanda campus, while these RAMP measurements were conducted about 5 km away in the Gacuriro neighborhood.

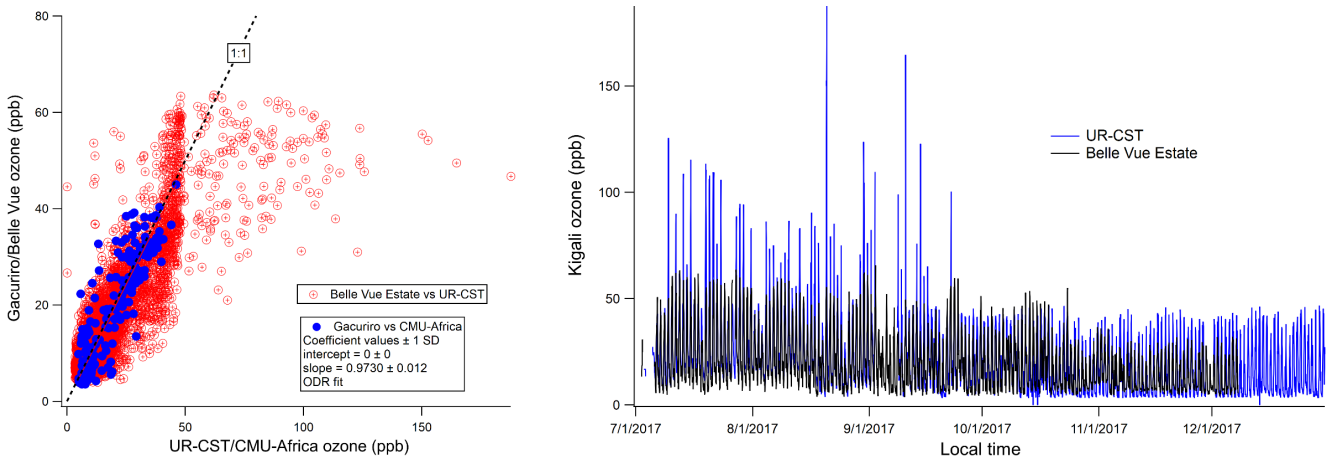


**Figure S4:** Ozone measurements in Kigali over the course of this study. (Left) Scatter plot shows most of the paired measurements across the city agree with each other. (Right) However, there are periods when the UR-CST  $O_3$  is much higher than at Belle Vue estate.

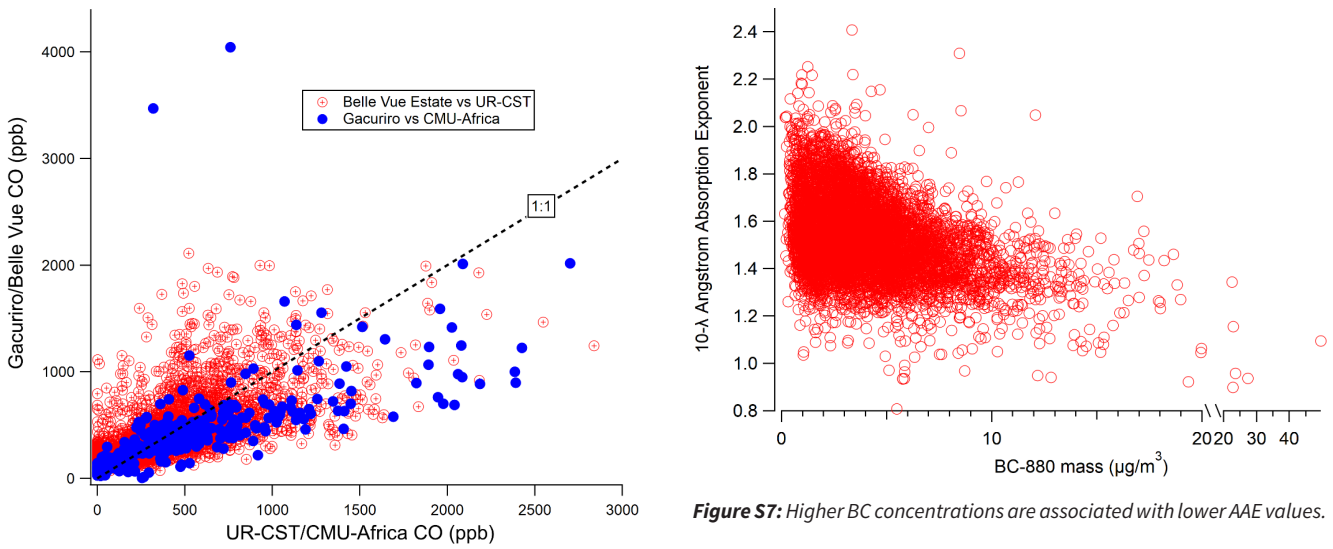


**Figure S7:** Higher BC concentrations are associated with lower AAE values.

**Figure S5:** Intraurban variability of 1-hour CO concentrations across Kigali.

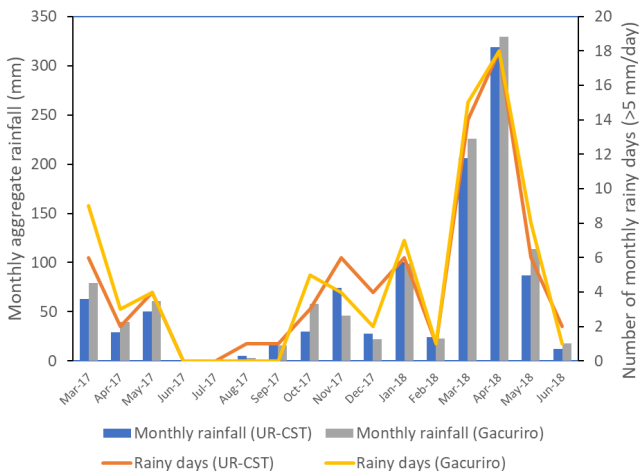


**Figure S6:** Spatially-resolved rainfall data using the ENACTS-Rwanda methodology, from the Rwanda Meteorological Agency. MAM 2018 saw significantly more rainfall and more rainy days than other periods.

## Gas Analysers



43iQ Sulfur Dioxide Analyser

## Multi-Parameter



GM-5000 Air Quality Monitor

## Particulate Analysers



Model 5028i Continuous Particulate Monitor

**thermo**  
scientific

Authorized Distributor

# Research article

## The impacts of commissioning coal-fired power stations on air quality in South Africa: insights from ambient monitoring stations

Itumeleng P. Morosele<sup>1</sup>, Kristy E. Langerman<sup>1\*</sup>

<sup>1</sup>Department of Geography, Environmental Management and Energy Studies, University of Johannesburg, Auckland Park, Johannesburg, South Africa, \*klangerman@uj.ac.za

Received: 26 August 2020 - Reviewed: 23 September 2020 - Accepted: 22 October 2020

<https://doi.org/10.17159/caj/2020/30/2.8833>

### Abstract

The South African electricity sector is known for its heavy reliance on coal. The aim of this study is to assess the impacts of increasing SO<sub>2</sub> and PM emissions from the three return-to-service power stations (Komati, Camden and Grootvlei), and the newly constructed Medupi power station on ambient air quality measured in the vicinities of these power stations. Trends in ambient pollution concentrations were determined using Theil-Sen analysis. The correlation between the emissions and ambient pollution concentrations at nearby monitoring stations was determined with the Spearman partial rank correlation coefficient. Lastly, compliance of ambient pollution concentrations with the South Africa National Ambient Air Quality Standards was assessed. Few statistically significant trends in ambient SO<sub>2</sub> and PM<sub>10</sub> concentrations are found, and there is little correlation between increasing power station emissions and ambient pollutant concentrations in the vicinity. It is only at Camden monitoring station where there are increases in PM<sub>10</sub> concentrations from the direction of Camden power station, and at Grootvlei monitoring station where increasing SO<sub>2</sub> concentrations are from the directions of Grootvlei and Lethabo power stations. A strong, positive correlation between power station emissions and ambient concentrations exists only for SO<sub>2</sub> at Grootvlei monitoring station and PM<sub>10</sub> at Medupi monitoring station (although it is likely that the correlation at Medupi is related to construction and vehicle activity, and not emissions from Medupi power station stacks). It is concluded that the establishment of monitoring stations in the vicinities of power stations is necessary but not sufficient to monitor their impact on air quality in the surrounds.

### Keywords

Coal-fired power stations, ambient air quality, SO<sub>2</sub>, PM<sub>10</sub>, trends, correlation, compliance, Theil-Sen analysis

### Introduction

Coal is the major source of electricity in South Africa, generating 85.7% of the country's power in 2016 (StatsSA, 2018). Eskom Holdings SOC Ltd (hereafter referred to as Eskom) generates more than 90% of South Africa's electricity and approximately 40% of Africa's electricity (Eskom, 2019). Coal-fired power station emissions have been flagged for their impact on ambient air quality and associated health issues (Xue et al., 2005; Keen and Altieri, 2016a; Keen and Altieri, 2016b; Holland, 2017; Mannucci and Franchini, 2017; Wright et al., 2017; Langerman and Pauw, 2018; Gray, 2019).

There is a global trend of decreasing emissions from coal-fired power stations, as power stations are decommissioned, converted to natural gas, or fitted with emission abatement technologies (Gouw et al., 2014; Wang et al., 2020; IEA, 2020). Reducing emissions from such large point sources is expected to result in improvements in ambient air quality. Indeed, such

improvements have been observed in many regions including south-eastern Australia (Crawford et al., 2018), north-eastern United States (Russell et al., 2017) and China (Ma et al., 2019). In the developing world, new power stations are still being commissioned. New coal-fired power stations are planned and/or under construction in Turkey (Akyuz and Kaynak, 2019) and India, for example. In South Africa, three previously mothballed power stations – Camden, Grootvlei and Komati – were returned to service between 2005 and 2013, and two large new power stations, Medupi and Kusile, are currently being commissioned (since 2015 for Medupi and 2016 for Kusile).

The threat posed by coal-fired power station emissions to ambient air quality in South Africa is only in small part due to the direct emissions of particulate matter (ash), since more than 99% of it is removed from the flue gas stream before release to the atmosphere. The concern is rather the large quantities of sulphur dioxide (SO<sub>2</sub>), which is of concern when inhaled at

high concentrations in the close vicinity of power stations. SO<sub>2</sub> oxidises to form secondary sulphate aerosols which elevate fine particulate matter (PM<sub>2.5</sub>) levels across the region and cause acid deposition. PM<sub>2.5</sub> negatively affects human health by increasing the risk of cardiovascular and cerebrovascular disease, cancer, diabetes and several other illnesses (Xue et al., 2005; Keen and Altieri, 2016a; Keen and Altieri, 2016b; Mannucci and Franchini, 2017; Wright et al., 2017), and altering local climate (by reflecting shortwave radiation) (Coakley et al., 1983; Kaufman et al., 2002).

Surface ambient air quality monitoring stations are commonly used to observe the impact of the commissioning and decommissioning of large point sources on ambient pollution levels (as was done by Russell et al., 2017 and Crawford et al., 2018). However, Akyuz and Kaynak (2019) contend that ambient monitoring stations are not sufficient to detect the impact on ambient air quality because the concentrations measured at the monitoring stations are highly dependent on the siting of the monitoring station. In South Africa, the establishment of at least one ambient monitoring station is usually a condition of the environmental authorization granted for the construction of a power station (or other polluting facility).

The aim of this study is to assess the impact of changing emission levels from three return-to-service power stations, Komati, Camden and Grootvlei, and the newly constructed Medupi power station on ambient air quality in the vicinities of these power stations, using measurements from ambient monitoring stations. Two criteria pollutants, SO<sub>2</sub> and PM<sub>10</sub>, are selected for analysis. Three research objectives were formulated: to identify and quantify trends in power station emissions and ambient air pollution concentrations; to determine whether there is a statistically significant correlation between power station emissions and ambient air pollution concentrations; and to assess compliance of ambient SO<sub>2</sub> and PM<sub>10</sub> concentrations with the National Ambient Air Quality Standards. We also evaluate the value of surface monitoring stations in detecting the effect of emissions from large point sources on ambient air quality levels.

To the authors' knowledge, this is the first research paper to investigate how the commissioning of the new Medupi power station has affected ambient air quality. It is also the only study seeking to establish a direct correlation between emissions from power stations and the ambient air quality in the immediate vicinities of these power stations. The study sheds light on the trends of pollutants identified in the Highveld and Waterberg-Bojanala Priority Areas. The findings should influence legislation and policies that have been created to regulate ambient air quality, especially in the event of non-compliance.

## Methods

### Study Sites

Komati, Camden and Grootvlei power stations are located in Mpumalanga, in the Highveld Priority Area (HPA), and Medupi power station in Limpopo, in the Waterberg-Bojanala Priority

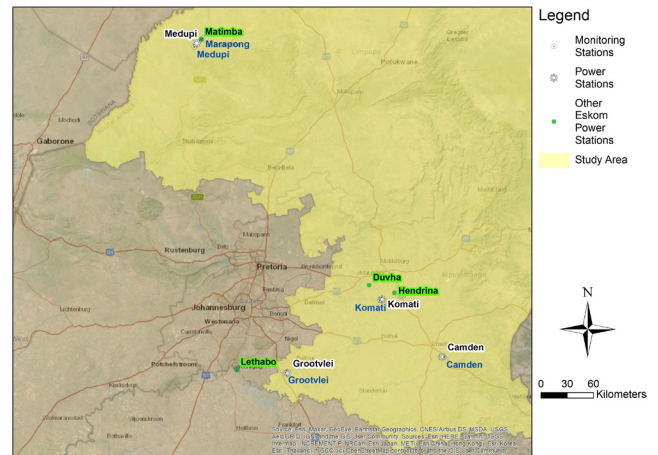


**Figure 1:** Locations of the coal-fired power stations (white and green labels) and ambient air quality monitoring stations (blue labels) in Mpumalanga and Limpopo

**Table 1:** Locations of return-to-service and new coal-fired power stations, and monthly emissions data received from Eskom

Power station	Coordinates	Commissioning dates	Monthly emissions data	Parameters
Camden	26.62°S; 30.09°E	1968-1969 2005-2008	Apr 2006 – Dec 2014	SO <sub>2</sub> PM (ash)
Grootvlei	26.77°S; 28.50°E	1989-1990 2008-2011	Jan 2008 – Dec 2013	
Komati	26.09°S; 29.47°E	1961-1996 2009-2013	Apr 2009 – Dec 2015	
Medupi	23.70°S; 27.57°E	2015-2020	Apr 2015 – Mar 2018	

**Table 2:** Location and pollutants monitored at the ambient air quality monitoring stations near the power stations and ambient air quality data received from Eskom

Ambient monitoring station	Coordinates	Nearby power station	Data received	Parameters
Camden	26.62°S 30.11°E	Camden	Jan 2005 – Dec 2014	SO <sub>2</sub> PM <sub>10</sub> Temperature Pressure Wind direction Wind speed
Grootvlei	26.76°S 28.48°E	Grootvlei	Jan 2007 – Dec 2013	
Komati	26.10°S 29.45°E	Komati	Jan 2006 – Dec 2015	
Marapong	23.66°S 27.63°E	Medupi	Jan 2014 – April 2018	
Medupi	23.69°S 27.32°E	Medupi	Jan 2015 – April 2018	

Area (WBPA) (Figure 1). The three return-to-service power stations (Camden, Grootvlei and Komati) were recommissioned between 2005 and 2013, while commissioning of Medupi power station commenced in 2015 (Table 1).

Komati monitoring station is located 2 km southwest of Komati power station, Camden monitoring station is 1.6 km east-southeast of Camden power station, Grootvlei monitoring station is 1.7 km northwest of Grootvlei power station in Grootvlei town. Marapong monitoring station is 8 km northeast of Medupi and 2 km northeast of Matimba power station, and Medupi monitoring station is 4.8 km south-southwest of Medupi power station (Figure 1 and Table 2).

### Data and analysis

Monthly emissions of SO<sub>2</sub> and PM (ash) (tons) from the four power stations were obtained from Eskom for the years indicated in Table 1. The SO<sub>2</sub> emissions are calculated using mass balance, based on the amount of coal burnt and the sulphur content of the coal, which is sampled twice a day. The PM emissions are continuously monitored with opacity monitors that are correlated with isokinetic samples every two years.

10-minute and hourly ambient SO<sub>2</sub> and PM<sub>10</sub> concentration data, from the five monitoring stations were provided by Eskom for the dates indicated in Table 2. Temperature, pressure, wind direction and wind speed data were also provided. SO<sub>2</sub> and PM<sub>10</sub> concentrations were converted from 10-minute or hourly values into monthly averages to reflect the same time interval as the emissions data. All zero and error values were deleted. Monthly concentrations with data availability below 50% were excluded from the analyses as they do not adequately represent the months.

To identify trends in power station emissions, a linear trend line was fitted to the monthly power station emissions using the method of least squares. For the ambient air pollution concentrations, Theil-Sen analysis was performed using the Openair package in R. The option to de-seasonalize the data was selected because some of the datasets are fairly short and include partial years. The trends were also calculated for each of the eight cardinal wind directions. The analysis produces an overall trend, the 95 % confidence intervals in the slope, and the statistical significance of each trend estimate (p-value). A p-value of less than 0.001 indicates a highly statistically significant trend, while a p-value of less than 0.05 indicates a statistically significant trend. When p > 0.1, there is no statistically significant trend. The following symbols are used to indicate the statistical significance on the plots: \*\*\* denotes p < 0.001, \*\* denotes p < 0.01, \* denotes p < 0.05 and + denotes p < 0.1 (Carslaw and Ropkins, 2012; Carslaw, 2015).

The Spearman partial rank correlation (SPRC) test was adopted to determine the relationship between trends in monthly SO<sub>2</sub> and PM (ash) emissions and trends in ambient SO<sub>2</sub> and PM<sub>10</sub> concentrations, since the emissions and ambient data is not normally distributed. IBM SPSS Statistics Version 25 ('SPSS') package was employed to perform the correlation analysis.

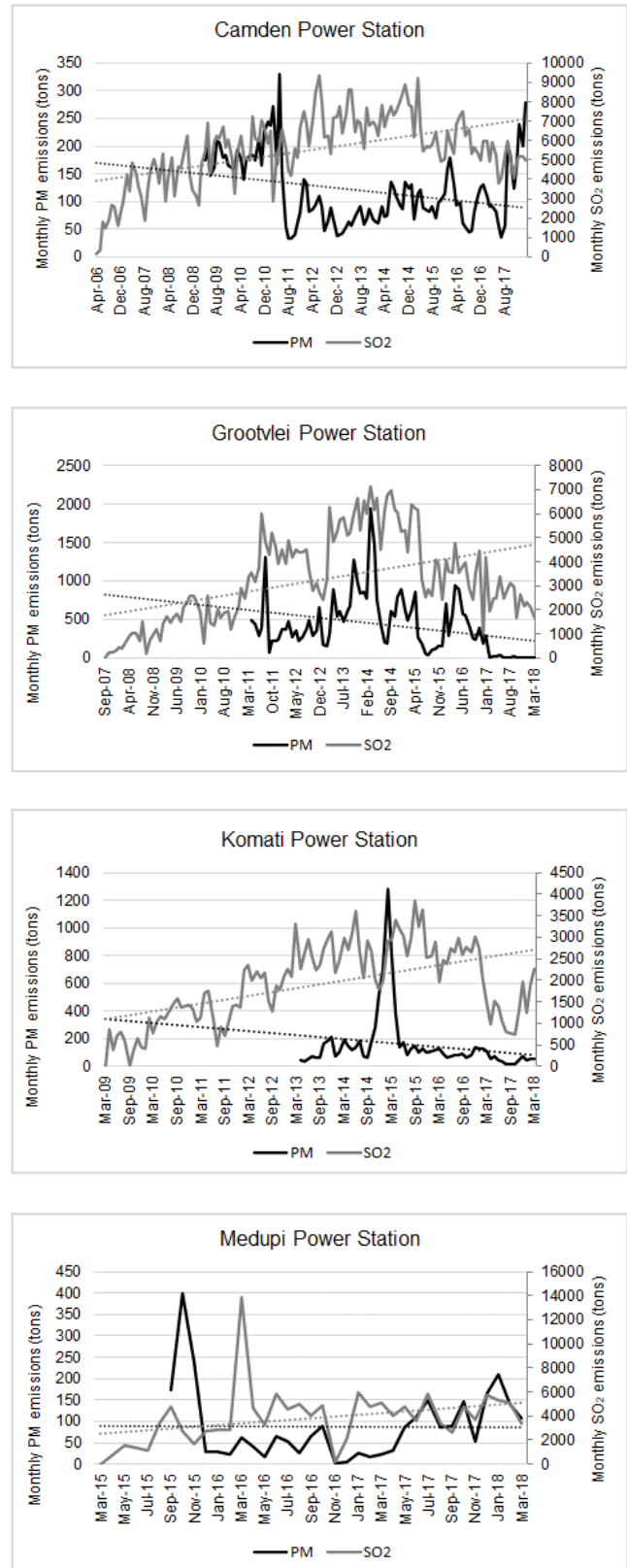


**Figure 2:** SO<sub>2</sub> and PM (ash) emission trends at Camden, Grootvlei, Komati and Medupi power stations. Monthly emissions are shown in solid lines and the trends in dotted lines.

**Table 3:** Summary of Theil-Sen analysis of SO<sub>2</sub> and PM<sub>10</sub> trends at the ambient air quality monitoring stations (NS = not significant)

Monitoring station	Period	SO <sub>2</sub> trends		PM <sub>10</sub> trends	
		Trend [95% confidence interval] (µg/m <sup>3</sup> /year)	Significance (p-value)	Trend [95% confidence interval] (µg/m <sup>3</sup> /year)	Significance (p-value)
Komati	2006-2015	-0.09 [-0.59, 0.45]	NS	-0.87 [-1.64, 0.06]	NS
Camden	2005-2014	0.36 [-0.04, 0.84]	NS	1.22 [0.72, 1.72]	0.001
Grootvlei	2007-2013	1.64 [1.23, 2.03]	0.001	0.28 [-0.29, 0.88]	NS
Marapong	2014-2018	-1.22 [-3.48, 1.01]	NS	-2.04 [-3.28, -0.74]	0.01
Medupi	2015-2018	-0.15 [-2.19, 2.44]	NS	0.38 [-1.4, 2.41]	NS

Compliance with the 1-hour SO<sub>2</sub> and 24-hour PM<sub>10</sub> National Ambient Air Quality Standards was determined by calculating the 99th percentile of the hourly SO<sub>2</sub> concentrations and 24-hour PM<sub>10</sub> concentrations for all years and comparing the 99th percentile values with the limit values. Compliance with

the annual National Ambient Air Quality Standards was also determined for SO<sub>2</sub> and PM<sub>10</sub>.

## Results

### Trend Analysis

#### Power station emissions

There is an increasing trend in unabated power station SO<sub>2</sub> emissions as power station units are commissioned (in 2005-2008 for Camden, 2008-2011 for Grootvlei and 2009-2013 for Komati) and as load is ramped up after commissioning at the return-to-service stations (Figure 2). A decline in SO<sub>2</sub> emissions is evident at the return-to-service stations from around 2016 as the load factor is decreased again. As of 2019, three of Grootvlei's six units and five of Komati's nine units have been placed in cold storage. Between March 2015 and March 2018, three of Medupi's six units were commissioned.

The decreasing trends in PM emissions (Figure 2) reflect the improving removal efficiency of the PM abatement technology (electrostatic precipitators and flue gas conditioning plants at Komati and 3 units at Grootvlei initially, and fabric filter plants at Medupi, Camden and 3 units at Grootvlei) as defects are rectified and performance is optimised. The extremely low PM emissions at Grootvlei from 2017 are due to the fabric filter plant retrofits on units 2, 3 and 4.

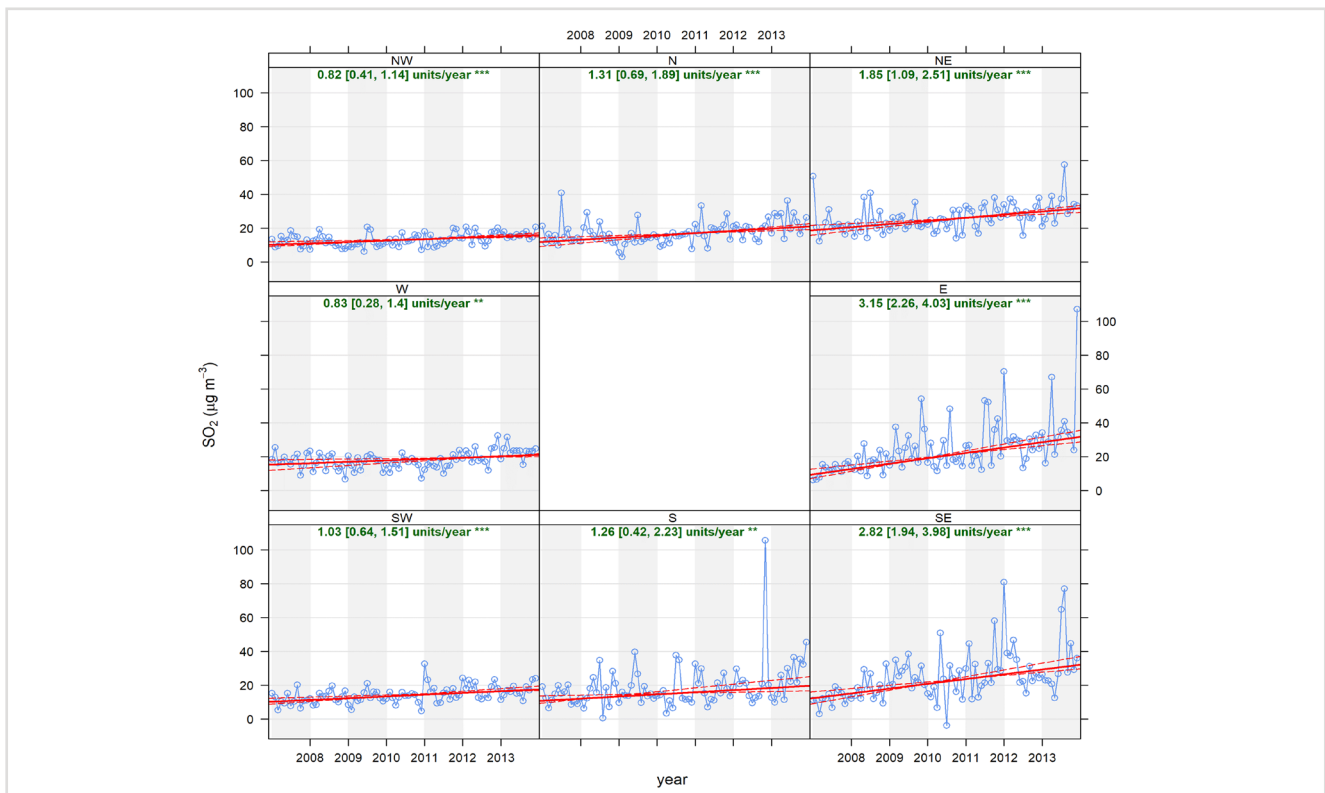


**Figure 3:** Theil-Sen trend analysis for monthly mean SO<sub>2</sub> concentrations at Grootvlei monitoring station

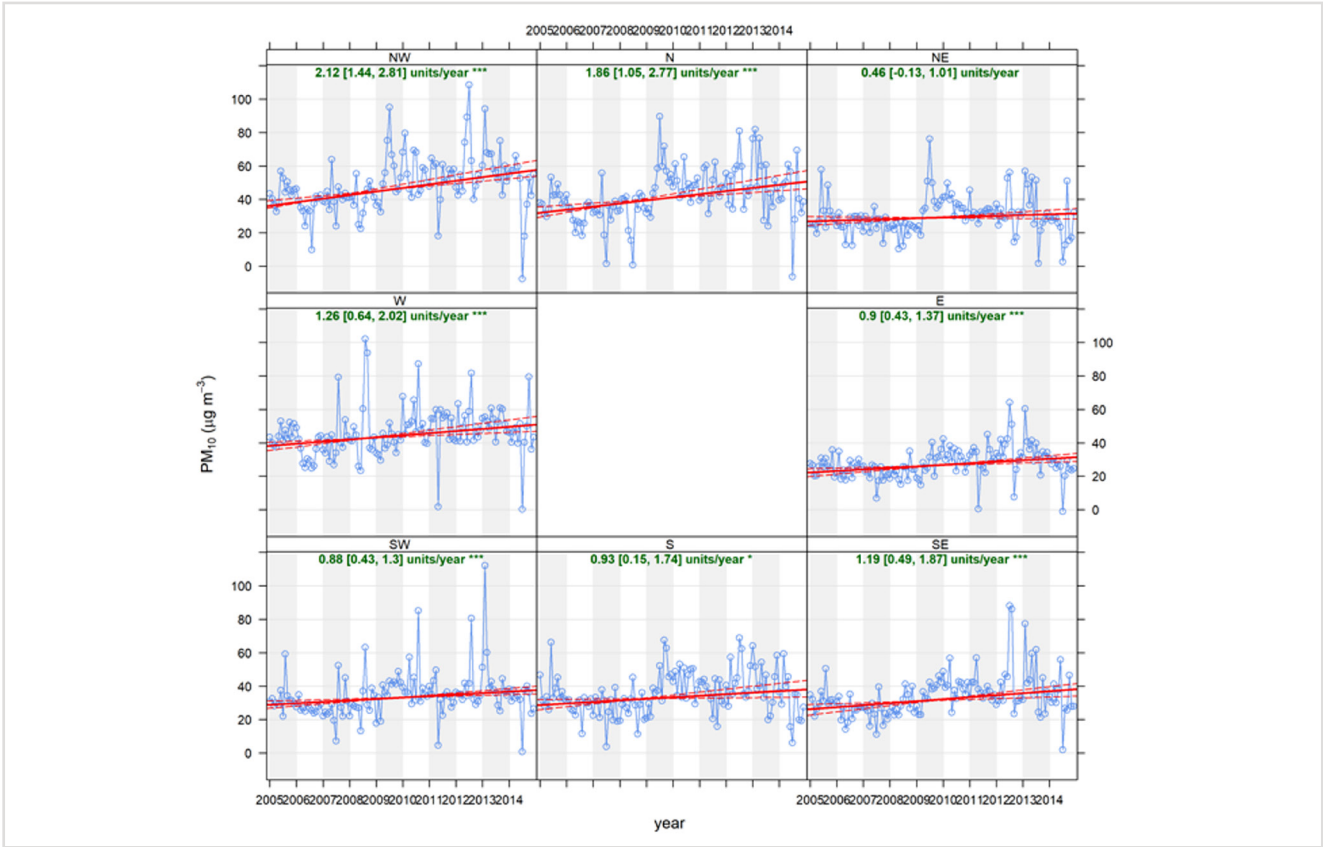


Figure 4: Theil-Sen trend analysis for monthly mean PM<sub>10</sub> concentrations at Camden monitoring station

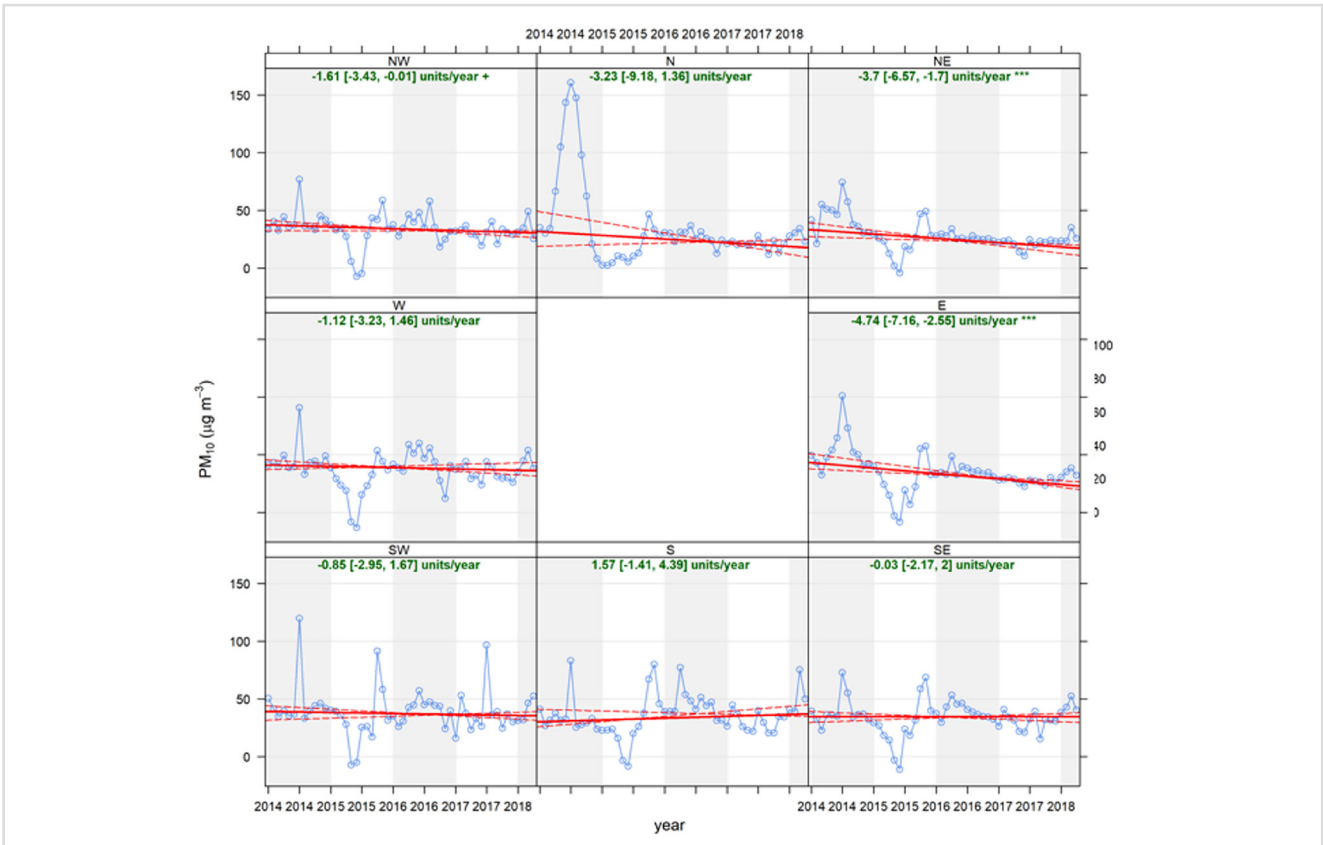


Figure 5: Theil-Sen trend analysis for monthly mean PM<sub>10</sub> concentrations at Marapong monitoring station at Camden monitoring station

**Table 4:** Spearman's rho correlation between power station SO<sub>2</sub> emissions and ambient SO<sub>2</sub> concentrations

Power station	Ambient air monitoring station	Correlation coefficient (r)	p-value
Komati	Komati	-0.008	0.953
Camden	Camden	0.105	0.306
Grootvlei	Grootvlei	0.546**	0.000
Medupi	Marapong	-0.071	0.700
	Medupi	0.369	0.076

\* Correlation is significant at the 0.05 level (2-tailed)  
 \*\* Correlation is significant at the 0.01 level (2-tailed)

**Ambient air pollution concentrations**

Despite the increase in SO<sub>2</sub> emissions from the power stations, there are no statistically significant increasing trends in SO<sub>2</sub> concentrations at most monitoring stations during the period when the power stations were commissioned (Table 3). There is only a statistically significant increase of 1.64 µg/m<sup>3</sup>/year (p<0.001) at Grootvlei monitoring station. The increase occurs in association with airflow from all directions (Figure 3). Highest annual increases in SO<sub>2</sub> concentrations occur in association with easterly (3.15 µg/m<sup>3</sup>/year) and south-easterly (2.82 µg/m<sup>3</sup>/year) flow, from the direction of Grootvlei power station.

There is a statistically significant increasing trend in PM<sub>10</sub> concentrations of 1.22 µg/m<sup>3</sup>/year (p<0.001) at Camden monitoring station, and a statistically decreasing trend of 2.04 µg/m<sup>3</sup>/year (p<0.1) at Marapong monitoring station. The most significant increases in PM<sub>10</sub> concentrations at Camden monitoring station occur in association with NW (2.12 µg/m<sup>3</sup>/year) and N (1.86 µg/m<sup>3</sup>/year) flow, and also with W flow (1.26 µg/m<sup>3</sup>/year) from the direction of Camden power station (Figure 4). The decrease in PM<sub>10</sub> concentrations at Marapong is presumably due to the reduction in emissions from local sources in Marapong to the E and NE of the monitoring station (Figure 5). Average diurnal variations in PM<sub>10</sub> concentrations at the monitoring stations show that PM is mainly from surface sources like vehicle activity. These surface sources typically emit more in the early morning and evening, and the pollutants are trapped by stable conditions at these times.

**Correlation Analysis**

There is no strong positive correlation between SO<sub>2</sub> emissions from Komati, Camden and Medupi power station and the ambient SO<sub>2</sub> concentrations at the nearby Komati, Camden, Marapong and Medupi monitoring stations. A strong positive correlation exists only between SO<sub>2</sub> emissions from Grootvlei power station and ambient SO<sub>2</sub> concentrations detected at the Grootvlei monitoring station (r = 0.546 and p-value = 0.000) (Table 4). The pollution roses and diurnal variations provide insight into potential sources of SO<sub>2</sub> measured at the monitoring

**Table 5:** Spearman's rho correlation between power station PM<sub>10</sub> emissions and ambient PM<sub>10</sub> concentrations

Power station	Ambient air monitoring station	Correlation coefficient (r)	p-value
Komati	Komati	-0.443*	0.011
Camden	Camden	-0.029	0.830
Grootvlei	Grootvlei	-	-
Medupi	Marapong	0.282	0.146
	Medupi	0.498*	0.035

\* Correlation is significant at the 0.05 level (2-tailed)  
 \*\* Correlation is significant at the 0.01 level (2-tailed)

stations. Ambient SO<sub>2</sub> levels at the Komati monitoring station are affected by emissions from Duvha (NNW) and Hendrina (NE) power stations. SO<sub>2</sub> concentrations at Phola monitoring station are affected by emissions from Duvha (ENE) and Kendal (SSW) power stations and low-level sources, presumably the domestic burning of coal (Thomas and Scorgie, 2006). Ambient SO<sub>2</sub> concentrations at the Medupi monitoring station are affected also by emissions from Matimba power station (NE).

A strong positive correlation exists between PM emissions from Medupi power station and the ambient PM<sub>10</sub> concentrations at the Medupi monitoring station (r = 0.498 and p-value = 0.035; Table 5). This correlation is probably due to the construction activities at Medupi. There is a negative correlation between PM emissions from Komati power station and ambient PM<sub>10</sub> concentrations. PM emissions from Komati's stacks decrease between 2013 and 2018 as the efficiency of the electrostatic precipitators increased (Figure 2). Presumably the negative correlation is due to changes in other sources affecting Komati monitoring station. The average diurnal ambient PM<sub>10</sub> profiles confirm that PM<sub>10</sub> is mainly derived from surface sources at all monitoring stations. At the Medupi monitoring station, an ash dump located to the ENE is a potential source of PM<sub>10</sub>. The correlation between PM emissions and ambient PM<sub>10</sub> concentrations at Grootvlei could not be analysed due low emissions data availability.

**Compliance with the National Ambient Air Quality Standards**

**Compliance with the 1-hour and annual SO<sub>2</sub> standards**

99<sup>th</sup> percentile 1-hour SO<sub>2</sub> concentrations at all the monitoring stations did not exceed the 1-hour limit value of 350 µg/m<sup>3</sup>. Annual average SO<sub>2</sub> concentrations exceeded the annual SO<sub>2</sub> standard of 50 µg/m<sup>3</sup> only at Komati monitoring station in 2009 (Table 6).

**Compliance with the 24-hour and annual PM<sub>10</sub> standards**

99<sup>th</sup> percentile 24-hour average PM<sub>10</sub> concentrations exceeded

the 24-hour standard of 75  $\mu\text{g}/\text{m}^3$  at all the monitoring stations, with compliance achieved only at Marapong monitoring station in 2017 and 2018. Compliance with the annual  $\text{PM}_{10}$  standard of 40  $\mu\text{g}/\text{m}^3$  is also a challenge at all monitoring stations except at Grootvlei, Marapong and Medupi monitoring stations (Table 7).

## Discussion

### Relationship between power station emissions and ambient air quality

Overall, there is not a strong correlation between the ambient air pollution concentrations detected by the five ambient air quality monitoring stations and the increasing emissions from the four coal-fired power stations near them. Strong positive correlations are only recorded for  $\text{SO}_2$  concentrations at Grootvlei and  $\text{PM}_{10}$  concentrations at Medupi monitoring station. There is a weak positive correlation between emissions at Medupi power station and ambient  $\text{PM}_{10}$  concentrations at Marapong monitoring station. It is likely that the correlation between PM emissions from Medupi and ambient  $\text{PM}_{10}$  concentrations in the vicinity is due to construction activity at Medupi, increased vehicle activity and an increase in the population of Marapong due to Medupi's construction, and not PM emissions from Medupi's stacks.

Within the HPA, this study found a statistically significant increasing trend in  $\text{SO}_2$  concentrations at Grootvlei monitoring station. A statistically significant increasing trend in  $\text{PM}_{10}$  concentrations was found at Camden monitoring station. The increase in  $\text{PM}_{10}$  levels at Camden contrasts with the decreasing trend observed by Feig et al. (2019) in Ermelo, which suggests that activities at Camden may be affecting  $\text{PM}_{10}$  concentrations downwind. In terms of compliance, this study indicates compliance with the annual  $\text{SO}_2$  National Ambient Air Quality Standard at all monitoring stations except at Komati monitoring station in 2009. Furthermore, compliance with the annual ambient  $\text{PM}_{10}$  standard was not achieved at all the monitoring stations except at Grootvlei monitoring station from 2007 to 2013. Feig et al. (2019) found similar results in the HPA with the only exceedance of the annual ambient  $\text{SO}_2$  standard at the Witbank monitoring station between 2008 and 2014, and an exceedance of the annual ambient  $\text{PM}_{10}$  standard at all monitoring stations except at the Hendrina and Middelburg stations.

This study attributes  $\text{PM}_{10}$  ambient concentrations at the Marapong monitoring station to local domestic combustion and/or traffic sources, as indicated by early morning and evening diurnal peaks. Feig et al. (2016) found similar results for  $\text{PM}_{10}$  concentrations in the WBPA. The association between high  $\text{SO}_2$  concentrations at Matimba Power Station and Grootegeluk Coal Mine was also found by Feig et al. (2016). In terms of trends, this study found a statistically significant decreasing trend in  $\text{PM}_{10}$  concentrations of 2.04  $\mu\text{g}/\text{m}^3/\text{year}$  ( $p < 0.01$ ) at Marapong monitoring station between 2014 and 2018. Feig et al. (2016) also found a statistically significant decreasing trend of 6.5  $\mu\text{g}/\text{m}^3/\text{year}$  ( $p < 0.01$ ) in Lephalale between 2012 and 2015. This study found there to be compliance with the annual ambient

$\text{SO}_2$  standard at the Marapong (between 2014 and 2018) and Medupi (between 2015 and 2018) monitoring stations, as was found by Feig et al. (2016) elsewhere in the WBPA. There was also compliance with the annual ambient  $\text{PM}_{10}$  standard at the Marapong and Medupi monitoring stations, although Feig et al. (2016) found that the annual ambient  $\text{PM}_{10}$  standard was exceeded elsewhere in the WBPA.

Coal combustion industries are one of the biggest atmospheric polluters globally (Pretorius et al., 2015; Rohde and Muller, 2015, Lourens et al., 2011, SOGA, 2018), however the contribution of other industries to air pollution is well documented. These include mines (Ekosse, 2005, Banza, 2009, Wright et al., 2017); road traffic (Khedo et al., 2010, Shirinde et al., 2014, SOGA, 2018); domestic burning and open burning (Balashov et al., 2014, Shirinde et al., 2014, Wright et al., 2017, SOGA, 2018). In the HPA, Lourens et al. (2011) found  $\text{SO}_2$  and  $\text{NO}_2$  concentrations were highest near industrial areas such as metallurgical operations, coal-based industries, mines, petrochemical industries, and steel smelters. In the WBPA,  $\text{SO}_2$  concentrations are linked mostly to industries, and a small percentage to residential burning and vehicle emissions.  $\text{PM}_{10}$  concentrations were linked to mining activities (WBPA Air Quality Management Plan, 2015).

### Non-compliance and human health

Compliance with the 24-hour  $\text{PM}_{10}$  standard of 75  $\mu\text{g}/\text{m}^3$  was achieved only at Camden monitoring station in 2006, Grootvlei monitoring station in 2007, and Marapong monitoring station in 2017 and 2018. Compliance with the annual  $\text{PM}_{10}$  standard was not achieved, with exceptions at the Marapong and Medupi monitoring stations. Compliance with the  $\text{SO}_2$  1-hour standard of 350  $\mu\text{g}/\text{m}^3$  was achieved at all the monitoring stations except at Komati monitoring station in 2009. The annual  $\text{SO}_2$  standard of 50  $\mu\text{g}/\text{m}^3$  was exceeded only at Komati monitoring station in 2009.

These findings indicate that  $\text{PM}_{10}$  pollution is a bigger problem than  $\text{SO}_2$  pollution in the HPA and the WBPA. Research findings have shown that exposure to air pollution is one of the major causes of poor health globally (Silva et al., 2016; Wright et al., 2017; Martinez et al., 2018; SOGA, 2019), and 4.9 million global deaths (SOGA, 2019). As a result, it is important to put measures in place to ensure that people are not impacted by poor ambient air quality. In South Africa, 1800 premature deaths in 2012 were attributed to the exposure to fine PM (Keen and Altieri, 2016b). In addition, Balashov et al. (2014) found that the concentrations of  $\text{NO}_x$ ,  $\text{SO}_2$ , PM, CO and  $\text{O}_3$  over the HPA exceeded the WHO guidelines, and contributed to respiratory infections.  $\text{PM}_{2.5}$  provides a better indication of exposure to human than  $\text{PM}_{10}$ , and should therefore be monitored more widely.

### The effectiveness of ambient air monitoring stations

From the results obtained, it is inferred that the establishment of monitoring stations in the vicinities of coal-fired power stations is necessary but not sufficient to measure the impact of the power stations on ambient air quality. The main limitation

**Table 6:** 99<sup>th</sup> percentile of 1-hour averages and annual average SO<sub>2</sub> concentrations (µg/m<sup>3</sup>) compared to 1-hour and annual concentration limits at the monitoring stations

	2005	2006	2007	2008	2009	2010	2011	2012	2013	2014	2015	2016	2017	2018
<b>1-hour standard (350 µg/m<sup>3</sup>)</b>														
Komati		250.8	280.5	240.4	98.7	267.2	221.3	263.1	282.9	277.3	206.6			
Camden	151.3	159.9	154.9	198.4	178.2	213	205.3	239.3	193.7	152.6				
Grootvlei			106.5	123.8	151.3	156.8	186.8	210.4	208.3					
Marapong										150.2	133.5	102	140.7	156.2
Medupi											282.4	280.4	289.1	321.4
<b>Annual standard (50 µg/m<sup>3</sup>)</b>														
Komati		36.9	38.6	34.9	55.2	37.1	34.8	37.8	42.0	30.8	36.8			
Camden	19.2	16.9	17.7	25.4	27.1	26.9	22.3	29.3	24.0	17.1				
Grootvlei			14.8	16.0	17.6	16.8	21.2	23.7	25.3					
Marapong										18.3	25.9	10.6	13.2	18.1
Medupi											34.1	26.4	27.5	29.7

**Table 7:** 99<sup>th</sup> percentile of 24-hour averages and annual average PM<sub>10</sub> concentrations (µg/m<sup>3</sup>) compared to 24-hour and annual concentration limits at the monitoring stations. Non-compliance with the standard is indicated in red.

	2005	2006	2007	2008	2009	2010	2011	2012	2013	2014	2015	2016	2017	2018
<b>24-hour standard (75 µg/m<sup>3</sup>)</b>														
Komati		140.8	161.6	158.9	168.5	233.3	169.1	178.2	176.1	139	157.7			
Camden	88.1	63.5	88.8	113.7	135.8	125.9	143.4	128.9	147.5	100.4				
Grootvlei			67.5	83.2	78.9	86.8	77.3	130.2	89.6					
Marapong										157.8	106.2	78.8	57.4	55.1
Medupi											126.5	86.5	75.5	92.4
<b>Annual standard (40 µg/m<sup>3</sup>)</b>														
Komati		72.7	63.2	72.8	70.8	83.7	64.1	67.4	64.1	56.1	65.3			
Camden	36.1	29.2	30.8	33.2	39.9	45.2	41.9	45.7	50.8	34.6				
Grootvlei			30.8	35.9	34.7	37.0	35.0	29.2	36.7					
Marapong										36.2	28.7	32.5	24.3	23.6
Medupi											33.5	33.0	30.3	37.3

of an ambient monitoring station is that it only provides a measurement at one point in a large domain (Akyuz and Kaynak, 2019). Monitoring ideally needs to be supplemented with other forms of impact assessments, like dispersion modelling, that covers the entire domain of influence.

The value of monitoring stations is particularly evident when monitoring stations are sited in residential areas, where the measurements give a fairly accurate reflection of levels of pollution that people are exposed to monitoring stations also detect the cumulative impacts of a multitude of sources related to the power station of interest. For example, at Marapong, impacts of construction vehicles, domestic emissions by people who are temporarily residing in Marapong while they work on Medupi’s construction, ash and coal handling at Matimba, and tall stack emissions from Medupi and Matimba are detected. Many smaller and fugitive emission sources are very difficult to accurately model and cannot be observed from satellites, and so are best measured at ambient monitoring stations.

## Conclusion

In this paper, we identified trends in air pollution concentrations monitored at the ambient monitoring stations intended to measure impacts of new and recommissioned coal-fired power stations in South Africa. We also attempted to use statistical techniques to determine the extent to which these trends can be statistically related to changing emission levels.

The only potential observed instance where pollutant emissions, emitted from a power station had an impact on ambient pollutant levels was observed for SO<sub>2</sub> emissions from Grootvlei Power Station, detected at the Grootvlei ambient monitoring station. The increasing trend in SO<sub>2</sub> concentrations was highest in association with airflow from the direction of the power station. Ambient PM<sub>10</sub> concentrations at the Medupi monitoring station downwind of Medupi power station are also significantly correlated with the commissioning of Medupi; however, the correlation is likely due to construction activity at Medupi, and

not ash emissions from the stacks. The diurnal profile of PM<sub>10</sub> concentrations at Medupi confirms that surface sources are the main contributor to ambient PM<sub>10</sub> levels in the area.

No other significant correlations were found between increasing emissions of SO<sub>2</sub> and PM from the power stations, and ambient air quality levels. This is probably due to the fact that ambient pollution levels reflect the accumulation of pollutants from a large number of sources, both local and regional. Also, ash emissions from power station stacks are a fairly small source of PM in comparison to other sources in the priority areas.

We conclude that ambient monitoring stations are a useful way of determining impacts from coal-fired power stations on ambient air quality. They should be preferentially sited in residential areas where they measure exposure levels. They are particularly valuable in showing the cumulative impacts of a number of other activities directly and indirectly associated with the construction and operation of a coal-fired power station. However, ambient measurements should be supplemented with dispersion modelling, both during impact assessment before construction, and also during and after construction, to estimate the impact of the power station throughout its domain of influence.

## Acknowledgements

Itumeleng Morosele's Masters studies were funded by the National Research Foundation (NRF). We would like to thank Eskom SOC Ltd (Bontle Monametsi) for the timeous provision of data, Mr Anesu Khuhudzai at UJ STATKON for his assistance with performing statistical analyses, and Kgomotso Langa, Ratanang Rantho, Masonwabe Gatyeni and Nhlanhla Zondo for their assistance with data preparation and results analyses. Gratitude is also extended to Ms Bianca Wernecke for reviewing a draft of this paper.

## Author contributions

Itumeleng Morosele analysed most of the data and compiled the first draft of this paper. Kristy Langerman conceived of the study and revised the manuscript.

## References

Akyuz, E. and Kaynak, B. 2019, Use of dispersion model and satellite SO<sub>2</sub> retrievals for environmental impact assessment of coal-fired power plants. *Science of the Total Environment*, 689: 808-819. <https://doi.org/10.1016/j.scitotenv.2019.06.464>.

Balashov, N.V., Thompson, A.M., Piketh, S.J. and Langerman, K.E. 2014, Surface ozone variability and trends over the South African Highveld from 1990 to 2007. *Journal of Geophysical Research*, 119(7): 4323 - 4342. <https://doi.org/10.1002/2013JD020555>.

Banza, C.L., Nawrot, T.S., Haufroid, V., Decree, S., De Putter, T., Smolders, E., Kabyla, B.I., Luboya, O.N., Ilunga, A.N., Mutombo,

A.M. & Nemery, B. 2009, High human exposure to cobalt and other metals in Katanga, a mining area of the Democratic Republic of Congo. *Environmental Research*, 109(6): 745-752. <https://doi.org/10.1016/j.envres.2009.04.012>.

Carslaw, D.C. and Ropkins, K. 2012, Openair – an R package for air quality data analysis. *Environmental Modelling & Software*, 27-28: 52–61. <https://doi.org/10.1016/j.envsoft.2011.09.008>.

Carslaw, D.C. 2015, The openair manual – open-source tools for analysing air pollution data. Manual for version 1.1-4, King's College London.

Coakley, J.A., Cess, R.D. and Yurevich, F.B. 1983, The effect of tropospheric aerosols on the earth's radiation budget: a parameterization for climate models. *Journal of the Atmospheric Sciences*, 40:116–138. [https://doi.org/10.1175/1520-0469\(1983\)040<0116:TEOTAO>2.0.CO;2](https://doi.org/10.1175/1520-0469(1983)040<0116:TEOTAO>2.0.CO;2).

Crawford, J., Cohen, D.D. and Atanacio, A. 2018, The impact of closure of coal-fired power stations on aerosol concentrations in the Sydney Basin. *Atmospheric Pollution Research*, 9: 1167-1176. <https://doi.org/10.1016/j.apr.2018.05.002>.

Ekosse, G.E. 2008, Environmental Effects of Nickel-Copper Exploitation on Workers Health Status at Selebi Phikwe Area, Botswana. *Journal of Applied Sciences*, 8(13): 2344-2356. <https://doi.org/10.3923/jas.2008.2344.2356>.

Eskom 2016, Research, Testing and Development (RT&D): Ambient Air Quality Annual Report (January - December 2016). Eskom Holdings Limited.

Eskom 2017, Medium-term System Adequacy Outlook 2017 to 2021. Eskom Holdings Limited. <https://www.eskom.co.za/Whatweredoing/SupplyStatus/cuments/2017to2021MedTermSysAdequacyOutlook31Jul2017.pdf>.

Eskom 2019, Applications for suspension, alternative limits and/or postponement of the minimum emission standards (MES) compliance timeframes for Eskom's coal and liquid fuel fired power stations: summary document. Eskom ENV18-R245 rev 2.1. <https://www.eskom.co.za/MESApplications/Documents/Annexure%203%20-%20ESKOMs%20MES%20Applications%20-%20Summary%2020%20March%202019%20rev%202.1.pdf>.

Feig, G.T., Naidoo, S. & Ncgukana, N. 2016, Assessment of ambient air pollution in the Waterberg Priority Area 2012-2015, *Clean Air Journal*, 26(1): 21-28. <https://doi.org/10.17159/2410-972X/2016/v26n1a9>.

Feig, G., Garland, R.M., Naidoo, S., Maluleke, A. and van der Merwe, M. 2019, Assessment of changes in concentrations of selected criteria pollutants in the Vaal and Highveld Priority areas. *Clean Air Journal*, 29(2): 1-13. <https://doi.org/10.17159/caj/2019/29/2.7464>.

- Gouw, J., Parrish, D., Frost, G., Trainer, M. 2014, Reduced emissions of CO<sub>2</sub>, NO<sub>x</sub>, and SO<sub>2</sub> from U.S. power plants owing to switch from coal to natural gas with combined cycle technology. *Earths Future*, 2: 75–82. <https://doi.org/10.1002/2013EF000196>
- Gray, H.A. 2019, Air quality impacts and health effects due to large stationary source emissions in and around South Africa's Mpumalanga Highveld Priority Area (HPA). <https://cer.org.za/wp-content/uploads/2019/06/Andy-Gray-Report.pdf>.
- Hirsikko, A., Vakkari, V., Tiita, P., Manninen, H.E., Gagne, S., Laakso, H., Kulmala, M., Mirme, A., Mirme, S., Mabaso, D., Beukes, J.P. & Laakso, L. 2012, Characterisation of sub-micron particle number concentrations and formation events in the western Bushveld Igneous Complex, South Africa. *Atmospheric Chemistry and Physics*, 12: 3951-3967. <https://doi.org/10.5194/acp-12-3951-2012>.
- Holland, M. 2017, Health impacts of coal fired power plants in South Africa, report for Groundwork (South Africa) and Health Care without Harm. <https://cer.org.za/wp-content/uploads/2017/04/Annexure-Health-impacts-of-coal-fired-generation-in-South-Africa-310317.pdf>.
- International Energy Agency (IEA) 2020, Energy policy review. Germany, <https://www.iea.org/reports/germany-2020>.
- Kaufman, Y.J., Tanré, D. and Boucher, O. 2002, A satellite view of aerosols in the climate system. *Nature* 419:215–223. <https://doi.org/10.1038/nature01091>.
- Keen, S. and Altieri, K. 2016a, The health benefits of attaining and strengthening air quality standards in Cape Town. *Clean Air Journal*, 26(2): 22-27. <https://doi.org/10.17159/2410-972X/2016/v26n2a9>.
- Keen, S. & Altieri, K. 2016b, The cost of air pollution in South Africa. International Growth Centre (IGC). <http://eprints.lse.ac.uk/81698/>.
- Khedo, K.K., Perseedoss, R. and Mungur, A. (2010). A wireless sensor network air pollution 797 monitoring system. *International Journal of Wireless & Mobile Networks*, 2(2): 31-45. <https://doi.org/10.5121/ijwmn.2010.2203>.
- Langerman, K.E. and Pauw, C.J. 2018, A critical review of health risk assessments of exposure to emissions from coal-fired power stations in South Africa. *Clean Air Journal*, 28(2): 1-12. <https://doi.org/10.17159/2410-972x/2018/v28n2a19>.
- Lourens, A.S., Beukes, J.P., van Zyl, P.G., Fourie, G.D., Burger, J.W., Pienaar, J.J., Read, C.E. & Jordaan, J.H. 2011, Spatial and temporal assessment of gaseous pollutants in the Highveld of South Africa. *South African Journal of Science*, 107(1/2): 1-8. <https://doi.org/10.4102/sajs.v107i1/2.269>.
- Ma, Z., Liu, R., Liu, Y., Bi, J. 2019, Effects of air pollution control policies on PM<sub>2.5</sub> pollution improvement in China from 2005 to 2017: a satellite-based perspective. *Atmos. Chem. Phys.* 19: 6861–6877. <https://doi.org/10.5194/acp-19-6861-2019>.
- Mannucci, P.M. & Franchini, M. 2017, Health Effects of Ambient Air Pollution in Developing Countries. *International Journal of Environmental Research and Public Health*, 14: 2-8. <https://doi.org/10.3390/ijerph14091048>.
- Martinez, G.S., Spadaro, J.V., Chapizanis, D., Kendrovski, V., Kochubovski, M. and Mudu, P. 2018, Health Impacts and Economic Costs of Air Pollution in the Metropolitan Area of Skopje. *International Journal of Environmental Research and Public Health*, 15(626): 1-11. <https://doi.org/10.3390/ijerph15040626>.
- Pretorius, I., Piketh, S., Burger, R. & Neomagus, H. 2015, A perspective on South African coal fired power station emissions. *Journal of Energy in Southern Africa*, 26(3): 27-40. <https://doi.org/10.17159/2413-3051/2015/v26i3a2127>.
- Rohde, R.A. & Muller, R.A. 2015, Air Pollution in China: Mapping of concentrations and Sources. *PLOS ONE*, 10(8): 1-14. <https://doi.org/10.1371/journal.pone.0135749>.
- Russell, M.C., Belle, J.H. and Liu, Y. 2017, The impact of three recent coal-fired power plant closings on Pittsburgh air quality: A natural experiment. *Journal of the Air & Waste Management Association*, 67(1): 3-16. <https://doi.org/10.1080/10962247.2016.1170738>.
- Shirinde, J., Wichmann, J. and Voyi, K. 2014, Association between wheeze and selected air pollution sources in an air pollution priority area in South Africa: a cross-sectional study. *Environmental Health*, 13(32): 1-12. <https://doi.org/10.1186/1476-069X-13-32>.
- Silva, R.A., Adelman, Z., Fry, M.M. & West, J.J. 2016, The Impact of Individual Anthropogenic Emissions Sectors on the Global Burden of Human Mortality due to Ambient Air Pollution. *Environmental Health Perspectives*, 124(11): 1776-1784. <https://doi.org/10.1289/EHP177>.
- SOGA (State of Global Air) 2018, A specialist report on global exposure to air pollution and its disease burden.
- SOGA (State of Global Air) 2019, A specialist report on global exposure to air pollution and its disease burden.
- StatsSA (Statistics South Africa) 2018, Electricity, gas and water supply industry, 2016, Report No. 41-01-02 (2016), Statistics South Africa.
- Thomas, R. and Scorgie, Y. 2006, Air quality impact assessment for the proposed new coal-fired power station (Kendal North) in the Witbank area, APP/06/NMS-01 Rev 0.2, Airshed Planning Professionals, [https://www.eskom.co.za/OurCompany/SustainableDevelopment/EnvironmentalImpactAssessments/Documents/Air\\_quality\\_part\\_1.pdf](https://www.eskom.co.za/OurCompany/SustainableDevelopment/EnvironmentalImpactAssessments/Documents/Air_quality_part_1.pdf).

Venter, A.D., Vakkari, V., Beukes, J.P., van Zyl, P.G., Laakso, H., Mabaso, D., Tiita, P., Josipovic, M., Kulmala, M., Pienaar, J.J. & Laakso, L. 2012, An air quality assessment in the industrialised western Bushveld Igneous Complex. South Africa. *South African Journal of Science*, 108(9/10): 1-10. <https://doi.org/10.4102/sajs.v108i9/10.1059>.

Wang, G., Deng, J., Zhang, Y., Zhang, Q., Duan, L., Hao, J. and Jiang, J. 2020, Air pollutant emissions from coal-fired power plants in China over the past two decades. *Science of the Total Environment*, 741: 140326. <https://doi.org/10.1016/j.scitotenv.2020.140326>.

WHO (World Health Organization) 2016, *Ambient air pollution: A global assessment of exposure and burden of disease*. World Health Organization, Geneva.

Wright, C.Y., Garland, R.M., Thambiran, T., Forbes, P., Diab, R. & Oosthuizen, M.A. 2017, Air quality and human health impacts in southern Africa. Available from: [https://www.researchgate.net/publication/320181172\\_Air\\_quality\\_and\\_human\\_health\\_impacts\\_in\\_southern\\_Africa](https://www.researchgate.net/publication/320181172_Air_quality_and_human_health_impacts_in_southern_Africa).

Xue, Z., Hao, J., Chai, F., Duan, N., Chen, Y., Li, J., Chen, F., Liu, S. & Pu, W. 2005, Air Quality Impact of the Coal-Fired Power Plants in the Northern Passageway of the China West-East Power Transmission Project. *Journal of the Air & Waste Management Association*, 55(12): 1816-1826. <https://doi.org/10.1080/10473289.2005.10464781>.

## SENHARE CONSULTING SERVICES (PTY) LTD

Registration number: 2015/032439/07

Consulting firm specializing in the design, implementation and maintenance of the ISO 17025, Iso 17034, ISO 17043, GLP and ISO 9001. The unique approach of blending the training of personnel, business process, the requirements of the standards and regulations, corporate governance and meeting customer's requirements have been key to our success.

Cell: 084 549 3710

Email: [martins.jenita@gmail.com](mailto:martins.jenita@gmail.com)



## ENVIRONMENTAL SERVICES

- Stack Emission Services
- ISO17025 Accredited Laboratory Services
- Equipment Supply
- NAEIS Reporting
- Passive Sampling and Dust Fall-out Monitoring
- Leak Detection and Repair



**LEVEGO**

*Levego provides a world class environmental service in line with our core company values of customer focus, quality, integrity, respect and trust.*

**011 608-4148**

**[www.levego.co.za](http://www.levego.co.za)**



Member of the  
Source Testing Association U.K.

**SABS**  
ISO 9001

**sanas**  
T0846

# Research article

## Chemical characterization of fine particulate matter, source apportionment and long-range transport clusters in Thohoyandou, South Africa

Rirhandzu J. Novela<sup>1</sup>, Wilson M. Gitari<sup>1</sup>, Hector Chikoore<sup>2</sup>, Peter Molnar<sup>3</sup>,  
Rabelani Mudzielwana<sup>1</sup>, Janine Wichmann<sup>4</sup>

<sup>1</sup>Environmental Remediation and Nano Science Research Group, University of Venda,  
Private bag X5050, Thohoyandou, 0950 South Africa. gitariw@gmail.com\*

<sup>2</sup>Unit for Environmental Sciences and Management, North-West University,  
1174 Hendrick Van Eck Boulevard, Vanderbijlpark, South Africa.

<sup>3</sup>Occupational and Environmental Medicine, Sahlgrenska University Hospital and University of Gothenburg,  
Medicinaregatan 16A, SE-40530, Sweden.

<sup>4</sup>School of Health Systems and Public Health, University of Pretoria, 31 Bophelo Road, Pretoria, 0001 South Africa.

Received: 5 August 2020 - Reviewed: 14 September 2020 - Accepted: 5 October 2020  
<https://doi.org/10.17159/caj/2020/30/2.8735>

### Abstract

This paper presents a chemical characterization of fine particulate matter (PM<sub>2.5</sub>) in air masses passing through Thohoyandou and further determines their sources. PM<sub>2.5</sub> samples were collected and quantified using the gravimetric method. X-ray fluorescence, smoke stain reflectometer, optical transmissometer and scanning electron microscopy - energy dispersive X-Ray spectroscopy were used to determine the chemical and morphological composition of the particulate matter. The source apportionment was done using principal component analysis while the HYSPLIT model was used to depict the long-range transport clusters. The mean of concentrations of PM<sub>2.5</sub>, soot, black carbon and UVP were 10.9 µg/m<sup>3</sup>, 0.69x10<sup>-5</sup> m<sup>-1</sup>, 1.22 µg/m<sup>3</sup> and 1.40 µg/m<sup>3</sup>, respectively. A total of 24 elements were detected in the PM<sub>2.5</sub> with Pd, Sn, Sb, Mg, Al, and Si being the dominant elements. SEM-EDS have shown the presence of irregular, flat and spherical particles which is associated with crustal material and industrial emissions. Source apportionment analysis revealed six major sources of PM<sub>2.5</sub> in Thohoyandou namely, crustal materials, industrial emissions, vehicular emissions, urban emissions, fossil fuel combustion and fugitive-Pd. Air parcels that pass through Thohoyandou were clustered into four groupings. The major pathways were from the SW Indian Ocean, Atlantic Ocean, and inland trajectories. Clusters from the ocean are associated with low concentration, while inland clusters are associated with high concentration of PM<sub>2.5</sub>. The PM<sub>2.5</sub> levels occasionally exceeded the daily WHO guideline (25 µg/m<sup>3</sup>) in Thohoyandou and the sources of PM<sub>2.5</sub> extend beyond the borders. This study recommends that further studies need to be carried out to assess the health impacts of PM<sub>2.5</sub> in Thohoyandou.

### Keywords

PM<sub>2.5</sub> characterization; source apportionment; long range clusters; principal component analysis; backward trajectories.

### Introduction

Ambient air pollution is a major environmental health issue globally due to several health implications associated with various air pollutants (Olaniyan et al., 2015). Of all air pollutants fine particulate matter (PM<sub>2.5</sub>) is of major concern since it is linked to a number of health implications including premature death in adults with heart and lung disease, strokes, heart attacks, chronic respiratory disease such as bronchitis, aggravated asthma and premature deaths of children from acute lower respiratory infections such as pneumonia (CCAC, 2019). It is estimated that about 7 million people die prematurely every year as a result of exposure to PM<sub>2.5</sub> (WHO, 2014). The World Health

Organization (WHO) has therefore set the daily guideline value of 25 µg/m<sup>3</sup> for PM<sub>2.5</sub> concentrations in ambient air and further issued recommendations to countries to lower PM<sub>2.5</sub> levels in ambient air (WHO, 2016). In South Africa, the daily standard for PM<sub>2.5</sub> is set at 40 µg/m<sup>3</sup> which is much higher compared to the WHO daily guideline.

Valsamakis (2015) conducted a study in Johannesburg, South Africa during winter and spring of 2013 and 2014 and recorded PM<sub>2.5</sub> concentrations at Petrus Molefe Eco Park ranging from 18.1-61.2 µg/m<sup>3</sup> during spring and 62.9-126 µg/m<sup>3</sup> during winter;

18.5-38.4 $\mu\text{g}/\text{m}^3$  during spring and 25.1-71.9  $\mu\text{g}/\text{m}^3$  during winter at Thokoza Park. Biomass burning, vehicle emissions, industrial activity, and wind erosion of exposed areas were identified as major sources of particulate matter. Prior to that, Engelbrecht et al. (2002) had done source apportionment in Qalabotjha, South Africa and revealed that biomass burning is a major source of  $\text{PM}_{2.5}$ , accounting 13.8% of the  $\text{PM}_{2.5}$  concentrations, and reported the daily range between 71 to 93  $\mu\text{g}/\text{m}^3$ . Biomass burning was also identified as a major contributor during the SAFARI 2000 dry season campaign through elemental analysis in Skukuza, South Africa (Petkova et al., 2013). In the Vaal Triangle and Johannesburg, biomass burning, and aged pollution-laden air have been responsible for 20-40% of inhalable particulates (DEA, 2009). The transportation industry is the second common source contributing to  $\text{PM}_{2.5}$  concentrations through exhaust emissions, tire wear and dust resuspension. The growth of many cities without expanding or building new roads, together with increasing vehicle ownership result in a transportation system characterized by severe traffic congestion (Petkova et al., 2013) resulting in localized ambient air pollution. In Cape Town vehicle emissions have been identified as sources of brown haze (DEA, 2016). In Limpopo high emissions from vehicles are expected from national highways (N1 and N11) in Vhembe districts due to a high flow of vehicles as these roads connect South Africa to Zimbabwe and Botswana. On the South Africa environment outlook, DEA (2012) listed agricultural activities amongst sources that can be considered significant contributors to particulate emissions. Particulate emissions are derived from windblown dust, tillage and harvesting, dust entrainment due to heavy vehicles travelling (LEDET, 2016), fertilizer and chemical treatment, as well as the burning of residue crops and vegetation (DEA, 2012). The outcome of the huge dependence on coal in South Africa, is the high emission of particulate matter in coal fired power stations (DEA, 2016). These power stations have been identified as one of the leading sources of particulate matter in Limpopo (LEDET, 2016).

Air is a shared resource, not prone to any barriers circulating around the globe, whether clean or dirty. The geographical origin of the air mass can be traced through a combination of measurements and calculations using meteorological models (Wichmann et al., 2014). According to Tang et al., (2014) the contribution of long-range transport can be quantified using trajectory models such as the HYSPLIT model. The pathways that transport air masses away from and into South Africa is the Indian Ocean plume, the recirculation plume, the Atlantic ocean plume, the African plume and the Southern Ocean plume (DEA, 2009). Air masses from the south and central Atlantic are most likely to be free from industrial emissions. Air masses from the Indian Ocean are also relatively free of industrial pollutants, leaving the African transport plume, and carrying industrial pollutants from southern Africa (DEA, 2009). HYSPLIT trajectories have shown that Zambian copper belt emissions are transported over southern Africa (DEA, 2012), while in spring ambient air quality is likely to be affected by the transport of pollutants associated with biomass burning in the sub-equator (LEDET, 2016). Air pollution in South Africa also affects the neighboring

countries (Swaziland, Lesotho, Mozambique, Zimbabwe and Botswana), with emissions from the Mpumalanga Highveld (Freiman and Piketh, 2002), while pollutants from Waterberg DM are anticipated to be transported and influence background concentrations in the North West Province (LEDET, 2016).

Although activities such as biomass burning, agricultural activities, construction and transportation are being carried out in Thohoyandou, no study has been conducted to quantify and characterize  $\text{PM}_{2.5}$ . These sources can be contributing to high  $\text{PM}_{2.5}$  that are exceeding the standards and most likely to be detrimental to human health. Thus, this study is the first of its own kind in Limpopo. This study therefore aims at quantifying the  $\text{PM}_{2.5}$  in Thohoyandou, Limpopo Province South Africa, the correlation between meteorological variables and  $\text{PM}_{2.5}$  and further determines the chemical composition of quantified  $\text{PM}_{2.5}$ . Lastly the source apportionment of the contaminants as well as geographical origin of the air masses were determined using gravimetric method, principal component analysis and HYSPLIT model respectively.

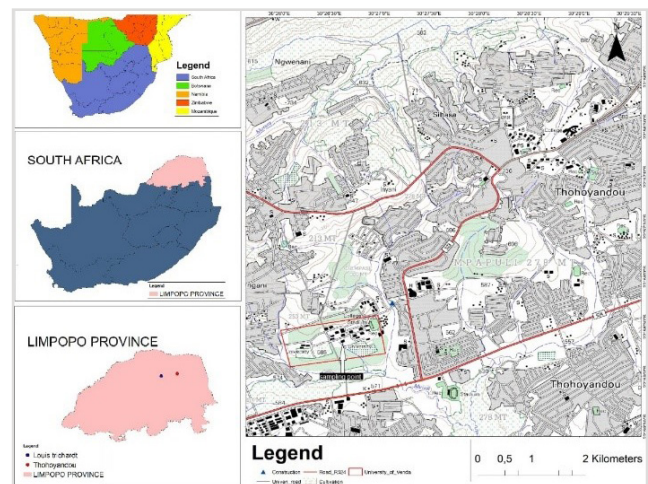


Figure 1: A map showing the location of South Africa and Thohoyandou.

## Methods

### Study area

Sampling of  $\text{PM}_{2.5}$  was undertaken on the roof of the School of Environmental Sciences building, University of Venda. Figure 1 demonstrates Thohoyandou in Limpopo province, South Africa. Limpopo shares borders with three countries, Mozambique, Zimbabwe, and Botswana, and they can also contribute to  $\text{PM}_{2.5}$ . The rainfall of Thohoyandou is highly seasonal, with most rainfall occurring during midsummer from December to February (Osidele, 2016). The monthly distribution of average daily maximum temperatures shows that the average midday temperatures for Thohoyandou range from 22°C to 26°C in winter and from 25°C to 40°C in January (Mzezewa et al., 2010). Activities that could result in particulate pollution in Thohoyandou include agricultural activities, construction, biomass burning, windblown dust and motor vehicles and long-

range transport as can be seen from Figure 1. The sampling site was selected to represent the urban background settings, since it is not near potential  $PM_{2.5}$  sources and the population of  $1629.49/km^2$  (SSA, 2012). The site was also chosen because it is close to the laboratory, and thus would minimize cross contamination. The coordinates of the sampling station are  $22^{\circ}58.650'S$  and  $030^{\circ}26.646'E$ . The height of the sampling point was 9m above ground and this was chosen as to avoid overloading the filters with crustal material at ground level, and hindrance from other buildings.

## Ambient air sampling

The single channel GilAir-5 personal air samplers (Sensidyne, Schauenburg Electronic Technologies Group, Mulheim-Ruhr, Germany) and 37 mm PTFE membrane filters (Zefon International, Florida, USA) (Figure 2) were used for sampling  $PM_{2.5}$  on a 24 hour period from April 2017 to April 2018 on a 3 day interval using Teflon filters 37 mm (Zefon International, Florida, USA). Filters were conditioned under climate-controlled conditions (Temperature:  $20.1-22.0^{\circ}C$ , RH: 43-54%) for 24 hours before weighing with a Mettler Toledo balance (Mettler-Toledo XP6) prior sampling. After sampling filters were removed and conditioned under the same climate-controlled conditions before weighing and stored in a freezer after weighing waiting for analysis. The pumps were calibrated using GilAir calibrator, the flow rate of 4L/ min was checked prior and after sampling using a field rotameter. Gravimetric analyses (See appendix 1) were conducted at the University of Pretoria. The total of 122 samples were collected and analysed.



**Figure 2:** Sampling train on the rooftop showing the GilAir pumps, cyclone, and filter cassette.

## Physicochemical characterization of $PM_{2.5}$

Soot measurement was performed using an EEL43 reflectometer at University of Pretoria. Black carbon (BC) and Ultraviolet absorbing particulate matter (UVP) were analyzed using a model OT21 optical transmissometer (Magee Scientific Corp. Berkeley, California, USA) at University of Gothenburg, Sweden. A wavelength-dispersive X-ray fluorescence (WD-XRF) spectrometer (PANALYTICAL AXIOS<sup>MAX</sup>) at North-West University was used to analyze the elemental composition of the collected filters in two seasons (summer and autumn). The morphology and elemental analysis of  $PM_{2.5}$  was performed with a FEI Quanta 250 scanning electron microscope with an integrated electron dispersion spectroscopy microanalysis system at North-West University.

## Determination of source apportionment and long-range transport clusters

Principal Component Analysis (PCA) with VARIMAX rotation was applied to the data of elemental concentrations to identify the main emission sources of elements in measured fine particulate matter. PCA was conducted in IBM SPSS statistics 26. Hybrid Single Particle Lagrangian Integrated Trajectory (HYSPLIT) model developed by National Oceanic and Atmospheric Administration Air Resources Laboratory (NOAA ARL) (Draxler and Rolph, 2003), driven by the National Center for Environmental Prediction/ National Center for Atmospheric Research (NCEP/NCAR) Global Reanalysis. Meteorological Data at the web server of the NOAA ARL was used to determine the transport trajectory of air parcels at the sampling site (Molnar et al, 2017). Daily trajectories were calculated for 72 h backwards. An analysis field (resolution  $2.5^{\circ} \times 2.5^{\circ}$  and 17 vertical levels) was provided every 6 h and the wind field was interpolated linearly between each analysis (Molnar et al, 2017). 12 trajectories were calculated daily in different height (250, 500, 750m), with 4 trajectories per height at different time interval (0, 6, 12, 18h). Since a single backward trajectory has a large uncertainty and is of limited significance, an ensemble of trajectories was used in this study. The cluster analysis was conducted seasonally due to the limitation of using very large sample sizes in the clustering function of the HYSPLIT software, as done in other studies (Tang et al., 2014; Molnar et al., 2017; Adeyemi, 2020). A total of 4384 backward trajectories were generated for the 365 days and applied in the cluster analysis. The clustering algorithm coupled in HYSPLIT was based on the distance between a trajectory endpoint and the corresponding cluster mean endpoint. Seasonal clusters and the whole year clusters were made. Each daily trajectory was assigned to a cluster, daily measured pollutants concentration was matched with cluster assigned to the corresponding daily trajectory and the descriptive statistics were measured for each cluster.

## Data analysis

Statistical analysis was performed using IBM SPSS statistics 26.

## Sampler quality assurance

To ensure data quality all aspects of air quality monitoring were subjected to recognized procedures to ensure standardization, conformity in approach so that the resultant data are representative and comparable. All the equipment used were checked, cleaned and calibrated according to manufacturer's specifications prior to each sampling and weighing session. To ensure quality control the filters were weighed and loaded in a clean lab with controlled environmental conditions. To avoid contamination weighed filter papers were placed in petri-dishes, during transportation the filters were sealed with a sellotape and placed in the ziplock bag inside a box filled with papers to ensure that there is no movement.

## Results and discussions

### PM<sub>2.5</sub>, Soot, Black carbon and UVPM analysis

Table 1 presents the descriptive statistics of PM<sub>2.5</sub>, soot, black carbon and UVPM determined throughout the sampling period (April 2017- April 2018). The PM<sub>2.5</sub> concentrations ranged from 1.06 to 37.52 µg/m<sup>3</sup> with an average of 10.9 µg/m<sup>3</sup>. The PM<sub>2.5</sub> concentrations exceeded the daily WHO guideline of 25 µg/m<sup>3</sup> on 9 occasions. However, the PM<sub>2.5</sub> concentrations were found to be within the South African National Ambient Air Quality Standard (NAAQS) of 40 µg/m<sup>3</sup> (See appendix 3). Seasons were defined as followed: Autumn (18/4/2017 to 31/5/2017 and 1/3/2018 to 16/4/2018), winter (1/6/2017 to 31/8/2017), spring (1/9/2017 to 30/11/2017) and summer (1/12/2017 to 28/2/2018). The highest mean of PM<sub>2.5</sub> level was observed in spring and four exceedances of the daily WHO guideline were recorded, followed by autumn with two exceedances, while the highest mean levels of soot and BC was observed in winter followed by spring (Table 1). For UVPM, the highest mean level was observed in autumn followed by winter.

Higher concentration of PM<sub>2.5</sub> in spring is attributed to biomass burning prior to the onset of rainfall during September, which is followed by agricultural activities after the first rainfall in October and November resulting in daily WHO guideline exceedances. Biomass burning and agricultural activities have been identified as major contributors to PM<sub>2.5</sub> (DEA, 2009; Engelbrecht et al., 2002; DEA, 2012; Petkova et al., 2013; Hersey et al., 2015; Valsamakis, 2015; DEA, 2016; LEDET, 2016). High concentrations measured in winter are attributed to household warming during June and July and the prevalence of stable conditions in these months also contributes to the increase in concentrations. Stable conditions occur with little to no rainfall and calmer winds, as was observed in June and July (See Appendix 2). This results in longer atmospheric residence times of PM<sub>2.5</sub> and PM<sub>2.5</sub> chemical composition due to limited wet deposition and high accumulation of the aerosol properties (Perrino et al., 2011; Valsamakis, 2015). Low PM<sub>2.5</sub>, soot, BC and UVPM levels in summer and autumn was due to unstable weather conditions. Unstable conditions are associated with high rainfall, increased wind speed. These conditions increase wet deposition and dispersion of PM<sub>2.5</sub>, soot, BC and UVPM leading to low concentrations and less exceedances of the daily WHO guideline. Dependence on public transport during summer, and no household warming reduces PM<sub>2.5</sub>, soot, BC and UVPM levels.

### Correlation between PM<sub>2.5</sub> and meteorological variables

Table 2 presents the correlation coefficients and the corresponding p-values for the whole study period. Relative humidity and rainfall played a major role in decreasing PM<sub>2.5</sub> concentrations, due to the significant correlation. Relative humidity and rainfall decrease the concentration of PM<sub>2.5</sub>, as deduced from negative correlation. PM<sub>2.5</sub> decreases with high

**Table 1:** Descriptive statistics for seasonal variation of PM<sub>2.5</sub>, soot, BC and UVPM, seasonally and for the entire sampling period.

	MEAN	MEDIAN	SD	MIN	MAX
<b>PM<sub>2.5</sub> (µg/m<sup>3</sup>)</b>					
Autumn	10.41	9.25	7.17	1.35	33.57
Winter	9.83	7.53	8.10	1.18	37.53
Spring	14.69	14.44	9.53	1.06	31.33
Summer	8.64	6.42	7.22	1.83	34.28
Annual	10.89	8.10	8.29	1.06	37.53
<b>SOOT (m<sup>-1</sup> 10<sup>-5</sup>)</b>					
Autumn	0.60	0.39	0.49	0.03	1.50
Winter	0.78	0.53	0.66	0.14	2.40
Spring	0.75	0.57	0.70	0.05	2.79
Summer	0.63	0.66	0.34	0.12	1.47
Annual	0.69	0.60	0.56	0.03	2.79
<b>BC (µg/m<sup>3</sup>)</b>					
Autumn	1.29	1.23	0.67	0.13	2.60
Winter	1.49	1.10	1.24	0.03	4.97
Spring	1.34	1.01	1.37	0.06	5.61
Summer	0.74	0.59	0.78	0.11	4.07
Annual	1.22	0.81	1.09	0.03	5.61
<b>UVPM (µg/m<sup>3</sup>)</b>					
Autumn	1.64	1.39	0.87	0.15	3.18
Winter	1.55	1.33	0.98	0.10	3.80
Spring	1.44	1.27	1.13	0.08	4.78
Summer	0.97	0.95	0.53	0.36	3.08
Annual	1.40	1.19	0.93	0.08	4.78

relative humidity due to hygroscopic growth (Wang and Ogawa, 2015) rendering the particles to be too heavy to stay suspended in the atmosphere, also particulate matter act as condensation nuclei, during cloud formation as humidity increases. Significant negative relationship with rainfall, is due to wet deposition as atmospheric washout takes place when rainfall increases. High relative humidity and rainfall were measured in summer and autumn when compared to winter and spring and this negative relationship explains why winter and spring had high concentrations compared to summer and autumn. Wind speed was positively correlated with PM<sub>2.5</sub>. Prevailing wind transports PM<sub>2.5</sub> from nearby sources to the receptor, and thus, as wind speed increases the PM<sub>2.5</sub> increases.

Temperature has shown an insignificant negative correlation. A study by Wang and Ogawa (2015) has also shown that high temperatures hindered formation of particles in summer. According to Tai et al., (2010) sulfate concentrations are expected to increase with increasing temperatures due to faster SO<sub>2</sub> oxidation, while semi-volatile components such as nitrates and organics are expected to decrease as they shift from particle phase to gas phase at high temperatures. Temperature has a decreasing and an increasing effect; in the case of Thohoyandou

it had a decreasing effect due to high temperatures. This can be seen from high concentration in winter where low temperature was measured and low concentrations in summer where there was high temperature.

**Table 2:** Correlation coefficients of  $PM_{2.5}$ ,  $PM_{2.5}$  chemical composition and meteorological variables in Thohoyandou from 18 April 2017 to 16 April 2018.

	$PM_{2.5}$ ( $\mu\text{g}/\text{m}^3$ )	Soot ( $\text{m}^{-1} \cdot 10^{-5}$ )	BC ( $\mu\text{g}/\text{m}^3$ )	UVP ( $\mu\text{g}/\text{m}^3$ )
<b>All year</b>				
Temperature ( $^{\circ}\text{C}$ )	$r = -0.06$ 0.4760 <sup>NS</sup>	$r = -0.04$ 0.5985 <sup>NS</sup>	$r = -0.20$ 0.0280*	$r = -0.18$ 0.0486*
Relative humidity (%)	$r = -0.26$ 0.0030**	$r = -0.40$ < 0.0001***	$r = -0.35$ < 0.0001***	$r = -0.24$ 0.0059**
Wind speed (m/s)	$r = 0.18$ 0.0485*	$r = -0.04$ 0.6297 <sup>NS</sup>	$r = -0.18$ 0.0400*	$r = -0.16$ 0.0654 <sup>NS</sup>
Precipitation (mm)	$r = -0.23$ 0.0085**	$r = -0.21$ 0.0183*	$r = -0.3903$ < 0.0001***	$r = -0.28$ 0.0017**

*P*-value less than 0.05 is significant and greater than 0.05 is considered insignificant.  
<sup>NS</sup>=Not significant. \*=Significant. \*\*=Very significant. \*\*\*=Extremely significant.  
 Bold text: *p*-value significant

## Chemical composition analysis

### Elemental composition

Figure 3 and 4 presents the seasonal variations of elements detected in  $PM_{2.5}$  in the air mass passing through Thohoyandou, in summer and autumn respectively. For each season two graphs were plotted one with high elemental concentrations and one with low elemental concentrations. The transition metals (Cr, Mn, Co, Ni, Cu, W, Zr, Au and Pd), alkali earth metals (Rb and Na), alkaline earth metals (Mg and Ca), other metals (Al, Bi, Ga and Sn), semi metals (Si, Ge, Sb and As), non-metals (S and Se) and halogens (I) were detected in the particulate matter (See appendix 4). In summer, 24 elements were detected and decreased monthly throughout the season. Higher concentrations of Na, Sb, Pd and Sn were measured followed by Mg, Si and S (Fig 3a). High concentrations of Na can be attributed to gusty winds and torrential rain brought by tropical cyclones from Indian ocean in summer. The elements with high concentrations are associated with long range transport (Pd, Sn, Sb) from the igneous bushveld complex, followed by the elements associated with crustal materials (Mg, Al, Si) and lastly elements from industrial activities (Cu, As, Co, Ni). The low concentrations of elements associated with crustal materials can be explained by the fact that the sampling period was also associated with rainfall, and thus the soil re-suspension was suppressed, and the dust was not easily suspended from the surface to become airborne while for industrial activities is due to limited industrial activities in Thohoyandou. The decrease in high concentration of the trace metals as the sampling period progresses is attributed to the fact that the beginning of the sampling was associated with unstable conditions,

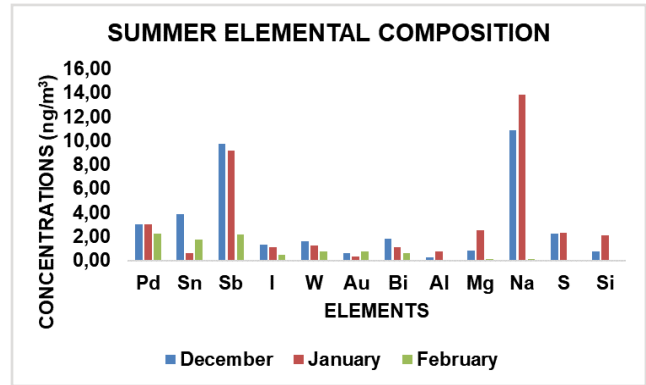


**Figure 3a:** Summer high elemental composition measured from  $PM_{2.5}$  filters in Thohoyandou.

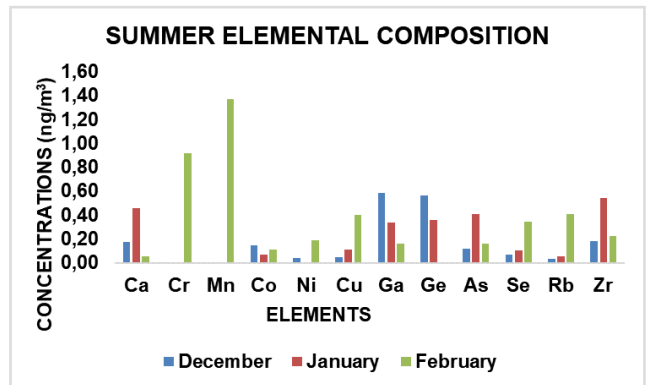


**Figure 3b:** Summer low elemental composition measured from  $PM_{2.5}$  filters in Thohoyandou.

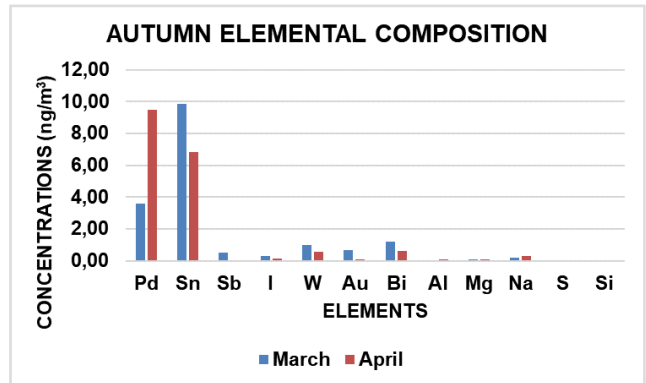


**Figure 4a:** Autumn high elemental composition measured from  $PM_{2.5}$  filters in Thohoyandou.

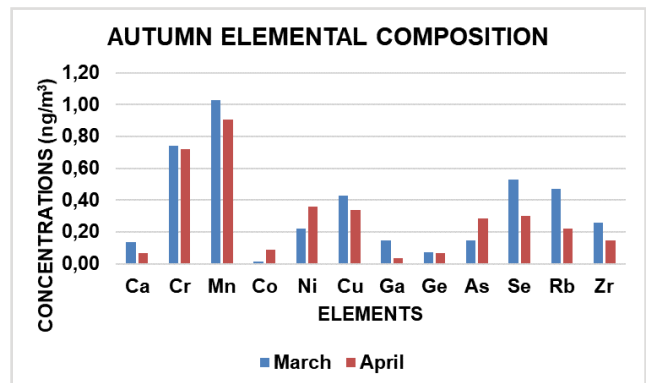


**Figure 4b:** Autumn low elemental composition measured from  $PM_{2.5}$  filters in Thohoyandou.

which facilitates dispersions and thus the high concentrations of these trace metals are highly dispersed. In autumn the high concentrations were Pd<Sn<S>Si. The concentrations of elements in autumn has decreased (Figure 4) this is attributed to increase in rainfall in this season which has scavenging properties. The concentrations of elements associated with crustal materials (Ca, Si, Mg) and Na significantly decreased in autumn this is because rainfall increased although the tropical cyclone season has passed, while Sn and Pd remained high as compared to other elements. Cr and Mn increased from February to April, the increase in these elements from industrial activities in autumn is attributed to change in backward trajectories which was dominated by Indian ocean origin in summer, wherein autumn has 25% backward trajectories originating from Zimbabwe picking up particles from industrial activities. A study by Hsu et al., (2016) has observed an abundance of Al followed by Ca, Mg, Fe and Zn in PM<sub>2.5</sub>. This trend can be justified by the high rainfall during the sampling season, which suppress the soil and prevent dust re-suspension.

**Morphological Analysis**

Figure 5(a) depicts the micrographs of particulate matter collected during 2017/2018 sampling period. In this study different kinds of morphologies were observed irregular, flat, and spherical (Figure 5a). Particles collected are clearly visible in the micrographs. A variety of particles shapes were observed from nearly perfect spherical shape to irregular shapes. The morphologies are consistent with the study by Li et al., (2019), wherein they observed irregular, flocculent, flat, rectangular, spheroidal, spherical, and regular particles. The shape of the particles is mainly depended on the source of the particles. Morphology and composition of these particles as done in previous studies (Van Zyl et al., 2014; Satsangi and Yadav, 2014) can help in identification of their sources. According to Van Zyl et al., (2014) the shapes of particles can be used to distinguish between windblown particles and anthropogenic particles. Well-rounded shapes are associated with anthropogenic sources, while unevenly shaped particles with natural sources. The particles in these micrographs are likely to be originating from natural emissions. As noted by Satsangi and Yadav (2014) PTFE filter is causing uncertainties because of its fiber structure observed from (Figure 5A).

In addition to visual inspection, EDS analysis was used to obtain the surface chemical composition. Figure 5b presents the micrograph of particulate matter and the subsequent chemical analysis of individual particles using EDS. The EDS as can be seen from the bar graphs (figure 5b) show the presence of Na, Mg, Al, Si, S, Cl, K, Ti, Cr, Fe. Majority of these oxygen-rich elements (Na, Mg, Al, Si, Cl, K, Ti, Cr, Fe) have been associated with natural sources such as crustal minerals erosion and surface winds, natural burning and from the oceans (Van Zyl et al., 2014). Additionally, a non-metallic species S, was detected, which suggests anthropogenic source. Flat particles and irregular (Figure 5b; Spectrum 1 and 4 respectively) comprises of C, O, Na, Mg, Al, Si, Ti, and Ca, these particles represent the

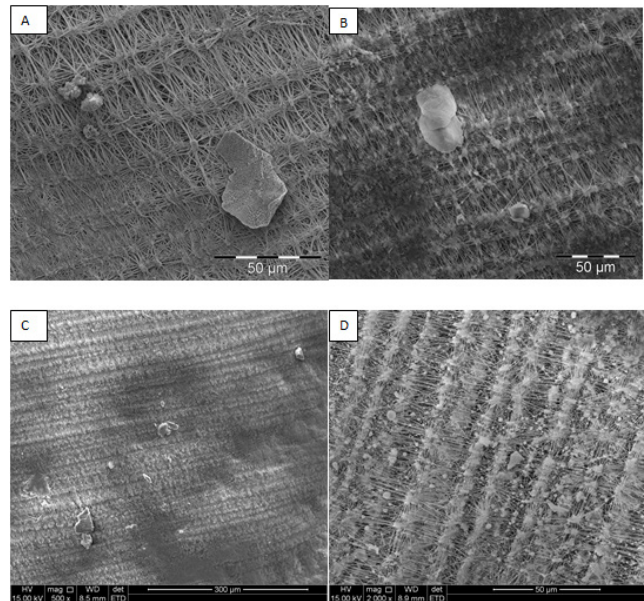
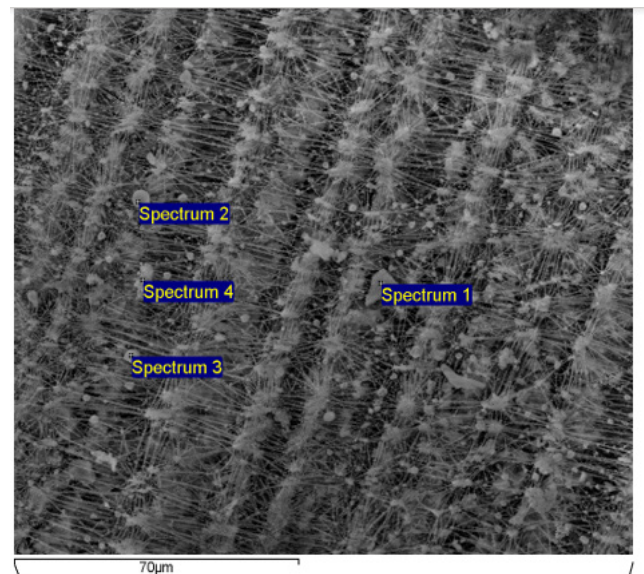


Figure 5a: SEM micrographs showing different particle morphology.



	C	O	Na	Mg	Al	Si	S	K	Ca	Ti	Cr	Fe
<b>Spectrum</b>												
<b>1</b>	71,7	21,5	1,31	0,5	0,84	1,05			3,12			
<b>2</b>	77,7	14,2	4,5	0,99		1,54		1,07				
<b>3</b>	62,2	22,4	1,95	1,45	1,25	1,69	0,28	3,61	1,57			0,67
<b>4</b>	33,8	31,3	0,76	0,45	10,8	11,3		1,22	2,72	0,5	0,66	

Figure 5b: SEM micrograph showing different particles that were used for EDS analysis.

crustal material. This type of particle primarily contained Si, Al, O, which is the elemental composition associated with phyllosilicates (AlSi)<sub>3</sub>O<sub>4</sub>. Spherical particles (Figure 5b: Spectrum 2) comprise of C, O, Na, Mg, Si and K. High content of C and K, show that its organic material and it was formed during biomass burning. Spheroid particles (Figure 5b: Spectrum 3), has shown additional elements such as Fe and S these morphologies represent industrial emissions.

## Sources of elemental composition

Figure 6 presents the principal component and the subsequent elements. Principal component analyses identified seven principal components with even eigenvalues > 1 that explained 84.70% of the % variance in elemental composition sources (See appendix 5). The last one was not included in the discussion because it had one element even though it explained 4.93% of the total variance. The first component is comprised of Na, Mg, Si, Al, Sb, S, Ca, Zr, and soot. Mg, Al, Si, Ca has been linked with crustal materials throughout the literature (Zhang et al., 2008; Xia and Gao, 2011; Santanna et al., 2016; Yu et al., 2013; Zhang et al., 2013; Cheng et al., 2016) and thus component one is showing emissions from crustal material i.e. dust resuspension. crustal materials explained 24.21% of the total variance. The study conducted by (Mohammed et al., 2017; Sammaritano et al., 2018) this source had a high percentage of variance. Although this component has soot that has not been previously linked with crustal material in this study it was assigned mainly with crustal material because of the number of the elements associated with this component and the diversity of the source.

The second component is comprised of S, Ga, W, Bi, I, Ge, Au and Co. Zhang et al., (2008) linked S with coal combustion. Co has also been linked with combustion of fuel (Xia and Gao, 2011). W, Co, and Ga has been used in jewelries; Ga and Ge have been used in electrodes, while Bi and W has been used as alloys. This source has been attributed to industrial activities and has explained to 21.06% of the cumulative variance. The third component is comprised of Sb, soot, Co. Co has been linked with vehicular emissions (Rizzo and Scheff, 2007; Hsu et al., 2016) from batteries and gasolin. Sb was found to be from abrasion and brake wear (Xia and Gao, 2011) since it has been used in automotive brakepad. soot is known to originate from incomplete combustion of fossil fuel and thus, can be emitted from internal combustion engines more especially diesel engines through vehicles tailpipes. Vehicular emission explained 10.31% of total variance. The fourth component is comprised of Au, Cu, Rb, and Mn. Mn emissions are also linked to transportation activities such as tailpipe emissions, brake, and tire wear (Yu et al., 2013), refuse burning (Begum et al., 2007) resuspended soil dust (Cheng et al., 2015). Cu has been linked to industrial dust (Lee et al., 2008), vehicle exhaust (Yu, et al., 2013) and brake wear. This source has been linked to urban emissions and contributed 9.56% of the total variance. The fifth component is comprised of Cr, BC, UVP and Pd. BC has been linked with combustion processes (Engelbrecht et al., 2002). Combustion processes include fossil fuel combustion, diesel engine exhaust, as well as open biomass fires and household combustion (Chiloane et al., 2017). Cr has been linked to biomass burning (Yu et al., 2013; Zhang et al., 2013). Some coal fired power stations are also located in Limpopo where fossil fuels are burned continuously to generate electricity, the use of firewood and agricultural burning also take place. This source has been attributed to a mixture of fossil fuel combustion and has contributed 8.76% of the total variance. The sixth component is comprised of Sb and Pd. This source has been attributed to fugitive Pd and explained

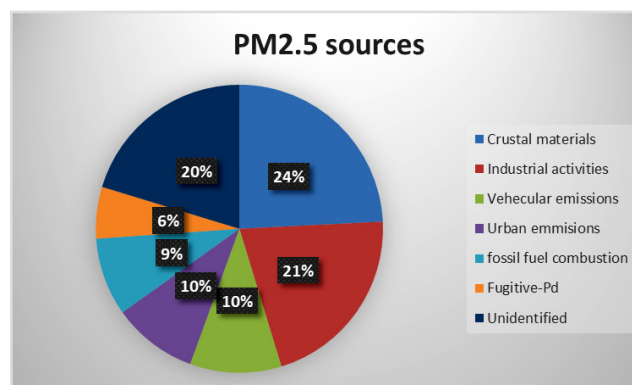
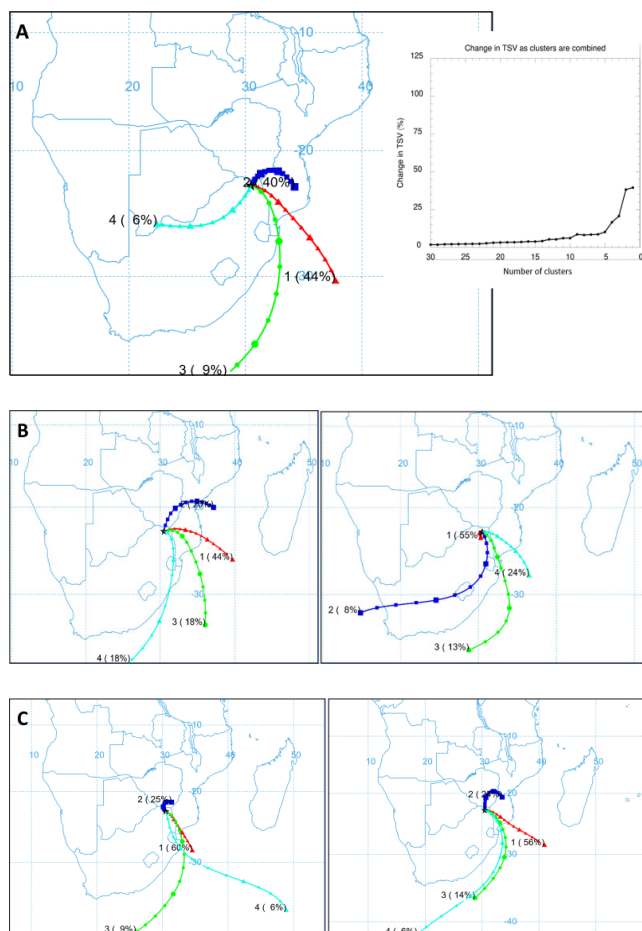


Figure 6: PM<sub>2.5</sub> concentrations sources during summer and autumn in Thohoyandou.

5.80% of the variance. Pd is emitted from mining activities in the bushveld igneous complex (Schouwstra et al., 2000). The approximate sources of PM<sub>2.5</sub> in Thohoyandou during summer and fall are crustal materials re-suspension (24.21%), industrial emissions (21.06%) vehicular emission (10.31%), urban emission (9.56%); fossil fuel combustion (8.76%) and fugitive-Pd (5.80%).

## Long range transport clusters

The clustered backward trajectories are presented in Figure 7 and the corresponding descriptive statistics per cluster are presented in Table 3. Four clusters were used in response to change in total spatial variance (TSV) as clusters are combined (Figure 7A). The clusters are from the Indian Ocean, Inland and recirculation. Cluster 2 (40%) and cluster 4 (6%) are associated with days of high PM<sub>2.5</sub> concentrations (Table 2). The high concentrations of these clusters can be explained by the fact that they are mainly inland, where there are many industrial activities. Cluster 2 is associated with air masses from Mozambique, although they occurred 40% of the time it was associated with days of high concentrations. Hersey, et al., (2015) observed that biomass burning emissions from Mozambique and Zimbabwe reach South Africa. A report by the Department of Environmental Affairs (DEA, 2009) indicated that biomass burning accounts for 20-40% of PM<sub>2.5</sub> concentration, and this explains the high concentration of PM<sub>2.5</sub> associated with air parcels that pass-through Mozambique. Cluster 4 is associated with air parcels from Botswana. DEA, (2009) points that among the air parcels that reach South Africa, there is an Indian plume, Atlantic plume and African plume. It was found that the African plume was associated with high pollutants. This explains the high concentrations associated with cluster 4, which is associated with days that exceeded the daily WHO guideline. Cluster 1 and cluster 3 are of oceanic origin and concentrations were lower on these days. This is because there are fewer emissions over the oceans. Air parcels from the Indian Ocean bring low concentrations of pollutants (DEA, 2009). Cluster 3 spent a lot of time over the ocean and thus, no exceedance, while cluster 1 spent less time and passed through Mozambique this explains the exceedances associated with this cluster. The Mozambican cluster is once again associated with high concentration of PM<sub>2.5</sub>. This emphasizes the high contribution of Mozambique to PM<sub>2.5</sub>



**Figure 7:** All year backward trajectories and TSV plot (A), spring and winter backward trajectories (B), autumn and summer backward trajectories (C) respectively in Thohoyandou, South Africa from April 2017 to April 2018.

concentration in South Africa and shows that there are major sources of  $PM_{2.5}$  in Mozambique that affect the South African air quality that need to be evaluated.

Spring season (Figure 7B left) has 82% (Cluster 1 44%, cluster 2 20% and cluster 3 18%) of backward trajectories originating Indian ocean passing through Mozambique 20% (cluster 2) of the 88% pass through Zimbabwe before reaching South Africa and 18% (cluster 4) of backward trajectories originating from Indian ocean reaching Thohoyandou. Besides different industrial activities these 3 countries have similar meteorological conditions with summer rainfall and spring onset rains and thus, biomass burning an agricultural activity in spring from all these countries has resulted in high concentrations in spring. Winter season (Figure 7B right) had 55% (cluster 1) of the backward trajectories closer to the receptor. This explains the high concentrations measured in winter due to limited dispersion, 8% (cluster 2) of the backward trajectories were from Atlantic Ocean and passed through Lesotho and Mozambique before reaching South Africa. This is because south Africa also experiences Mediterranean climate, with cold fronts approaching from the west coast. And the reimaging 37% (cluster 3 and 4) originated from Indian ocean and passed through Mozambique before reaching the receptor.

**Table 3:** Descriptive statistics of  $PM_{2.5}$  and  $PM_{2.5}$  components per cluster.

	Cluster 1 (44%)	Cluster 2 (40%)	Cluster 3 (9%)	Cluster 4 (6%)
<b><math>PM_{2.5}</math> (<math>\mu\text{g}/\text{m}^3</math>)</b>				
MEAN	9,55	12,42	8,59	12,28
SD	7,04	9,57	6,49	7,45
MIN	1,06	1,83	1,18	4,36
MAX	34,28	37,53	23,16	24,51
<b>Soot (<math>\text{m}^{-1}\cdot 10^{-5}</math>)</b>				
MEAN	0,52	0,85	0,57	0,95
SD	0,33	0,72	0,32	0,46
MIN	0,03	0,05	0,07	0,42
MAX	1,2	2,79	1,03	1,6
<b>BC (<math>\mu\text{g}/\text{m}^3</math>)</b>				
MEAN	0,95	1,48	0,85	1,66
SD	0,81	1,33	0,48	0,89
MIN	0,06	0,03	0,16	0,73
MAX	4,5	5,61	1,63	2,96
<b>UVPM (<math>\mu\text{g}/\text{m}^3</math>)</b>				
MEAN	1,05	1,64	1,33	2,11
SD	0,59	1,12	0,71	0,89
MIN	0,08	0,16	0,36	1,14
MAX	2,4	4,78	2,43	3,31

Autumn season (Figure 7C left) had 69% (cluster 1 and 3) originating from Indian ocean passing through Mozambique, 6% (cluster 4) originating from Indian ocean and 25% originating from Zimbabwe reaching the receptor. Summer season (Figure 7C right) has 76% (cluster 1, 3 and 4) of the clusters originating from Indian ocean passing through Mozambique, this explains the low concentrations measured in this season because tropical cyclones from Indian ocean not only control the prevailing winds but also brings the heavy rainfall with scavenging properties, and the remaining 24% cluster 2) originates in Mozambique pass through Zimbabwe before reaching South Africa. Precipitation has high decreasing effects, despite the similarities in the spring and summer cluster spring had the highest concentration measured while summer had the lowest concentrations.

## Conclusion

This study presented the chemical characterization of  $PM_{2.5}$  in Thohoyandou and further determined the sources of the  $PM_{2.5}$  as well as the long-range clusters. The  $PM_{2.5}$  concentrations were found to be ranging from  $1.06 \mu\text{g}/\text{m}^3$  to  $37.53 \mu\text{g}/\text{m}^3$  with the mean concentrations of  $10.89 \mu\text{g}/\text{m}^3$  over the sampling period. The concentration of  $PM_{2.5}$  was found to be higher than the daily WHO guideline on 9 occasions. The soot, UVPM and BC were found to be having an annual mean of  $0.69 \text{m}^{-1} \cdot 10^{-5}$ ,  $1.40 \mu\text{g}/\text{m}^3$  and  $1.22 \mu\text{g}/\text{m}^3$  respectively. The elemental analysis revealed the dominance of Pd, Sb, Sn, Mg, Al, Si elements. The source apportionment suggested that the  $PM_{2.5}$  could be originating from Crustal materials, industrial, vehicular, urban and biomass

burning emissions. HYSPLIT model showed that air parcel that pass-through Thohoyandou varies seasonally from four to six clusters. The results obtained showed that the air mass passing through Thohoyandou could pose some health effects on communalities living in the area. As such the study recommends the epidemiological studies assessing the health effects of PM<sub>2.5</sub> in Thohoyandou and more routine monitoring of PM<sub>2.5</sub>.

## Acknowledgements

The authors wish to acknowledge the South African Weather Service, for providing meteorological data.

This study was funded by the National Research Foundation grant (CPT160424162937; J. Wichmann was the PI; this study was part of a larger study that also included Cape Town and Pretoria) and supported by South African Department of Higher Education and Training Research incentive funds (W.M Gitari), University of Venda RPC (Grant G196), and NRF scholarship (R.J Novela).

The authors declare no conflict of interest.

## Authors contributions

Novela Rirhandzu (student): Conceptualization, design of the study, data collection and writing - original draft. Gitari Mugera, Chikoore Hector: Supervision, resources, review and editing, funding acquisition. Molnar Peter: Resources, filter analysis for BC and UVPM. Mudzielwana Rabelani: Proof reading and revising manuscript. Wichmann Janine: Conceptualization, design of the study, supervision, resources, review and editing, funding acquisition.

## References

Adeyemi, A., 2020. PM<sub>2.5</sub> chemical composition, source apportionment and geographical origin of air masses in Pretoria, South Africa. Pretoria: University of Pretoria.

Begum, B., Biswas, S. & Hopke, P., 2007. Source Apportionment of Air Particulate Matter by Chemical Mass Balance (CMB) and Comparison with Positive Matrix Factorization (PMF) Model. *Aerosol and Air Quality Research*, 7(4), pp. 446-468. <https://doi.org/10.4209/aaqr.2006.10.0021>.

CCAC, 2019. *Black Carbon*, <https://www.ccacoalition.org/en/slcps/black-carbon>: Climate and clean air coalition.

Cheng, Y. et al., 2015. PM<sub>2.5</sub> and PM<sub>10-2.5</sub> chemical composition and source apportionment near a Hong Kong roadway. *Particology*, 18, pp. 96-104. <https://doi.org/10.1016/j.partic.2013.10.003>.

Cheng, Y. & Yang, L., 2016. Characteristics of Ambient Black Carbon Mass and Size-Resolved Particle Number Concentrations during Corn Straw Open-Field Burning Episode Observations at a Rural Site in Southern Taiwan. *International Journal of Environmental Research and Public Health*. <https://doi.org/10.3390/ijerph13070688>.

Chiloane, K. et al., 2017. Spatial, temporal and source contribution assessments of black carbon over the northern

interior of South Africa. *Atmospheric Chemistry and Physics*, 17, p. 6177-6196. <https://doi.org/10.5194/acp-17-6177-2017>.

DEA, 2009. *State of Air Report 2005. A report on the state of air in South Africa*, Pretoria: Department of Environmental Affairs.

DEA, 2012. *South Africa environment outlook: Air quality draft*, Pretoria: Department of Environmental Affairs.

DEA, 2016. *2nd South Africa Environment Outlook. A report on the state of the environment*, Pretoria: Department of Environmental Affairs.

Draxler, R. & Rolph, G., 2003. *HYSPLIT (HYbrid Single-Particle Lagrangian Integrated Trajectory) model*, Silver Spring: NOAA ARL READY website (<http://www.arl.noaa.gov/ready/hysplit4.html>).

Engelbrecht, J.P., Swanepoel, L., Chow, J.C., Watson, J.G. and Egami, R.T., 2002. The comparison of source contributions from residential coal and low-smoke fuels, using CMB modeling, in South Africa. *Environmental Science & Policy*, 5(2), pp. 157-167. [https://doi.org/10.1016/S1462-9011\(02\)00029-1](https://doi.org/10.1016/S1462-9011(02)00029-1).

Freiman, M. & Piketh, S., 2002. Air Transport into and out of the Industrial Highveld Region of South Africa. *Journal of Applied Meteorology*, 42, pp. 994-1003. [https://doi.org/10.1175/1520-0450\(2003\)042<0994:ATIAOO>2.0.CO;2](https://doi.org/10.1175/1520-0450(2003)042<0994:ATIAOO>2.0.CO;2).

Hersey, S., Garland, R.M., Crosbie, E., Shingler, T., Sorooshian, A., Piketh, S. and Burger, R., 2015. An overview of regional and local characteristics of aerosols in South Africa using satellite, ground, and modeling data. *Atmospheric Chemistry and Physics*, 15, p. 4259. <https://doi.org/10.5194/acp-15-4259-2015>.

Hsu, C., Chiang, H., Lin, S., Chen, M., Lin, T., Chen, Y., 2016. Elemental characterization and source apportionment of PM<sub>10</sub> and PM<sub>2.5</sub> in the western coastal area of central Taiwan. *Science of the Total Environment*, p. 1139-1150. <https://doi.org/10.1016/j.scitotenv.2015.09.122>.

LEDET, 2016.  *Limpopo environmental outlook report*, Polokwane: Department of Economic Development, Environment and Tourism Limpopo.

Lee, S. Liu, W., Wang, Y., Russell, A.G. and Adgeron, E.S., 2008. Source apportionment of PM<sub>2.5</sub>: Comparing PMF and CMB results for four ambient monitoring sites in the southeastern United States. *Atmospheric Environment*, 42, p. 4126-4137. <https://doi.org/10.1016/j.atmosenv.2008.01.025>.

Li, Y. et al., 2019. Morphological characterization and chemical composition of PM<sub>2.5</sub> and PM<sub>10</sub> collected from four typical Chinese restaurants. *Aerosol Science and Technology*, pp. 1186-1196. <https://doi.org/10.1080/02786826.2019.1645292>.

Mohammed, G., K. G. & Mitchell, D., 2017. Trace Elemental Composition in PM<sub>10</sub> and PM<sub>2.5</sub> Collected in Cardiff, Wales. *Energy Procedia*, p. 540-547. <https://doi.org/10.1016/j.egypro.2017.03.216>.

Monlar, P., Tang, L., Sjoberg, K. & Whichmann, J., 2017. Long-range transport clusters and positive matrix factorization

- source apportionment for investigating transboundary PM<sub>2.5</sub> in Gothenburg, Sweden. *Environmental Science Process and Impacts*, 19, pp. 1270-1277. <https://doi.org/10.1039/C7EM00122C>
- Mzezewa, J., Misi, T. & van Rensburg, L., 2010. Characterisation of rainfall at a semi-arid ecotope in the Limpopo Province (South Africa) and its implications for sustainable crop production. *African Journal Online*, 36(1). <https://doi.org/10.4314/wsa.v36i1.50903>.
- Olaniyan, T., Dalvie, M. & Jeebhay, M., 2015. Ambient air pollution and childhood asthma: a review of South African epidemiological studies: allergies in the workplace. *Current Allergy & Clinical Immunology*, 28(2), pp. 122-127.
- Osidele, O., 2016. *An Analysis of Patterns and Trends of Road Traffic Injuries and Fatalities in Vhembe District, Limpopo Province, South Africa*. Thohoyandou: University of Venda.
- Perrino, C. et al., 2011. Chemical characterisation of atmospheric PM in Delhi, India, during different periods of the year including Diwali festival. *Atmospheric Pollution Research*, 2, pp. 418-427. <https://doi.org/10.5094/APR.2011.048>.
- Petkova, E., Jack, D., Volavka-Close, N. & Kinney, P., 2013. Particulate matter pollution in African cities. *Air Quality, Atmosphere & Health*, 6(3), pp. 603-614. <https://doi.org/10.1007/s11869-013-0199-6>.
- Rizzo, M. & Scheff, P., 2007. Fine particulate source apportionment using data from the USEPA speciation trends network in Chicago, Illinois: Comparison of two source apportionment models. *Atmospheric Environment*, 41, p. 6276-6288. <https://doi.org/10.1016/j.atmosenv.2007.03.055>.
- Sammaritano, M., Bustos, D., Poblete, A. & Wannaz, E., 2018. Elemental composition of PM<sub>2.5</sub> in the urban environment of San Juan, Argentina. *Environmental Science and Pollution Research*, p. 4197-4203. <https://doi.org/10.1007/s11356-017-0793-5>.
- Santanna, F. et al., 2016. Elemental composition of PM<sub>10</sub> and PM<sub>2.5</sub> for a Savanna (Cerrado) region of Southern Amazonia. *Química Nova*, pp. 1170-1176. <https://doi.org/10.21577/0100-4042.20160154>.
- Satsangi, P. & Yadav, S., 2014. Characterization of PM 2.5 by X-ray diffraction and scanning electron microscopy-energy dispersive spectrometer: its relation with different pollution sources. *International Journal of Environmental Science and Technology*, 11(1), pp. 217-232. <https://doi.org/10.1007/s13762-012-0173-0>.
- Schouwstra, R., Kinloch, E. & Lee, A., 2000. A short geological review of the Bushveld complex. *Platinum metals Review*, 44(1), p. 33.
- SSA, 2012. *Census 2011*, Pretoria: Stats SA Library Cataloguing-in-Publication (CIP) Data.
- Tai, A., Mickley, L. & Jacob, D., 2010. Correlations between fine particulate matter (PM<sub>2.5</sub>) and meteorological variables in the United States: Implications for the sensitivity of PM<sub>2.5</sub> to climate change. *Atmospheric Environment*, 44, pp. 3976-3984. <https://doi.org/10.1016/j.atmosenv.2010.06.060>.
- Tang, L. et al., 2014. Estimation of the long-range transport contribution from secondary inorganic components to urban background PM<sub>10</sub> concentrations in south-western Sweden during 1986-2010. *Atmospheric Environment*, 89, pp. 93-101. <https://doi.org/10.1016/j.atmosenv.2014.02.018>.
- Valsamakis, S., 2015. *Ambient air quality monitoring: a comparison between two urban parks in Soweto, South Africa*. Johannesburg: University of Witwatersrand.
- Van Zyl, P. et al., 2014. Assessment of atmospheric trace metals in the western Bushveld Igneous Complex, South Africa. *South African Journal of Science*, 110(3/4). <https://doi.org/10.1590/sajs.2014/20130280>.
- Wang, J. & Ogawa, S., 2015. Effects of Meteorological Conditions on PM<sub>2.5</sub> Concentrations in Nagasaki, Japan. *International Journal of Environmental Research and Public Health*, 12, pp. 9089-9101. <https://doi.org/10.3390/ijerph120809089>.
- WHO, 2014. *Seven million premature deaths annually linked to air pollution*, <http://www.who.int/mediacentre/news/releases/2014/air-pollution/en/>: WHO.
- WHO, 2016. *Sustainable Development Goals: Health and Health Related Targets*, [http://www.who.int/gho/publications/world\\_health\\_statistics/2016/EN\\_WHS2016\\_Chapter6.pdf](http://www.who.int/gho/publications/world_health_statistics/2016/EN_WHS2016_Chapter6.pdf): WHO.
- Wichmann, J. et al., 2014. The effect of secondary inorganic aerosols, soot and the geographical origin of air mass on acute myocardial infarction hospitalisations in Gothenburg, Sweden during 1985-2010: a case-crossover study. *Environmental Health*, 13(1), p. 61. <https://doi.org/10.1186/1476-069X-13-61>.
- Xia, L. & Gao, Y., 2011. Characterization of trace elements in PM<sub>2.5</sub> aerosols in the vicinity of highways in northeast New Jersey in the U.S. east coast. *Atmospheric Pollution Research*, pp. 34-44. <https://doi.org/10.5094/APR.2011.005>.
- Yu, L. et al., 2013. Characterization and Source Apportionment of PM<sub>2.5</sub> in an Urban Environment in Beijing. *Aerosol and Air Quality Research*, 13, p. 574-583. <https://doi.org/10.4209/aaqr.2012.07.0192>.
- Zhang, R., Fu, C., Han, Z. & Zhu, C., 2008. Characteristics of elemental composition of PM<sub>2.5</sub> in the spring period at Tongyu in the semi-arid region of Northeast China. *Advances in Atmospheric Sciences*, p. 922-931. <https://doi.org/10.1007/s00376-008-0922-7>.
- Zhang, R. et al., 2013. Chemical characterization and source apportionment of PM<sub>2.5</sub> in Beijing: seasonal perspective. *Atmospheric Chemistry and Physics*, Volume 13, p. 7053-7074. <https://doi.org/10.5194/acp-13-7053-2013>.

## Appendix

### A1: Gravimetric analysis

#### A1.1 Weighing procedure: reference and sample filters

1. Download logged data from data-logging environmental monitor
2. Check if environmental conditions in the laboratory was maintained for the previous 24 hours within the prescribed limits
  - Dry air temperature =  $21 \pm 1.0^\circ\text{C}$
  - Relative humidity =  $50 \pm 5\%$
3. Record environmental conditions immediately prior to weighing reference filters
4. Ensure balance is level
5. Weigh a mass of 2 grams repeatedly until repeatability is reached
6. Close balance doors and tare the balance
7. Open the balance doors and place three reference (control) filters on the weighing grid. Note: use 3 reference (control) filters for each 10 sample filters.
8. Close balance doors and start count down timer
9. Allow 30 seconds for balance to stabilize
10. Note reading on the balance immediately when settling time has expired
11. Remove reference (control) filters from the weighing chamber and hold it next to the weighing chamber. Take care not to breath over the filters
12. Close the balance door and wait for balance to return to zero
13. If balance does not return to zero:
  - Discard all weighing results
  - Inspect the balance pan for dust or any other obstacle
  - Tare the balance
  - Reweigh filters
  - Balance should not otherwise be tarred between weighing filters
14. Follow steps 7-13 to obtain 3 consecutive weights for the 3 reference (control) filters
15. Proceed to weigh 10 individual sample filters by following the above procedure (steps 7-13)
16. After weighing the 10 sample filters, weigh the 3 reference filters again using steps 7-13
17. Record environmental conditions immediately after weighing reference filters
18. If the maximum and minimum weight of reference filters differ more than 1% from average, discard results and re-weigh
19. Place weighed filters with a clearly marked support pad in a clean filter cassette holder

#### A1.2 Measuring concentrations

After sampling filters were conditioned for 24 hours and weighed under the same conditions.

Mass of the particulate matter was calculated using the same formulae:

$$M_{pm} = (m_o - m_f) - m_b \quad (1)$$

$M_{pm}$  = mass of the particulate matter,  $m_o$  = initial mass of the filter,  $m_f$  = final mass of the filter,  $m_b$  = mass of the blank filter.

The volume of air sampled was calculated using the following formulae:

$$V_a = Q_{ave} \times t \times 10^{-3} \quad (2)$$

$V_a$  = volume of the air sampled,  $Q_{ave}$  = average flow rate,  $t$  = time elapsed.

Then the concentration of  $\text{PM}_{2.5}$  was calculated using the following formula:

$$PM_{2.5 \text{ conc}} = \frac{M_{pm}}{V_a} \quad (3)$$

EEL43 reflectometer was used to measure soot. Absorption coefficients (prosy for soot) was expressed in  $\text{m}^{-1}10^{-5}$  (SOP RUPIOH 4.0, 2002) calculated using the following formulae:

$$a = \left[ \left( \frac{A}{2V} \right) \times \ln \left( \frac{R_o}{R_s} \right) \right] \quad (4)$$

(A-The loaded filter area, V-sampled volume,  $R_o$ -reflection of primary control filter,  $R_s$ -Reflectance of the sampled filter).

ATNIR and ATN UV were measured using a Model OT21 Optical Transmissometer (Magee Scientific Corp., Berkeley, California, USA). Thereafter used to calculate BC and UVPM using the following formulae;

$$BC \text{ Density} = \frac{ATN \text{ IR}}{\text{Sigma}_{BC}} \quad (5)$$

$$\text{Total BC} = \text{density} \times \text{Area} \quad (6)$$

$$BC = \frac{\text{Total BC}}{V_a} \quad (7)$$

$$UVPM \text{ Density} = \frac{UV \text{ ATN}}{\text{Sigma}_{UV}} \quad (8)$$

$$\text{Total UVPM} = \text{density} \times \text{Area} \quad (9)$$

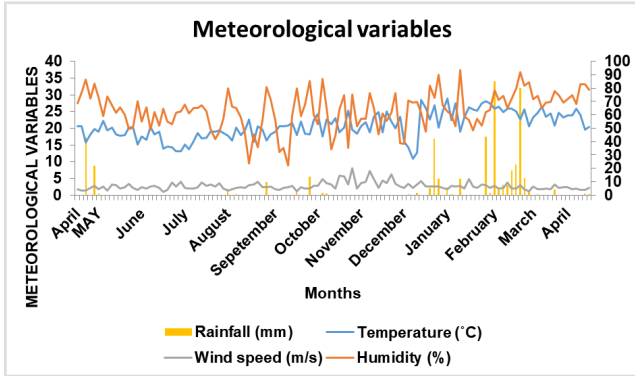
$$UVPM = \frac{\text{Total UVPM}}{V_a} \quad (10)$$

The elemental mass concentration obtained from wavelength dispersive X-ray fluorescence (WD-XRF) spectrometer (PANALYTICAL AXIOSMAX) analysis given in  $\mu\text{g}\cdot\text{cm}^{-2}$  and converted to  $\mu\text{g}\cdot\text{m}^{-3}$  using the following formulae:

$$EM = \frac{(EM_f - EM_b) A}{V_a} \quad (11)$$

EM = elemental mass concentration,  $EM_f$  = elemental concentration of the exposed filter,  $EM_b$  elemental concentration of blank filter.

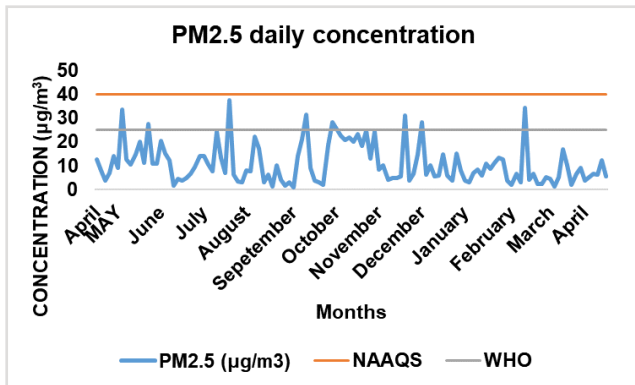
### A2: Meteorological variables for the whole study period April 2017- April 2018



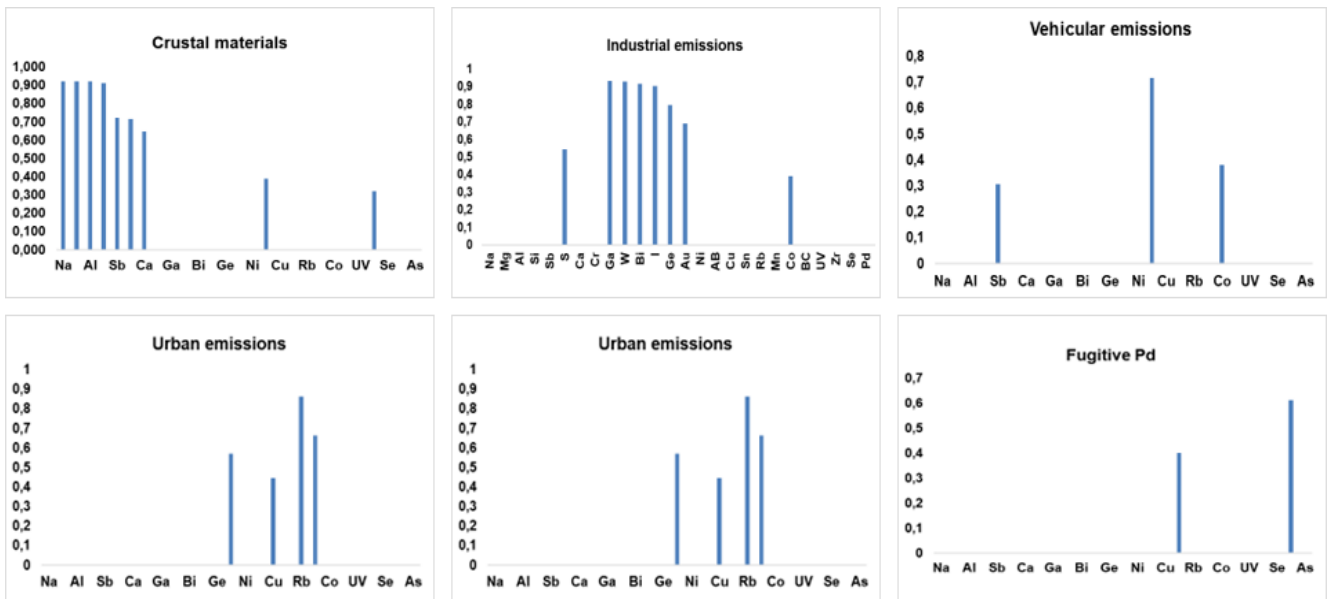
### A4: Monthly average concentrations of the 24 detected elements (ng/m<sup>3</sup>)

	December	January	February	March	April
Ca	0,17	0,46	0,06	0,13	0,07
Cr	0,00	0,00	0,92	0,74	0,72
Mn	0,00	0,00	1,37	1,03	0,90
Co	0,15	0,07	0,11	0,01	0,09
Ni	0,04	0,00	0,19	0,22	0,36
Cu	0,04	0,11	0,40	0,43	0,34
Ga	0,58	0,34	0,16	0,15	0,04
Ge	0,56	0,36	0,00	0,07	0,07
As	0,12	0,40	0,16	0,14	0,29
Se	0,07	0,10	0,34	0,53	0,30
Rb	0,03	0,05	0,41	0,47	0,22
Zr	0,18	0,54	0,23	0,26	0,14
Pd	3,01	3,02	2,21	3,59	9,49
Sn	3,88	0,58	1,72	9,83	6,81
Sb	9,72	9,17	2,16	0,52	0,00
I	1,33	1,12	0,44	0,32	0,11
W	1,59	1,26	0,75	1,00	0,59
Au	0,64	0,33	0,75	0,69	0,10
Bi	1,82	1,10	0,61	1,18	0,64
Al	0,26	0,74	0,03	0,04	0,07
Mg	0,85	2,54	0,12	0,09	0,06
Na	10,84	13,87	0,11	0,17	0,31
S	2,20	2,28	0,01	0,01	0,00
Si	0,72	2,10	0,01	0,02	0,03

### A3: PM<sub>2.5</sub> concentrations against WHO guideline and NAAQS standards for the whole study period April 2017- April 2018



### A5: Principal component factor analysis



## AQT400 SERIES AIR QUALITY MONITOR



Measures 4 pollutant gases.

Available gases: NO<sub>2</sub>, NO, CO, O<sub>3</sub>, SO<sub>2</sub>, and H<sub>2</sub>S

Temperature, Relative Humidity, Barometric Pressure

Intelligent algorithms that compensate for Environmental conditions and for the ageing of the sensor element.

Low power consumption (typically 0.5 W).

Wireless Internet connection with Vaisala Multi-Observation Gateway MOG100 to the Cloud.

RS-232 and RS-485 interfaces for local connectivity (such as Modbus support).

Easy integration and open API.

Solar Power option available.

AQT410 for gases only and AQT420 for gases and particulates. The AQT is available in 3 different gas configurations plus PM<sub>10</sub> and PM<sub>2.5</sub>.

- NO<sub>2</sub>, NO, O<sub>3</sub>, and CO
- NO<sub>2</sub>, O<sub>3</sub>, CO, and SO<sub>2</sub>
- NO<sub>2</sub>, CO, SO<sub>2</sub>, and H<sub>2</sub>S

The measurement performance of AQT400 series is based on proprietary advanced algorithms that enable parts per billion (ppb) measurements at an affordable price by using electrochemical sensors.

The algorithms compensate for the impact of ambient conditions and aging on the sensor elements and remove the need for costly gas sampling and maintenance equipment.

Easy to Deploy in Networks

AQT400 series is specifically designed for air quality monitoring networks in urban areas, road networks, or around industrial sites and transportation hubs.

Thanks to its small weight and compact size, it is ideally suited for deployment even in large air quality networks. The measurement data is sent wirelessly to a web-based database with a gateway solution or is available locally through a serial interface.

Depending on local conditions, AQT400 series devices have a maintenance and calibration interval of 12/ 24 months

**T: 011 4767323**

**[www.envirocon.co.za](http://www.envirocon.co.za)**

**[sales@envirocon.co.za](mailto:sales@envirocon.co.za)**

# Research article

## Morphology and elemental analysis of freshly emitted particles from packed-bed domestic coal combustion

Masilu Daniel Masekameni<sup>1\*</sup>, Tafadzwa Makonese<sup>3</sup>, Isaac Tebogo Rampedi<sup>2</sup>,  
Goitsewang Salvation Keretete<sup>1</sup>

<sup>1</sup>Occupational Health Division, School of Public Health, Faculty of Health Sciences, University of the Witwatersrand, South Africa

<sup>2</sup>Department of Geography, Environmental Management and Energy Studies, University of Johannesburg, Johannesburg, South Africa

<sup>3</sup>Process, Energy & Environmental Technology Station, Faculty of Engineering and the Built Environment, University of Johannesburg, Johannesburg, South Africa

\*Correspondence: daniel.masekameni@wits.ac.za

Received: 18 July 2020 - Reviewed: 1 September 2020 - Accepted: 30 November 2020

<https://doi.org/10.17159/caj/2020/30/2.8582>

### Abstract

This study was conducted in a laboratory-controlled environment to analyse the physical properties and elemental composition of coal combustion particles in a brazier. Particles were sampled ~1 m above the stove, using a partector. Particles were collected on gold transmission electron microscopy (TEM) grids, and polycarbonate filters for TEM and inductively coupled plasma mass spectrometry (ICP-MS) analysis, respectively. Particles for elemental analysis were collected on a 37 µm polycarbonate filter, and the exhaust was drawn in using a GilAir Plus pump. During sampling, a 2.5 µm cyclone was attached to the sampling cassette to isolate larger particles. Combustion particles emitted during the early stage of combustion were single organic spherical particles with similar characteristics to tarballs. As the combustion progressed, the particle diameter gradually decreased (from 109 nm), and the morphology changed to smaller particles (to 34.3 nm). The particles formed accretion chain structures, showing evidence of agglomeration. Furthermore, a fluffy microstructure, resembling the formation of soot, was formed in the post flaming phase. In the char-burning phase, an irregular structure of semi-spherical particles was formed, showing evidence of mineral particles infused with small carbonaceous particles. Similarly, with the findings of previous studies, the present research also observed organic spherical particles similar to tarballs. Given that during the ignition phase there was a simultaneous burning of wood as kindling and coal, the provenance of these particle emissions can be attributed to both coal and wood.

### Keywords

physical properties, D-grade coal, brazier, transmission electron microscopy, inductively coupled mass spectrometry, elemental composition

### Introduction

Despite efforts to reduce dependence on solid fuel, more than 3 billion people continue to burn coal and wood for cooking and space heating (Naeher et al., 2007; Gordon et al., 2014). Small diameter (< 2.5 µm) particulate matter has been singled out as posing a significant threat to both the environment and human health. Suspension of fine particles has been associated with household emissions from wood and coal burning (Mc Donald and Biswas, 2004; Chafe et al., 2015).

Several epidemiological studies have shown that particles below PM<sub>2.5</sub> are strongly associated with infection of the lower respiratory tract, cardiovascular system disruption, and morbidity (Lim et al., 2012, 2013). Despite severe health

effects, the source to exposure mechanisms from domestic coal and wood-burning has not yet been established. Researchers recommend that an understanding of particle evolution from its point of release to the microenvironment of the receptor is important for source and hazard mapping (Shen et al., 2013; Torvela et al., 2014). Therefore, the correct determination of the physicochemical properties of coal/ wood emissions particles is essential for source identification and characterisation. However, very few studies have been conducted on the physicochemical properties of particles emitted from small scale coal combustion technologies, even though significant associated health risks have been reported in countries such as China, India and Finland (Niemi et al., 2006; Wilkinson et al., 2009; Zhang and Tao, 2009).

Characterisation of the organic fractions emitted from domestic coal-burning technologies has been reported globally (Bazilian et al., 2012; Zhang et al., 2012). However, very few studies have focused on the characterisation of trace elements emitted from residential coal burning (Bazilian et al., 2012; Silva et al., 2012). Studies conducted in China have reported possible health effects of trace elements emitted from residential coal burning (Smith et al., 2014; Zhang, Zou, et al., 2018). In 2004 it was reported that, in Guizhou province, more than 3 000 people had suffered arsenic poisoning, bone deformation, human selenosis and fluorosis because of exposure to residential coal burning (Finkelman, 2004; Zhou et al., 2015). Furthermore, it was established that the health effects of trace elements from coal-burning vary according to the properties of the coal, and exposure scenarios (Masekameni, Makonese and Annegarn, 2014; Zhang, Zou, et al., 2018). In South Africa, especially in the central plateau of the Highveld region, coal burning, using unvented stoves, continues to be a significant source of energy for domestic cooking and heating (Balmer, 2007; Makonese et al., 2017). Efforts to reduce dependence on coal at the domestic level in South Africa have been commissioned, although they have not yet been fully implemented (Bonjour et al., 2013; GroundWork, 2016).

Household air pollution inventories in South Africa are limited due to inadequate data from source apportionment studies. Only a few studies used scanning electron microscopy (SEM) to confirm the physical properties of particles emitted from domestic coal and wood burning. Nevertheless, data generated from SEM analysis are not sufficient for source apportionment. Contrary to SEM, transmission electron microscopy (TEM) analysis is considered to provide a better characterisation of the internal structures of particles and is the preferred method for studying the shape and morphology of aerosol particles (Schneider et al., 2006; Gwaze, 2007).

Equipped with energy dispersive X-ray (EDX) or electron energy loss (ELL) spectroscopy, the instruments provide information about the elemental composition of the analysed particles (Nussbaumer et al., 2001). For TEM, very thin grids (often copper/gold), coated with a carbon or gold film are used. The quality of the film is essential to obtain good resolution (Mathis et al., 2005). If samples are used for quantitative analysis (e.g. the size distribution), care must be taken to have defined size fractions during the sampling process (Nussbaumer et al., 2001; Bond et al., 2006). In addition to particle morphology, the correct identification and determination of the elemental composition rely on the use of effective analytical techniques. Inductively coupled mass spectrometry (ICP-MS) has been widely used to study the elemental composition of combustion particles. In this study, we analysed the physical properties and selected elemental composition (Na, Mg, Al, Si, K, Ca, Ti, V, Cr, Mn, Fe, Co, Ni, Cu, Zn) of particles generated during residential coal burning during three combustion phases (ignition, flaming and coking).

Currently, in South Africa, several studies on emissions from industries are underway, but there are limited studies to

apportion the contribution of domestic coal/wood burning to air pollution. Our study aimed to examine the morphology and chemical analysis of particles emitted during the combustion of D-grade coal, during three combustion phases (ignition, flaming and char burning), to determine the source contribution of particulate matter and to further our understanding of pollutant source distribution.

We used lumps of D-grade type coal that were burned in a high-ventilated stove and lit with a top-lit updraft (TLUD) ignition method in three combustion phases (ignition, flaming and char burning). The limitation of D-grade coal was fostered, as it is the most common fuel available in the informal settlements and townships of South Africa. D-grade coal is considered poor quality coal with ash content of over 14%, carbon content of 55% and volatiles at about 25%.

## Materials and methods

### Experimental stove and fuel analysis

D-grade coal was burned in a high-ventilated stove lit using a Top-lit Updraft (TLUD) ignition method in a laboratory-controlled environment. Particles emitted during three combustion phases (ignition, flaming and char burning) were analysed. Due to variations of field-based factors, several variables were kept constant (i.e. ventilation rates, the position of the fuel grate inside the stove, size of coal lumps, ignition method and kindling fuel). The stove characteristics are shown in Figure 1.

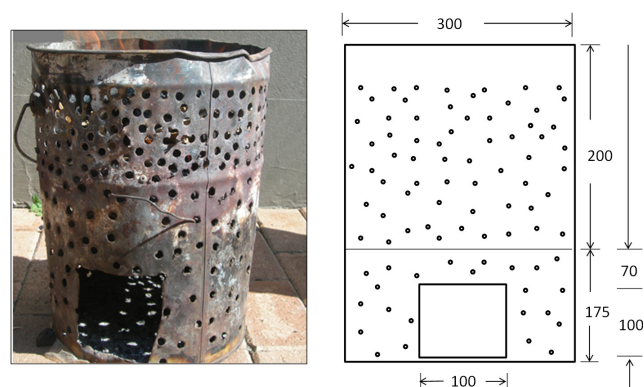


**Figure 1:** A photograph and schematic representation of a high ventilation field purchased brazier stove used in the experiments (Not drawn to scale – dimensions are in mm).

Coal particle size was determined by sieving the coal using a 40 mm x 60 mm diameter mesh. The coal was analysed by Bureau Veritas Inspectorate Laboratories (Pty) Ltd., using the standard methods. Experimental results are based on the proximate and ultimate air-dried D-grade coal analyses (Table 1).

During the TLUD ignition method, 2 500 g of coal were placed on the grate, followed by 35 g of paper, 400 g of wood kindling, and another 1 500 g of coal. Details on the division of the combustion phases, fuel properties and ignition method are detailed in a previous paper (Masekameni et al., 2018).

**Table 1:** Proximate and ultimate analysis values for the coal (merchants and colliery) on an air-dried basis

Parameter (air-dried basis)	Standard method	Slater mine D-grade coal
Moisture content (%)	ISO 5925	1.8
Volatiles (%)	ISO 562	20.3
Ash (%)	ISO 1171	24.2
Fixed carbon (%)	By difference	57.5
Calorific value (MJ kg <sup>-1</sup> )	ISO 1928	23.4
Calorific value (Kcal kg <sup>-1</sup> )	ISO 1928	5590
Total sulphur (%)	ASTM D4239	0.63
Carbon (%)	ASTM D5373	62.6
Hydrogen (%)	ASTM D5373	2.76
Nitrogen (%)	ASTM D5373	1.0
Oxygen (%)	By difference	5.0
Total silica as SiO <sub>2</sub> (%)	ASTM D4326	58.6
Aluminium as Al <sub>2</sub> O <sub>3</sub> (%)	ASTM D4326	27.6
Total iron as Fe <sub>2</sub> O <sub>3</sub> (%)	ASTM D4326	6.63
Titanium as TiO <sub>2</sub> (%)	ASTM D4326	0.82
Phosphorous as P <sub>2</sub> O <sub>5</sub> (%)	ASTM D4326	0.55
Calcium as CaO (%)	ASTM D4326	2.30
Magnesium as MgO (%)	ASTM D4326	0.83
Sodium as Na <sub>2</sub> O (%)	ASTM D4326	0.42
Potassium as K <sub>2</sub> O (%)	ASTM D4326	0.79
Sulphur as SO <sub>3</sub> (%)	ASTM D4326	1.10
Manganese as MnO <sub>2</sub> (%)	ASTM D4326	0.12

## Particle sampling

Particles were collected on TEM gold grids and polycarbonate membrane filters, for TEM and ICP-MS analyses, respectively. The gold grids were placed on a grid holder from the partector aerosol dosimeter TEM sampler (Naneos particle solutions, Switzerland), and the particles were deposited directly onto the grid. The sampling train included a Teflon tube, connecting the partector inlet to the sampling cassette that was fitted with a 2.5 µm cyclone, with a PM4 cutoff point at 50%. The partector was set at a flow rate of 2.8 L/minute, according to the cyclone's specification. Sampling for inductively coupled plasma Mass spectrometry (ICP-MS) was done using polycarbonate membrane filters (37 mm diameter). The exhaust was drawn onto the membrane filter inside a cassette, using a GilAir Plus pump (Model) set at a flow rate of 2.2 L/minute. The filters were changed at the start of each combustion phase (ignition, flaming and char burning/coking).

### Preparation of filters

A total of 12 (four samples for each combustion phase), 37 mm diameter polycarbonate membrane filters, with a pore size of 0.08 µm, were stored in a controlled laboratory environment before sampling campaign. The temperature ranged from 22 – 23 °C and the humidity was recorded as 35 %. The filters were conditioned for 24 hours and pre-weighed, using a Sartorius

electronic microbalance (model CPA225D, supplied with a balance pan) with a minimum resolution of 0.001 mg and a precision of 0.001 mg. The same procedure was repeated after a three-hour burn sequence of sampling particulate matter was completed. A field blank was handled in the same way as the field filter. However, the field blank was not exposed to the particulate matter. The objective of using a field blank is to overcome or account for moisture loss due to meteorological conditions, particularly during transportation and contamination when handling the filters. The determination of the final mass was calculated using equation 1.

$$\text{Final mass} = \text{Field filter (post-pre)} + \text{field blank (post-pre)} \quad (1)$$

where the field filter (post) mass is the mass collected from the filter after sampling while the field pre-mass is the mass recorded before sampling. The field blank 'post' and 'pre' are the masses recorded after and before transportation of the filters, respectively.

### Inductively coupled mass spectrometry

The sample filters for ICP-MS analysis were folded and placed inside pre-cleaned microwave digestion vessels; about 9 mL supra pure (Merc) nitric acid (HNO<sub>3</sub>) and 1 mL supra pure (Merc) hydrogen peroxide (H<sub>2</sub>O<sub>2</sub>) were added to each vessel. A reagent blank was included with the batch as a control. The vessels were closed and placed in a Mars 6 microwave. The digestion method made the vessels ramp to 200 °C for 20 minutes, and hold the temperature for another 15 minutes. The samples were then quantitatively transferred to 50 mL volumetric flasks and made up to the mark using 18.2 M Ω /cm ultrapure water. Calibration standards of 0 µg/L, 0.1 µg/L, 0.5 µg/L, 1.0 µg/L, 5.0 µg/L and 10 µg/L were prepared from 100 mg/L NIST traceable stock standards. The samples were then filtered using a 0.45 µm syringe filter and diluted 10 times (1 ml diluted to 10 ml) before analysis by ICP-MS. The blank filter analysis, using the ICP-MS technique, was carried out in the same manner as the sample filters. Since our samples were mostly carbon from a combustion process, we did not use hydrogen fluoride (HF) which is often used in dissolving samples of non-carbonaceous nature. For quality assurance, the instruments were optimized with a tune solution before analysis and calibrated with NIST traceable standards.

In this study, we noted that ICP-MS is a sensitive technique and that caution should be exercised when analysing samples. Many sources can contribute to the overall accuracy and precision of the analysis. Therefore, internal standards with a mass number close to that of the analyte element(s) were used to minimise errors inherent in the analytical method. The internal standards assist to correct for matrix differences between calibration standards and samples. Since samples can easily suffer from Easy Ionizable Elements (EIE) effect, the loss of ionization efficiency can be corrected. Moreover, imprecision arising from small variations in dilutions can also be corrected. The correction procedure followed in this study is similar to that detailed in Vanhaecke et al. (1992).

### Transmission electron microscopy (TEM)

Combustion smoke particles were imaged for their morphologies, using JEM-2100, in a multipurpose, 200 kV analytical electron microscope, at the University of Johannesburg, South Africa (Jeol Ltd from Akishima, Tokyo, Japan, manufactures the instrument). TEM has been used to study the semi-structure especially respirable particles, in contrast to optical microscopy, which uses light as an illumination source for imaging. TEM uses electrons which provide an opportunity to separate arrangements of atoms in small structure/ combustion soot aggregates (Kocbach et al., 2005; Wang et al., 2018). TEM combines the JEM-2100 optic system with an advanced control system for ease of operation.

### Physical properties of coal emissions

In an earlier study, Masekamani et al. (2018) reported physical properties of coal emissions particles for similar combustion activities. Particle size distribution (PSD) of around 109 nm, 54 nm and 31 nm for the ignition, flaming and coking phase were reported respectively (Table 2). The particle morphology shown by Masekamani et al. (2018), suggests that particle diameter was larger at the ignition phase and gradually decreased as the combustion process progressed.

**Table 2:** PSD of coal emission particles in a brazier

Phase	Duration (minutes)	GMD (nm)	GSD (nm)
Entire Combustion Sequence	180	51.9	2.1
Ignition	20	109.8	18.4
Flaming	60	54.9	5.9
Coking	100	34.3	5,1

## Results and discussion

### Morphology of coal particles from TEM analysis

#### Morphology of smoke particles emitted during the ignition phase

The morphology of particles observed using a TEM for the ignition phase shows giant single spherical particles. Moreover, we used TEM analysis to study and distinguish different smoke particle morphologies similar to previously conducted studies (Pósfai et al., 2004; Chakrabarty et al., 2010; Tóth et al., 2014a). Figure 2 shows the morphology of smoke particles emitted during the ignition phase of coal combustion.

Figure 2a shows a spherical organic particle, with the characteristics of tarballs, collected from low-temperature combustion during the ignition phase. Emission of spherical organic particles is synonymous with smouldering combustion conditions. This suggests that the spherical particles are emitted because of low-temperature combustion. Posfai et al. (2003) contended that these carbonaceous particles are formed in smouldering fires and that they increase in abundance in the atmosphere as the smoke plume ages.

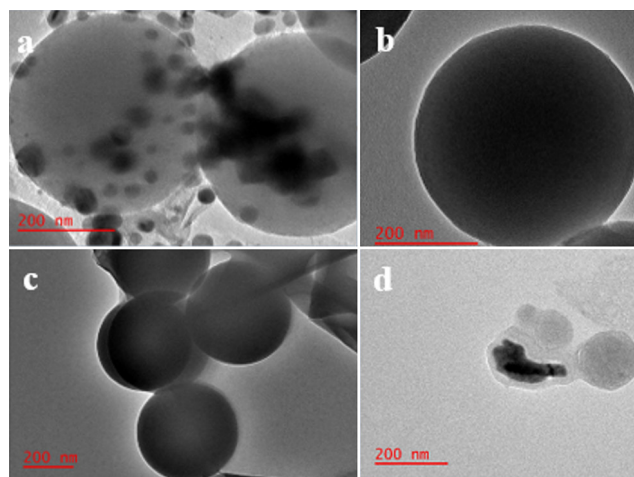


**Figure 2:** TEM images of particles emitted during the ignition phase of coal combustion. a) carbonaceous spherical particle, b) internal structure of spherules with evidence of aggregates, c) onion-like structured soot particles, d) single-particle exposed to high beam resolution.

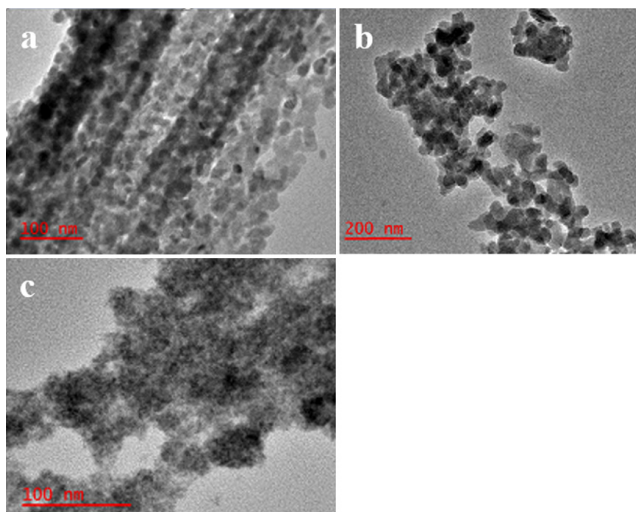
Furthermore, Posfai et al. (2004) reported similar morphologies to the ones reported in this study. However, the source contribution in their study was veld fires, which are often dominated by biomass burning. Figure 2b shows large organic spherical particles infused with diffusion accretion chains, forming soot. It was observed that, since these particles were collected at 1 m above the stove, the morphology might change with an increase in the height of sampling due to ageing of the particles.

Figure 2c shows particle growth as the spherical organic particles fuse, probably due to collision. Thajudeen et al. (2015) suggested that particle-particle collision is the dominant particle growth mechanism during combustion, even though the particles may restructure or rearrange after the collision and fail to coalesce. Particles with similar morphologies to those found in our study were observed from biomass burning fires (Shraim et al., 2003; Thajudeen, Jeon and Hogan, 2015). Figure 2d shows the onion-like structure of emitted organic particles, with disordered graphic layers, observed in the high-resolution TEM image.

Spherical organic particles shown in Figure 2 indicate a homogeneous structure (spherical), showing darker and lighter areas under TEM. The spherical organic particles have properties similar to tarballs produced during biomass burning. Similar morphologies were observed in previous studies (Pósfai et al., 2003; Tóth et al., 2014a). However, the literature suggests that tarballs are only released as a consequence of smouldering wood-burning fires. Several scholars have reported that tarballs are not emitted during coal or oil combustion (Pósfai et al., 2003; Tissari et al., 2008; Tóth et al., 2014b, 2014a).

#### Morphology of coal particles emitted during the flaming phase

During the flaming phase, particle diameter (54.9) was smaller than that during the ignition phase (Figure 3a, 3b and 3c). The



**Figure 3:** TEM images of carbonaceous particles emitted during the flaming phase- a) carbonaceous soot particles showing as aggregates, b) a more established and well-arranged accretion chain, c) fluffy microstructure, resembling soot particles, d) single-particle exposed to high beam resolution.

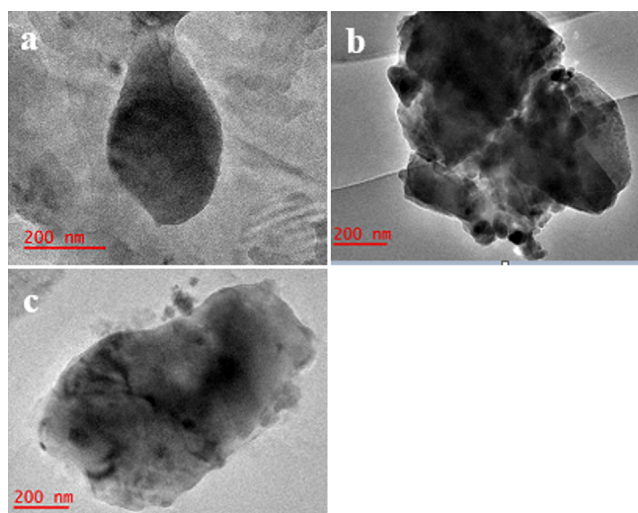


**Figure 4:** TEM images of particles emitted during the char burning phase- a) irregular structure of semi-spherical particles, b) mineral particles infused with small carbonaceous particles, c) a fully established macrostructure, indicating the presence of non-water soluble compounds.

formation of the spherical particles during ignition is thought to be influenced by the release of polar compounds from smouldering fires. During flaming, fewer polar compounds, which affect particle growth, are emitted than during the ignition stage (Pósfai et al., 2004). The particles observed, using TEM, resemble fused small particles with diffusion accretion chains that have characteristics similar to soot (Figure 3 a, b and c). Soot contains aggregates of small particles often less than 60 nm in the diameter. A morphology similar to the present study was reported from a study in Guizhou Province, China (Shraim et al., 2003). However, the researchers who conducted that study investigated the morphology of particles in ageing smoke, from a wood fire. It is important to note that, in the study reported in this paper, the images were obtained from freshly produced particles. A well-arranged morphology, consisting of single

particles, can be seen in figure 3b. Other researchers have also reported that the particle diameter decreases as the combustion conditions progress (Niemi et al., 2006).

Shraim et al. (2003) and Posfai et al. (2004) reported that there was an increase on the number of tar balls in samples collected at further distances from the emitting source, suggesting that there was particle growth because of condensation of organic gases, or transformation due to collision with other organic atmospheric particles. In our study, we have shown a mechanism to which particles transform as the combustion progresses (Figure 3c). We established that, as coal heats up, it swells and cracks. It is through these cracks that organic particles are released and, depending on the ignition method and combustion conditions, a brown to thick white plume is evident, which may pass through a cold zone above the burning coal into the ambient air. We previously demonstrated that, as combustion progresses, fine particles, often enriched with low volatile organic gases, are emitted (Masekameni et al., 2018). Furthermore, particle growth is as a result of the water injection in the coal and which is released as water vapour during coal pyrolysis (Chang et al., 2004). Therefore, accretion chains may be caused by coagulation of particles emitted during the flaming phase (Makonese, 2015; Makonese, Masekameni and Annegarn, 2017). As the coal fully pyrolyze, fluffy microstructures are formed, which have the same characteristics as soot particles.

In summary, the findings from our study build on the work of Makonese (2015) and Toth et al. (2014b), who recommended that further studies be conducted to affirm the existence of spherical organic particles, tarballs and related particle formation mechanisms in domestic combustion processes. We confirm that spherical organic particles with similar characteristics to tarballs are emitted as a consequence of smouldering combustion conditions. In this study, we have demonstrated that residential coal burning may be a source of - spherical organic particle-like tarball emissions. However, since wood kindling was used during the ignition phase, it might be that some of the emissions of the spherical organic particles similar to tarballs could have been released from the simultaneous combustion of wood kindling and coal.

### Morphology of coal particles emitted during the char burning phase

Figure 4 shows images of particles collected during the char burning stage of coal-combustion, in a typical brazier used in South African informal settlements. During the char-burning phase, almost all volatile organic compounds have been released during the ignition and flaming phases (Masekameni et al., 2018). This results in the emission of non-carbonaceous matter during the coking phase, usually in the form of mineral particles from the burning char (Figure 4 a, b and c). In this stage, the fire burns uniformly if there is sufficient oxygen supply, and particles emitted during this stage are similar to those particles reported in studies of ash. The mineral particles are irregular in shape and tend to have a much smaller diameter (34.3 nm) than soot and homogeneous spherical organic particles (Figure 4a).

In Figure 4b, a closer look on the mineral particle indicates that there are several smaller particles of irregular shapes fused or agglomerated. Existing literature recognizes these particles as being composed of several mineral elements, including Si, Ca, Al, Fe, Na, K, Mg, and P (Wang and Luo, 2009). In Figure 4c, a mineral enriched irregular particle was imaged under the TEM. This particle is different from particles shown for the ignition and flaming phases, respectively.

This study did not employ EDX to determine the composition of each mineral particle semi-quantitatively. It is recommended that further studies be carried out to determine the elemental composition of specific mineral particles emitted during the char burning stage of domestic fixed-bed coal combustion. This study has employed ICP-MS to ascertain the elemental contribution of each combustion stage to the overall emissions of elements across the entire burn cycle sequence.

**Elemental analysis of coal combustion particles during the ignition, flaming and char burning phases**

Table 3 lists the ICP-MS results of selected trace elements collected during the three combustion phases (ignition, flaming, and char/coking burning), and across the entire burn cycle. During the ignition phase, Ca, Si, Fe and K were released in the highest proportions. The elemental composition derived from the total PM is expressed in mg, while the total trace elements are expressed in µg as shown in Table 3 and Table 5. These results, especially the emission of Si and K, suggest a particle partitioning, similar to that shown in previous studies (Hand et al., 2005; Meij and te Winkel, 2007; Zhang, Liu, et al., 2018). The smoke particles with high Si content can be used as a marker for coal combustion emissions, while the smoke particles with a high K percentage suggest emissions from biomass burning (in this case, wood kindling was used during the ignition phase).

During the ignition phase, the percentages of both Si and K were high because wood fuel was used as kindling to ignite the coal nuggets. In the flaming phase, the percentage contribution of K was higher than in the ignition and char burning phases. The increase in the percentage of K during flaming is possibly due to the pyrolysis of the wood kindling. A noticeable decline in the percentage of potassium can be seen during the char burning phase. For the marker of coal emissions, a relatively steady increase in Si emission confirms that the particles are from

coal combustion. All trace element emissions, except Ca and K, steadily increased as the combustion progressed. K and Ca emissions are thought to be associated with the pyrolysis wood kindling which often completes in the second half of the flaming stage (Makonese et al., 2014).

In previous studies, the elemental composition of emissions from coal-burning boilers/ furnaces was limited to fly ash, with little emphasis on the elemental composition of smoke emissions from the different combustion phases (McElroy et al., 1982; Petaloti et al., 2006). Particles emitted during the coking phase are enriched with volatile organic trace elements categorized as class one (i.e. Al, Ca, Ce, Cs, Eu, Fe, Hf, K, La, Mg, Sc, Sm, Si, Sr, Th and Ti) and are comparable to emissions in ash. During coal combustion, the minerals in the coal are deposited as bottom ash, and some are given off as fly ash (Lu et al., 2017). The types of mineral elements released are related to the mineral content of the fuel (Table 4).

A comparison of the composition of the fuel burned with corresponding elements is provided in Table 4. Although there was a relatively low amount of K in the coal, the emitted particles contained K. This was expected as wood was used as kindling to ignite the coal. The results reported in this study on trace elements are similar to those described for emissions of ash in other studies (Makonese, Meyer and Solms, 2019).

Table 5 shows the percentage and mass concentration of trace element composition of particles emitted during the three combustion phases. With decreasing volatile matter from the burning fuel, mineral particles dominated the char burning phase. The mass of the trace elements emitted during the char burning phase was 3 times higher than that emitted during the ignition phase, and twice that emitted during the flaming phase. As expected, the bulk of the elements was emitted during the char burning phase relative to the flaming and ignition phases (Zhang, Liu, et al., 2018). This finding suggests that the majority of particles emitted during the ignition and flaming phases could be dominated by volatile organic compounds (Zhou et al., 2016). During the char-burning phase, most non-water-soluble trace elements are expected to be released.

**Table 3:** Elemental composition results from inductively coupled plasma mass spectrometry (ICP-MS) analysis

Combustion phase	Element (µg/g)														
	Na	Mg	Al	Si	K	Ca	Ti	V	Cr	Mn	Fe	Co	Ni	Cu	Zn
Ignition (µg/g)	0.8	0.2	0.2	2.3	1.4	3.9	0.1	0.0	0.1	0.0	0.8	0.0	0.1	0.0	0.2
% contribution	8.3	2.3	2.0	22.5	13.8	38.4	0.7	0.0	1.4	0.2	7.5	0.1	0.5	0.1	2.2
Flaming (µg/g)	0.9	0.4	2.0	3.8	3.2	1.6	0.1	0.0	0.3	0.1	2.6	0.0	0.0	0.0	1.1
% contribution	5.3	2.7	12.5	23.3	20.0	9.9	0.9	0.0	1.6	0.4	16.0	0.1	0.1	0.2	7.0
Char burning (µg/g)	1.3	1.0	6.3	8.1	4.8	2.3	0.4	0.0	0.2	0.2	5.7	0.0	0.0	0.1	1.7
% contribution	4.1	3.1	19.7	25.3	14.9	7.3	1.1	0.0	0.6	0.5	17.9	0.0	0.1	0.2	5.3

**Table 4:** Comparison of trace elemental composition of fuel and particles emitted during the overall combustion process

Coal Analysis Results			
Element	% Contribution	Standard Method	% Contribution
Si	23.7	ASTM D4326	58.6
Al	11.4	ASTM D4326	27.6
Fe	13.8	ASTM D4326	6.6
Ti	0.9	ASTM D4326	0.8
Cr	1.2	ASTM D4326	0.6
Ca	18.5	ASTM D4326	2.3
Mg	2.7	ASTM D4326	0.8
Na	5.9	ASTM D4326	0.4
K	16.2	ASTM D4326	0.8
S	1.1	ASTM D4326	1.1
Mn	0.4	ASTM D4326	0.1

**Table 5:** Percentage contribution of detected elements emitted per combustion phase

Combustion phase	Total trace elements (µg/g)	% Contribution
Ignition	10.1	17
Flaming	16.2	28
Char burning	31.9	55
<b>Sum</b>	<b>58.2</b>	<b>100</b>

## Conclusion

This study was conducted to examine the morphology and elemental characteristics of freshly emitted individual particles emitted during three distinct combustion phases in domestic packed-bed coal. Three types of particles were classified viz., spherical organic particles with characteristics similar to tarballs, soot particles, and mineral particles. Spherical organic compounds were predominant in the ignition stage due to smouldering combustion conditions, while soot particles dominated the flaming stage. The identification of spherical organic particles is essential to understand how particles evolve once released into the atmosphere. Spherical organic compounds have been previously reported in smouldering wood-burning fires (Makonese, Meyer and von Solms, 2019). This finding brings new knowledge, suggesting that organic spherical particles may also be released during coal smouldering combustion conditions. This was demonstrated in a study conducted by Makonese et al. (2019) where coal was ignited using burning coal embers instead of wood kindling. As wood was used as kindling in this study, some of the emissions of organic spherical particles resembling tarballs could have been released from the wood fuel.

Mineral particles were predominant in the char burning stage where > 55% of the elements were released, suggesting that the combustion conditions were taking place at sufficient oxygen and temperature resulting in almost all volatiles being

completely given off and burned. Elemental composition analysis showed that the particles were rich in Si, K, Al, Fe, Ca, Zn, Na, Mg, and Ti, depending on the combustion phase. The type of mineral elements released was related to the mineral content of the fuel.

This information is essential for updating emission inventory sources, understanding radiation forcing potential, and providing a basis for warming estimation. In addition to information about the morphology of the emitted particles, the information on trace elements may be useful in source identification due to chemical signatures or emission markers. Both Si and K were high during the ignition phase indicating simultaneous combustion of wood kindling and coal. For the marker of coal emissions, a relatively steady increase in Si emission was confirmed across the entire combustion sequence indicating that the particles were emitted from coal combustion instead of wood. Further studies should be conducted to describe the morphology of emitted particles at distances further from the source.

## Acknowledgement

Sincere appreciation goes to Mr Shalala Mgwambani and Mr Kevin Kasangana for their assistance during laboratory experiments, to Mr Siyasanga Mpelane for assisting with TEM analysis, and to Mr Philip Pieterse for assisting with ICP-MS analysis. Many thanks to Professor Gill Nelson for her excellent language editing skills and moral support provided in completing this work. The article is published as a non-peer reviewed as preprints by the Atmospheric Science Journal on the 29th of November 2019. doi: 10.20944/preprints201911.0363.v1.

## Author contributions

Daniel Masekameni conceptualized and prepared the manuscript. He also experimented and wrote the first draft of the paper. Tafadzwa Makonese developed the methodology for coal emission capturing and analysis. He further supervised the sampling of particulate matter, data analysis, interpretation, and the presentation of arguments, and assisted in the editing of the manuscript. Isaac Rampedi assisted with the manuscript structure and write-up. Goitsemang Keretsetse edited the manuscript and validated methodology for elemental analysis. She further worked on aligning the manuscript to the journal style.

## References

- Balmer, M. (2007) 'Household coal use in an urban township in South Africa', *Journal Of Energy In Southern Africa*, 18(3), pp. 27-32. Available at: <http://www.erc.uct.ac.za/jesa/volume18/18-3jesa-balmer2.pdf>. <https://doi.org/10.17159/2413-3051/2007/v18i3a3382>
- Bazilian, M. et al. (2012) 'Energy access scenarios to 2030 for the power sector in sub-Saharan Africa', *Utilities Policy*. Elsevier Ltd, 20(1), pp. 1-16. <https://doi.org/10.1016/j.jup.2011.11.002>

- Bond, T. C. et al. (2006) 'Emission Factors and Real-Time Optical Properties of Particles Emitted from Traditional Wood Burning Cookstoves', *Environ. Sci. Technol.*, 40(21), pp. 6750-6757. <https://doi.org/10.1021/es052080i>
- Bonjour, S. et al. (2013) 'Solid fuel use for household cooking: Country and regional estimates for 1980-2010', *Environmental Health Perspectives*, 121(7), pp. 784-790. <https://doi.org/10.1289/ehp.1205987>
- Chafe, Z. A. et al. (2015) 'Household cooking with solid fuels contributes to ambient PM<sub>2.5</sub> air pollution and the burden of disease', *Environmental Health Perspectives*, 122(12). <https://doi.org/10.1289/ehp.1206340>
- Chakrabarty, R. K. et al. (2010) 'Brown carbon in tar balls from smoldering biomass combustion', *Atmospheric Chemistry and Physics*, 10(13), pp. 6363-6370. <https://doi.org/10.5194/acp-10-6363-2010>
- Chang, M. C. O. et al. (2004) 'Measurement of ultrafine particle size distributions from coal-, oil-, and gas-fired stationary combustion sources', *Journal of the Air and Waste Management Association*, 54(12), pp. 1494-1505. <https://doi.org/10.1080/10473289.2004.10471010>
- Finkelman, R. B. (2004) 'Potential health impacts of burning coal beds and waste banks', *International Journal of Coal Geology*, 59(1-2), pp. 19-24. <https://doi.org/10.1016/j.coal.2003.11.002>
- Gordon, S. et al. (2014) 'Respiratory risks from household air pollution in low and middle-income countries', *Lancet Respiratory Medical*, 2(10), pp. 823-860. doi: 10.1016/S2213-2600(14)70168-7. [https://doi.org/10.1016/S2213-2600\(14\)70168-7](https://doi.org/10.1016/S2213-2600(14)70168-7)
- GroundWork (2016) *The Destruction of the Highveld: Digging Coal*.
- Gwaze, P. (2007) 'Physical and Chemical Properties of Aerosol Particles in The Troposphere: An Approach from Microscopy Methods'.
- Hand, J. L. et al. (2005) 'Optical, physical, and chemical properties of tar balls observed during the Yosemite Aerosol Characterization Study', *Journal of Geophysical Research Atmospheres*, 110(21), pp. 1-14. <https://doi.org/10.1029/2004JD005728>
- Kocbach, A. et al. (2005) 'Analytical electron microscopy of combustion particles: A comparison of vehicle exhaust and residential wood smoke', *Science of the Total Environment*, 346(1-3), pp. 231-243. <https://doi.org/10.1016/j.scitotenv.2004.10.025>
- Lim, J. et al. (2013) 'a Rights-Based Approach To Indoor Air Pollution', *Health and Human Rights*, 15(2), pp. 160-167.
- Lim, S. S. et al. (2012) 'A comparative risk assessment of burden of disease and injury attributable to 67 risk factors and risk factor clusters in 21 regions, 1990-2010: A systematic analysis for the Global Burden of Disease Study 2010', *The Lancet*, 380(9859), pp. 2224-2260. [https://doi.org/10.1016/S0140-6736\(12\)61766-8](https://doi.org/10.1016/S0140-6736(12)61766-8)
- Lu, S. et al. (2017) 'Single-particle aerosol mass spectrometry of coal combustion particles associated with high lung cancer rates in Xuanwei and Fuyuan, China', *Chemosphere*. Elsevier Ltd, 186, pp. 278-286. <https://doi.org/10.1016/j.chemosphere.2017.07.161>
- Makonese, T. et al. (2014) 'Aerosol particle morphology of residential coal combustion smoke', 24(2), pp. 24-28. <https://doi.org/10.17159/caj/2014/24/2.7064>
- Makonese, T. (2015) 'Systematic investigation of smoke emissions from packed-bed residential coal combustion devices', (April).
- Makonese, T. et al. (2017) 'Influence of fire-ignition methods and stove ventilation rates on gaseous and particle emissions from residential coal braziers', *Journal of Energy in Southern Africa*, 26(4), p. 16. <https://doi.org/10.17159/2413-3051/2016/v26i4a2089>
- Makonese, T., Masekameni, D. M. and Annegarn, H. J. (2017) 'Influence of coal properties on the performance of fixed-bed coal-burning braziers', *Journal of Energy in Southern Africa*, 28(2), pp. 40-51. <https://doi.org/10.17159/2413-3051/2017/v28i2a1374>
- Makonese, T., Meyer, J. and von Solms, S. (2019) 'Characteristics of spherical organic particles emitted from fixed-bed residential coal combustion', *Atmosphere*, 10(8), pp. 1-16. <https://doi.org/10.3390/atmos10080441>
- Makonese, T., Meyer, J. and Solms, S. Von (2019) 'Characteristics of Spherical Organic Particles Emitted from Fixed-Bed Residential Coal Combustion', pp. 1-16. <https://doi.org/10.3390/atmos10080441>
- Masekameni, D. et al. (2018) 'Size Distribution of Ultrafine Particles Generated from Residential Fixed-bed Coal Combustion in a Typical Brazier', *Aerosol and Air Quality Research*, 18(10), pp. 2618-2632. <https://doi.org/10.4209/aaqr.2018.03.0105>
- Masekameni, D., Makonese, T. and Annegarn, H. J. (2014) 'Optimisation of ventilation and ignition method for reducing emissions from coal-burning imbaulas', *Proceedings of the 22nd Conference on the Domestic Use of Energy, DUE 2014*. <https://doi.org/10.1109/DUE.2014.6827755>
- Masekameni, M. et al. (2018) 'Risk Assessment of Benzene, Toluene, Ethyl Benzene, and Xylene Concentrations from the Combustion of Coal in a Controlled Laboratory Environment', *International Journal of Environmental Research and Public Health*, 16(1), p. 95. <https://doi.org/10.3390/ijerph16010095>
- Mathis, U. et al. (2005) 'Influence of diesel engine combustion parameters on primary soot particle diameter', *Environmental Science and Technology*, 39(6), pp. 1887-1892. <https://doi.org/10.1021/es049578p>

- Mc Donald, R. and Biswas, P. (2004) 'A methodology to establish the morphology of ambient aerosols', *Journal of the Air and Waste Management Association*, 54(9), pp. 1069-1078. <https://doi.org/10.1080/10473289.2004.10470986>
- McElroy, M. W. et al. (1982) 'Size distribution of fine particles from coal combustion', *Science*, 215(4528), pp. 13-19. <https://doi.org/10.1126/science.215.4528.13>
- Meij, R. and te Winkel, H. (2007) 'The emissions of heavy metals and persistent organic pollutants from modern coal-fired power stations', *Atmospheric Environment*, 41(40), pp. 9262-9272. <https://doi.org/10.1016/j.atmosenv.2007.04.042>
- Naeher, L. P. et al. (2007) 'Woodsmoke health effects: A review', *Inhalation Toxicology*, 19(1), pp. 67-106. <https://doi.org/10.1080/08958370600985875>
- Niemi, J. V. et al. (2006) 'Changes in background aerosol composition in Finland during polluted and clean periods studied by TEM/EDX individual particle analysis', *Atmospheric Chemistry and Physics*, 6(12), pp. 5049-5066. <https://doi.org/10.5194/acp-6-5049-2006>
- Nussbaumer, T. et al. (2001) *Aerosols from biomass combustion, International Seminar by IEA Bioenergy Task.*
- Petaloti, C. et al. (2006) 'Trace elements in atmospheric particulate matter over a coal-burning power production area of western Macedonia, Greece', *Chemosphere*, 65(11), pp. 2233-2243. <https://doi.org/10.1016/j.chemosphere.2006.05.053>
- Pósfai, M. et al. (2003) 'Individual aerosol particles from biomass burning in southern Africa: 1. Compositions and size distributions of carbonaceous particles', *Journal of Geophysical Research: Atmospheres*, 108(D13), p. n/a-n/a. <https://doi.org/10.1029/2002JD002291>
- Pósfai, M. et al. (2004) 'Atmospheric tar balls: Particles from biomass and biofuel burning', *Journal of Geophysical Research: Atmospheres*, 109(D6), p. n/a-n/a. <https://doi.org/10.1029/2003JD004169>
- Schneider, J. et al. (2006) 'Mass spectrometric analysis and aerodynamic properties of various types of combustion-related aerosol particles', *International Journal of Mass Spectrometry*, 258(1-3), pp. 37-49. <https://doi.org/10.1016/j.ijms.2006.07.008>
- Shen, G. et al. (2013) 'NIH Public Access', 44(18), pp. 7157-7162. doi: 10.1021/es101313y.Emission.
- Shraim, A. et al. (2003) 'Arsenic speciation in the urine and hair of individuals exposed to airborne arsenic through coal-burning in Guizhou, PR China', *Toxicology Letters*, 137(1-2), pp. 35-48. [https://doi.org/10.1016/S0378-4274\(02\)00379-X](https://doi.org/10.1016/S0378-4274(02)00379-X)
- Silva, L. F. O. et al. (2012) 'Applied investigation on the interaction of hazardous elements binding on ultrafine and nanoparticles in Chinese anthracite-derived fly ash', *Science of the Total Environment*. Elsevier B.V., 419(July 2007), pp. 250-264. <https://doi.org/10.1016/j.scitotenv.2011.12.069>
- Smith, K. R. et al. (2014) 'Millions Dead: How Do We Know and What Does it Mean? Methods Used in the Comparative Risk Assessment of Household Air Pollution', *Ssrn*. <https://doi.org/10.1146/annurev-publhealth-032013-182356>
- Thajudeen, T., Jeon, S. and Hogan, C. J. (2015) 'The mobilities of flame synthesized aggregates/agglomerates in the transition regime', *Journal of Aerosol Science*. Elsevier, 80, pp. 45-57. <https://doi.org/10.1016/j.jaerosci.2014.11.003>
- Tissari, J. et al. (2008) 'Fine particle and gaseous emissions from normal and smouldering wood combustion in a conventional masonry heater', *Atmospheric Environment*, 42(34), pp. 7862-7873. <https://doi.org/10.1016/j.atmosenv.2008.07.019>
- Tiwari, M. et al. (2014) 'Particle size distributions of ultrafine combustion aerosols generated from household fuels', *Atmospheric Pollution Research*. Elsevier, 5(1), pp. 145-150. <https://doi.org/10.5094/APR.2014.018>
- Torvela, T. et al. (2014) 'Effect of wood combustion conditions on the morphology of freshly emitted fine particles', *Atmospheric Environment*. Elsevier Ltd, 87, pp. 65-76. <https://doi.org/10.1016/j.atmosenv.2014.01.028>
- Tóth, A. et al. (2014a) 'Atmospheric tar balls: Aged primary droplets from biomass burning?', *Atmospheric Chemistry and Physics*, 14(13), pp. 6669-6675. <https://doi.org/10.5194/acp-14-6669-2014>
- Tóth, A. et al. (2014b) 'Atmospheric tar balls: Aged primary droplets from biomass burning?', *Atmospheric Chemistry and Physics*, 14(13), pp. 6669-6675. <https://doi.org/10.5194/acp-14-6669-2014>
- Vanhaecke, Frank, et al. (1992). 'The use of internal standards in ICP-MS', *Talanta*, 39(7), pp. 737-742. [https://doi.org/10.1016/0039-9140\(92\)80088-U](https://doi.org/10.1016/0039-9140(92)80088-U)
- Wang, A. Q. C. and Luo, B. Y. H. (2009) 'Application SEM to analysis formation characteristic of soot aerosol emitted from lump-coal combustion in fixed-bed', *Asia-Pacific Power and Energy Engineering Conference, APPEEC*, pp. 2-5. <https://doi.org/10.1109/APPEEC.2009.4918190>
- Wang, W. et al. (2018) 'Characteristics of Individual Particles Emitted from an Experimental Burning Chamber with the Coal from Lung Cancer Area of Xuanwei, China', *Aerosol and Air Quality Research*, pp. 1-9. <https://doi.org/10.4209/aaqr.2018.05.0187>
- Wilkinson, P. et al. (2009) 'Public health benefits of strategies to reduce greenhouse-gas emissions: household energy', *The*

Lancet, 374(9705), pp. 1917-1929. [https://doi.org/10.1016/S0140-6736\(09\)61713-X](https://doi.org/10.1016/S0140-6736(09)61713-X)

Zhang, Zou, X., et al. (2018) 'Decoupling greenhouse gas emissions from crop production: A case study in the Heilongjiang land reclamation area, China', *Energies*, 11(6). <https://doi.org/10.3390/en11061480>

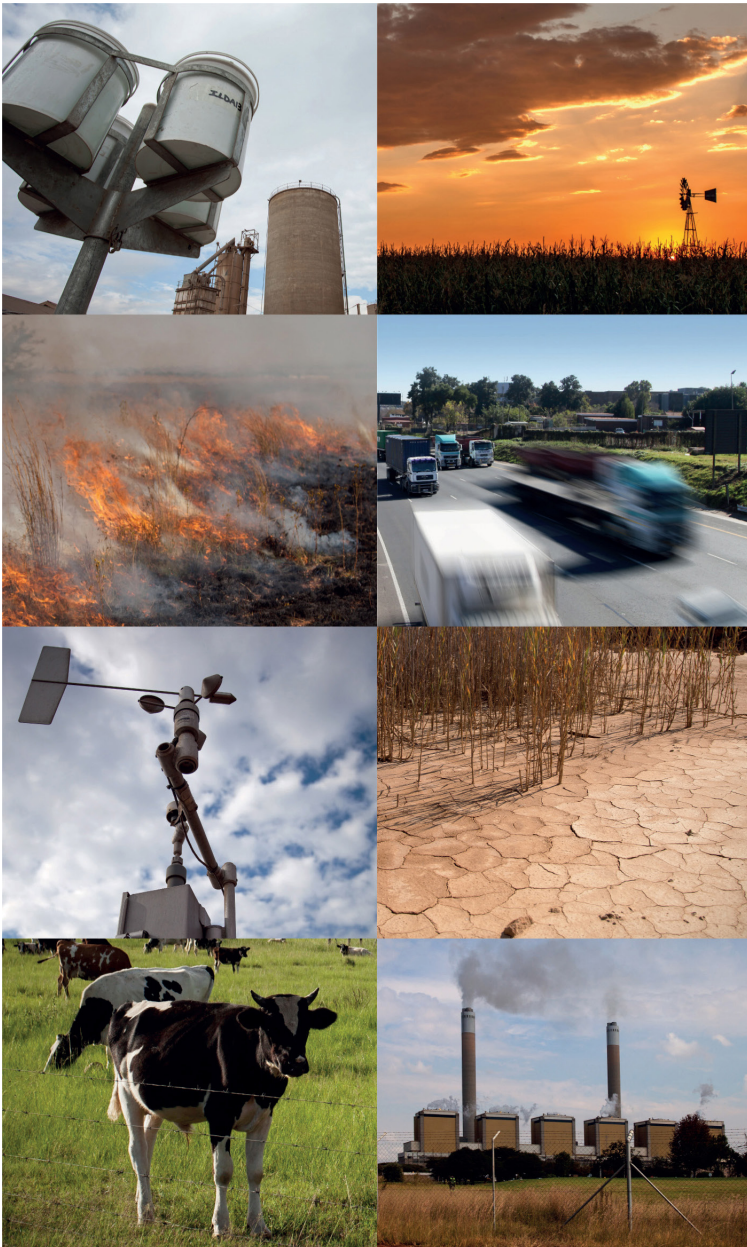
Zhang, Liu, C., et al. (2018) 'Morphology and property investigation of primary particulate matter particles from different sources', *Nano Research*, 11(6), pp. 3182-3192. <https://doi.org/10.1007/s12274-017-1724-y>

Zhang, H. et al. (2012) 'Chemical and size characterization of particles emitted from the burning of coal and wood in rural households in Guizhou, China', *Atmospheric Environment*. Elsevier Ltd, 51, pp. 94-99. <https://doi.org/10.1016/j.atmosenv.2012.01.042>

Zhang, Y. and Tao, S. (2009) 'Global atmospheric emission inventory of polycyclic aromatic hydrocarbons (PAHs) for 2004', *Atmospheric Environment*. Elsevier Ltd, 43(4), pp. 812-819. <https://doi.org/10.1016/j.atmosenv.2008.10.050>

Zhou, M. et al. (2015) 'Smog episodes, fine particulate pollution and mortality in China', *Environmental Research*. Elsevier, 136, pp. 396-404. <https://doi.org/10.1016/j.envres.2014.09.038>

Zhou, W. et al. (2016) 'Evolution of submicrometer organic aerosols during a complete residential coal combustion process', *Environmental Science and Technology*, 50(14), pp. 7861-7869. <https://doi.org/10.1021/acs.est.6b00075>



# GONDWANA

ENVIRONMENTAL SOLUTIONS



## Air Quality Management

- Air Quality Management Plans (AQMP)
- Air Quality Impact Assessments (AQIA)
- Emissions Inventories (EI)
- Dispersion Modelling (DM)
- Atmospheric Emission License (AEL) Applications

## Air Quality Monitoring

- Continuous Ambient Air Quality And Meteorological Monitoring
- Stack Monitoring
- Dustfall Monitoring (SANAS Accredited)

## Climate Change

- Framework Strategies
- GHG Emission Inventories

---

011 472 3112  
 info@gondwanagroup.co.za  
 www.gondwanagroup.co.za

# Environmental Solutions



Gonwana is a SANAS approved testing laboratory

## Technical article

# An exploratory characterisation of the carbon and stable isotope composition of atmospheric particulate matter from opencast coal mining activities and adjacent communities

Lerato Khumalo<sup>1</sup>, Gerrit Kornelius<sup>2\*</sup>, Pieter van Zyl<sup>3</sup>, Grant Hall<sup>4</sup>

<sup>1</sup>Department of Chemical Engineering, University of Pretoria, Private Bag X20, Hatfield 0028, South Africa.

<sup>2</sup>Department of Chemical Engineering, University of Pretoria, South Africa. gerrit.kornelius@up.ac.za

<sup>3</sup>Department of Chemistry, North West University, Potchefstroom, North West Province, South Africa.

<sup>4</sup>Mammal Research Institute, University of Pretoria, South Africa.

\*Corresponding author

Received: 27 June 2020 - Reviewed: 14 September 2020 - Accepted: 5 October 2020

<https://doi.org/10.17159/caj/2020/30/2.8564>

## Abstract

Standard source apportionment techniques for atmospheric particulate (PM) collected near opencast coal mines using inorganic markers only are limited by the similarity in the mineral components in the overburden and at adjacent residential locations. This study explores the use of the stable carbon (C) and nitrogen (N) isotope ratios ( $^{13}\text{C}/^{12}\text{C}$  and  $^{15}\text{N}/^{14}\text{N}$ ) and thermal optical methods to differentiate sources of carbonaceous material in the atmospheric PM samples from the opencast coal mines and adjacent communities. Results show isotopic and OC/EC ratio differences between atmospheric PM samples from the opencast coal mines and communities, although distinguishing between the contributions of coal combustion, liquid fuel combustion and the domestic use of biomass requires further analysis.

## Keywords

Atmospheric PM, coal, opencast, elemental carbon, organic carbon, IRMS, thermal optical.

## Introduction

### Atmospheric particulate matter

Air pollution in South Africa has been identified as one of the critical threats to human health, the environment and sustainability in general (see for instance Lim et al. 2011). High air pollution levels in some of the highly industrialised parts of the country have resulted in severe air quality degradation and the declaration of priority air quality management areas. The three priority areas which have been declared thus far in South Africa include the Vaal Triangle Airshed Priority Area (VTAPA) in Gauteng Province, the Highveld Priority Area (HPA) in Mpumalanga Province and Waterberg-Bojanala Priority Area (WBPA) in the North West and Limpopo Provinces. Anthropogenic sources of air pollution in all these areas include industrial facilities, power generation, transport, agricultural activities and coal mining (DEA, 2011). Elevated atmospheric concentrations of criteria pollutants such as sulphur dioxide ( $\text{SO}_2$ ), nitrogen oxides (NOx) and atmospheric particulate matter ( $\text{PM}_{10}$  and  $\text{PM}_{2.5}$ ; particles with an aerodynamic diameter less than  $10\ \mu\text{m}$  and  $2.5\ \mu\text{m}$ , respectively) have been observed in

these priority areas, resulting in stakeholder concerns on the resultant negative health and environmental impacts thereof (DEA, 2017). The health impact of atmospheric PM is historically measured by the concentration of particulate smaller than  $10\ \mu\text{m}$  or  $\text{PM}_{10}$  (Albers et al. 2015; Kunzli and Tager 2000; Mannucci and Franchini 2017) while  $\text{PM}_{2.5}$  is increasingly recognised as being of importance due to its higher toxicity and increased penetration into the gas exchange regions of the respiratory system (Hartmann et al. 2016).

Opencast coal mining activities have been associated with significant contributions to atmospheric PM emissions (Gautam et al. 2012). During opencast coal mining, atmospheric PM is generated from various sources which include drilling and blasting, excavation, materials handling, vehicle entrainment of dust, crushing and screening, wind erosion of mine residue dumps, tailings dams and open areas (Chaulya 2004). The handling of overburden, defined as the earth and rock that must be removed to gain access to the coal layers, can play a major part in dust generation, as the ratio of overburden to coal (also called the stripping ratio) in South African opencast coal mines

varies between 2 and 6 (Mohutsiwa 2015, Moolman 2000). The impact of these activities on air quality in adjacent communities has become a matter of concern (see for instance Huertas et al. 2012, 2014); for Mpumalanga, this has been quantified by the Highveld Priority Area baseline study (DEA 2012).

### Source apportionment

Source apportionment techniques such as principal component analysis (PCA) and principal matrix factorisation (PMF) are frequently used for atmospheric particulate matter (see for instance McGuire et al. 2011). As the inorganic components of atmospheric particulates from opencast mines and from other sources in their vicinity are often very similar, this paper explores the use of carbon- and nitrogen-related parameters of the atmospheric PM<sub>10</sub> collected from opencast coal mines and from sites in adjacent residential communities to establish whether significant differences occur. Such differences could occur if the fuel mix used in the residential areas contains components originating from sources other than the adjacent mine and, if found, could augment existing source apportionment techniques. In this paper, the possible use of these parameters by the analysis of single samples taken at three pairs of mine and adjacent residential locations is explored.

## Methodology

### Selection of study areas

Areas located in the HPA and WBPA air quality management priority areas were selected for the study and consisted of

three opencast coal mines and an adjacent community for each mine. Selection criteria for the community samples take into consideration site accessibility, security considerations for placement of PM<sub>10</sub> monitoring equipment and the distance from industrial or commercial activities. Two opencast coal mines were selected in Mpumalanga due to a high concentration of opencast coal mining activities in the province. The adjacent communities to these mines are Delmas and Clewer in Emalaheni (Figure 1 and Figure 2). In the case of Delmas, a site in a residential backyard as close as possible to the centre of the Delpark residential area was used. At Clewer, the grounds of the local primary school were used. One opencast coal mine was selected in Limpopo given its proximity to the adjacent community of Marapong in Lephalale (Figure 3). The community monitoring site in this case was located at the local public library. Mine samples were taken as close as possible to the coal processing facilities so as to represent coal properties; in one of the Mpumalanga mines and for the Limpopo mine, samples were also taken in areas where overburden handling took place so as to represent the composition of overburden material.

### Sampling

Portable Minivol (Airmetrics, Springfield, Oregon) samplers were deployed for the active sampling of atmospheric PM<sub>10</sub> over 24h at 5 l/min at the selected opencast coal mines and adjacent communities during March 2018. PM<sub>10</sub> impactors were used to selectively sample PM<sub>10</sub> with quartz fibre filters (47 mm in diameter). After sampling, each filter was removed from the filter holder using forceps and was placed in a marked container for post sampling weighing and analysis using Isotope Ratio Mass

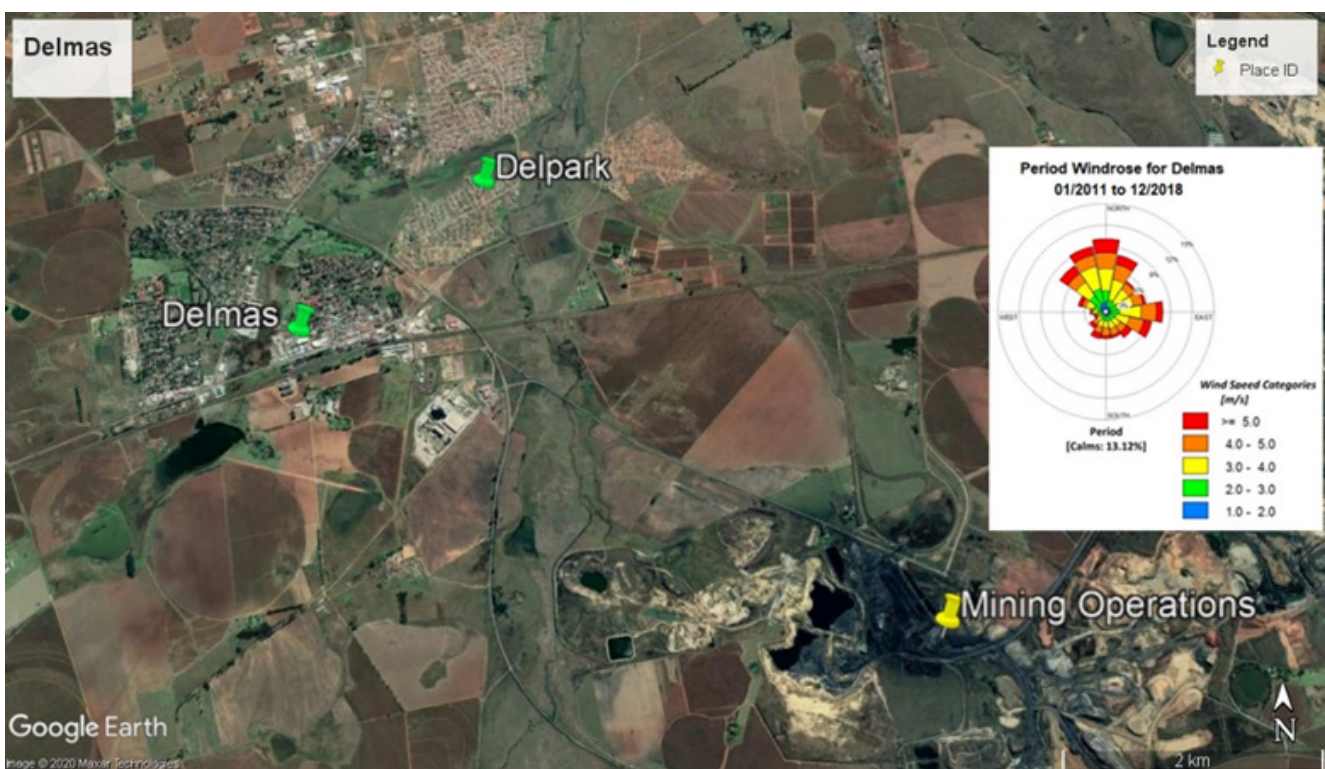


Figure 1: Location of the community of Delpark in relation to current opencast coal mining activities in the town of Delmas, Mpumalanga (Google Earth Maps, 2018).

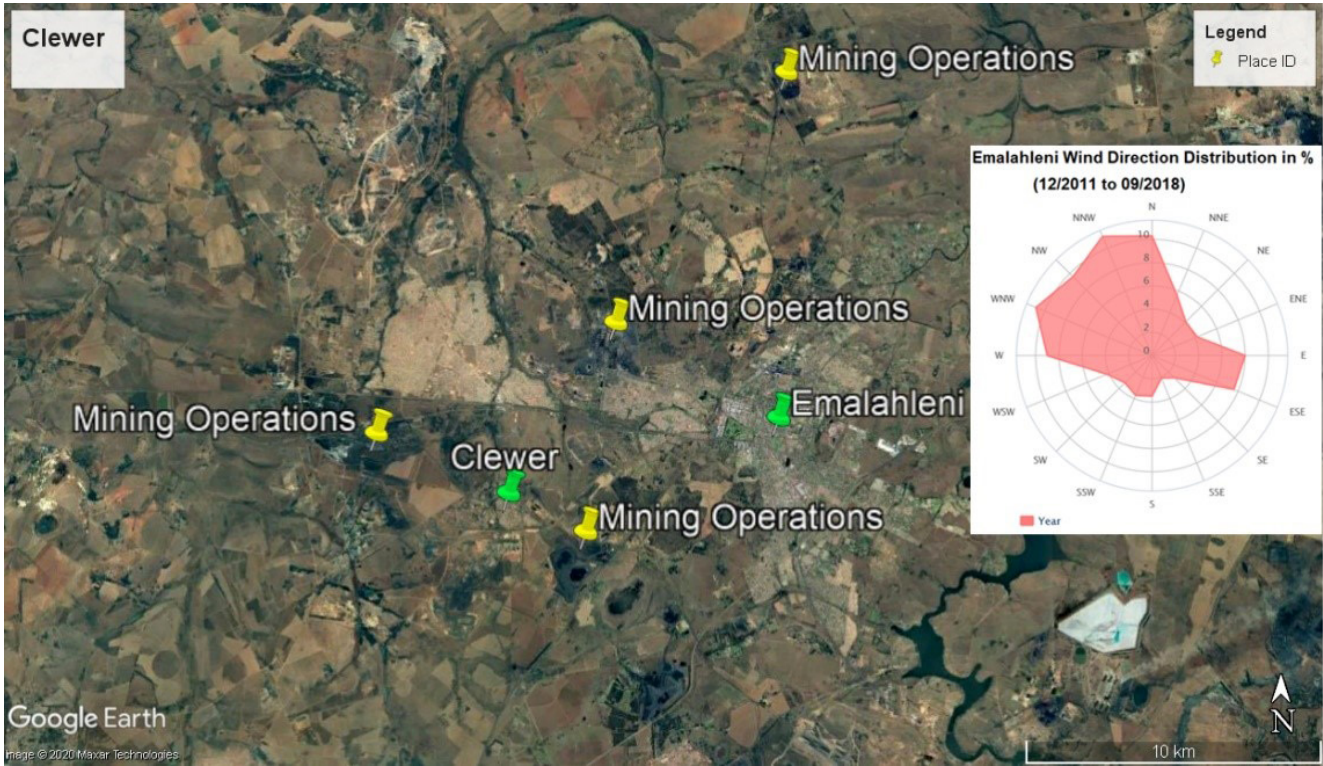


Figure 2: Location of the community of Clewer in relation to current opencast coal mining activities in the town of Emalahleni, Mpumalanga (Google Earth Maps, 2018).

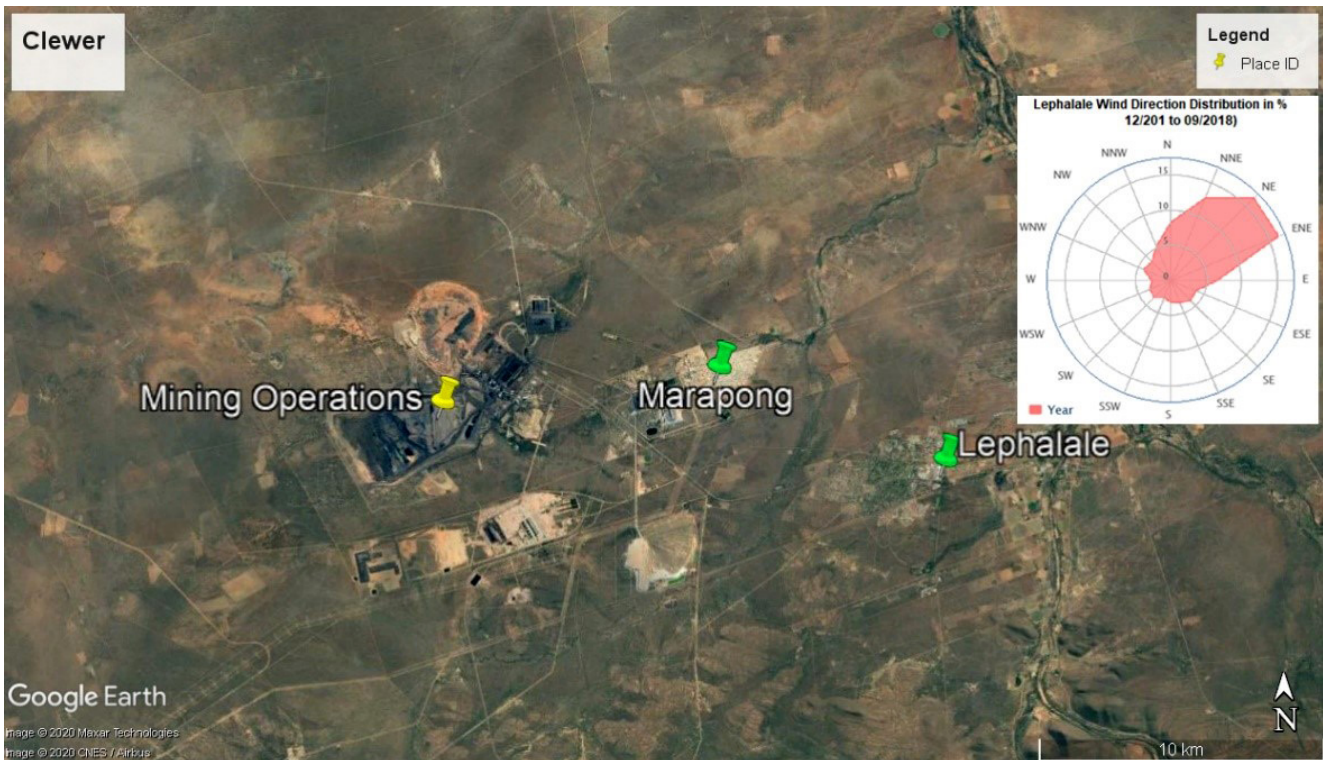


Figure 3: Location of the community of Marapong in relation to current opencast coal mining activities in the town of Lephalale, Limpopo (Google Earth Maps, 2018).

Spectrometry (IRMS) and thermal optical techniques. Within the mine area, samplers were located in coal handling areas and overburden handling areas to determine possible differences in the properties being evaluated.

## Analysis

### Isotope Ratio Mass Spectroscopy

Atmospheric PM samples were combusted at a temperature of 1020°C using an elemental analyser (EA) (Flash EA 1112 Series) coupled to a Delta V Plus stable light isotope ratio mass spectrometer (IRMS) via a ConFlo IV system (all equipment supplied by Thermo Fischer, Bremen, Germany), housed at the UP Stable Isotope Laboratory, Mammal Research Institute, University of Pretoria. Two laboratory running standards (Merck Gel:  $\delta^{13}\text{C} = -20.26\text{‰}$ ,  $\delta^{15}\text{N} = 7.89\text{‰}$ ,  $\text{C}\% = 41.28$ ,  $\text{N}\% = 15.29$ ) and (DL-Valine:  $\delta^{13}\text{C} = -10.57\text{‰}$ ,  $\delta^{15}\text{N} = -6.15\text{‰}$ ,  $\text{C}\% = 55.50$ ,  $\text{N}\% = 11.86$ ) and a blank sample were run after every 11 unknown samples. Data corrections were done using the values obtained for the Merck Gel during each run. The standard deviations of the nitrogen and carbon values for the DL-Valine standard provided the  $\pm$  error for  $\delta^{15}\text{N}$  and  $\delta^{13}\text{C}$  values for the samples. The C and N ratios for all secondary (NIST) and lab running (Merck & DL-Valine) standards were all calibrated using the following primary standards:

- IAEA-CH-3 (Cellulose),
- IAEA-CH-6 (Sucrose),
- IAEA-CH-7 (Polyethylene foil),
- IAEA N-1 & IAEA N-2 (Ammonium sulphate),
- IAEA NO-3 (Potassium nitrate).

All the results were referenced to Vienna Pee-Dee Belemnite for carbon isotope values and to air for nitrogen isotope values. Results were expressed in delta notation using a per mille scale using the standard equation:

$$\delta X (\text{‰}) = \left[ \left( \frac{R_{\text{sample}}}{R_{\text{standard}}} - 1 \right) \right]$$

where  $X = ^{15}\text{N}$  or  $^{13}\text{C}$  and R represents  $^{15}\text{N}/^{14}\text{N}$  or  $^{13}\text{C}/^{12}\text{C}$  respectively.

### Thermal Optical Characterisation of OC and EC

The quartz filters from the  $\text{PM}_{10}$  active monitoring campaign were analysed using a thermal-optical carbon analyser (Sunset Laboratory Inc Lab OC-EC Aerosol Analyser). The blank filters were pre-fired in air (700°C for one hour) for the removal of residual carbon contaminants. The detection limit of the instrument is  $0.2 \mu\text{g cm}^{-2}$  and the relative standard deviation (RSD) 5%. The instrument and analysis process followed during this investigation is shown in Figure 4.

Punch aliquots of  $1.5 \text{ cm}^2$  of the filter deposits were used for the analysis. Each aliquot was heated in a sample oven in four increasing temperatures of 140°C (OC1), 280°C (OC2), 480°C (OC3) and 580°C (OC4) in a non-oxidizing helium (He) atmosphere (Afrox Ltd, 99.999%) for the removal of all organic carbon (OC) on the filter. The carbon that evaporated at each temperature was catalytically oxidized by  $\text{MnO}_2$  into  $\text{CO}_2$  in the oxidiser oven. The  $\text{CO}_2$  entrained in the He gas flow, was converted to  $\text{CH}_4$  in the methanator oven. The detection and quantification of methane was undertaken through a flame ionisation detector while the pyrolytic conversion was continuously monitored by measuring the transmission of a He-Ne laser through the quartz filter. The darkness of the filter was also continuously monitored throughout all stages of the analysis. Ramping up to the next temperature or atmosphere was undertaken when the flame ionization detector's response returned to baseline or a constant value (subject to the condition of the time spent in any segment (OC1, OC2, etc).

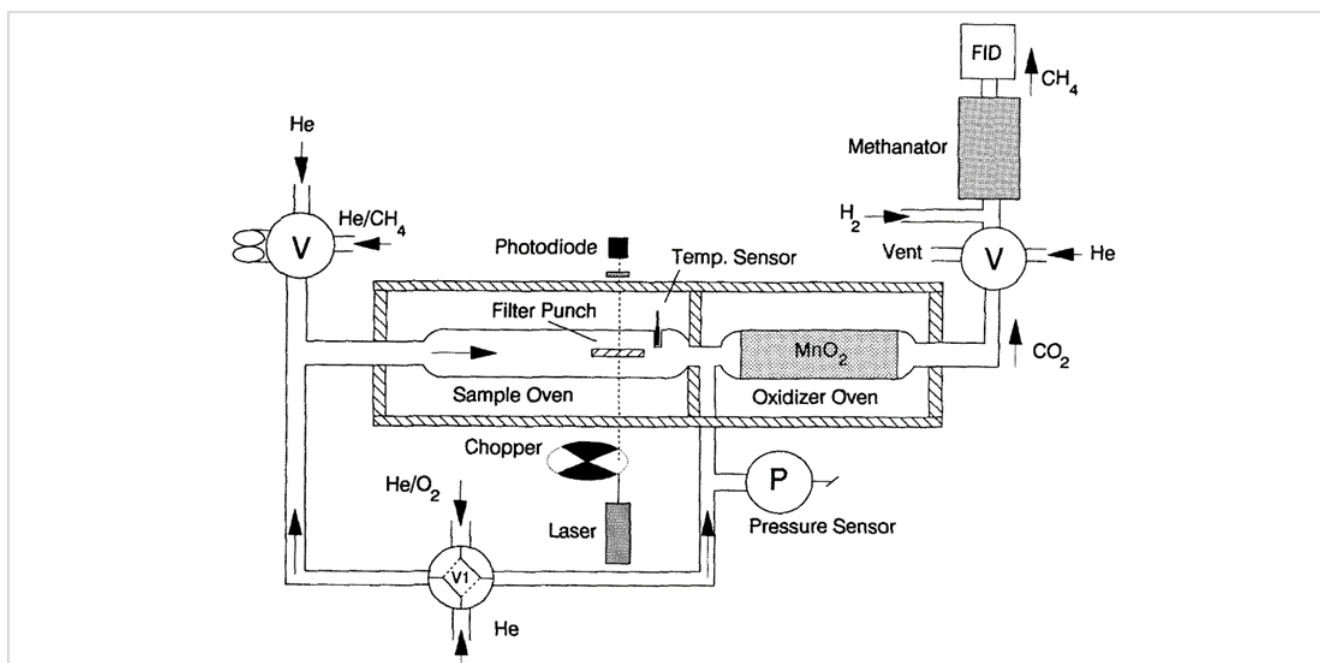


Figure 4: Schematic of thermal-optical instrumentation (Birch & Cary, 1996).

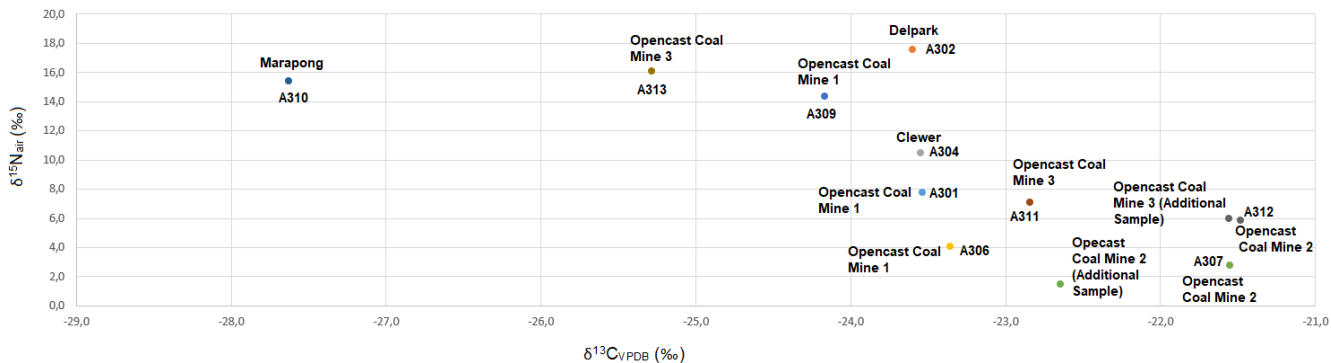


Figure 5: Biplot of mean carbon and nitrogen isotope ratios for opencast coal mines and adjacent communities.

Table 1: Results of stable carbon and nitrogen isotope analysis for atmospheric PM samples.

Sample ID	Weight	δ <sup>15</sup> N (‰)	%N	δ <sup>13</sup> C (‰)	%C	C/N ratio
A301 Opencast Coal Mine 1 Sample 1	10,1	7,8	0,13	-23,5	1,21	10,8
A302 Delpark Community	12,4	17,5	0,24	-23,6	2,89	14,3
A304 Clewer Community	17,6	10,5	0,03	-23,6	0,53	18,4
A306 Opencast Coal Mine 1 Sample 2 (plant area)	10,7	4,1	0,06	-23,4	1,80	34,8
A307 Opencast Coal Mine 2 Sample 1 (overloaded)	2,8	2,8	1,37	-21,6	56,55	48,1
A309 Opencast Coal Mine 1 (overburden area)	13,0	14,4	0,08	-24,2	1,08	16,5
A310 Marapong Community	14,6	15,4	0,07	-27,6	0,83	14,7
A311 Open cast Coal Mine 3 Sample 1	10,0	7,1	0,23	-22,8	5,27	27,1
A312 Open Cast Coal Mine 2 Sample 2	12,9	5,8	0,39	-21,5	12,87	38,9
A313 Opencast Coal Mine 3 Sample 2 (overburden area)	16,4	16,1	0,04	-25,3	0,33	9,7
Opencast Coal Mine 2 Additional Sample 2	2,8	1,5	1,02	-22,6	33,58	38,5
Opencast Coal Mine 3 Additional Sample	9,8	6,00	0,46	-21,6	16,32	41,2

Table 2: Organic, elemental and total carbon concentrations for the opencast coal mines and adjacent communities atmospheric PM samples.

Sample ID	OC (µg cm <sup>-2</sup> )	EC(µg cm <sup>-2</sup> )	TC(µg cm <sup>-2</sup> )	OC/EC Ratio
A301 Opencast Coal Mine 1 Sample 1	24	16	39	1.53
A302 Delpark Community	112	25	136	4.50
A304 Clewer Community	21	4	25	6.03
A306 Opencast Coal Mine 1 Sample 2	30	19	48	1.60
A307 Opencast Coal Mine 2 Sample 1 (filter overloaded)	4,7E+09	5,1E+09	9,9E+09	0.92
A309 Opencast Coal Mine 1 Sample 3 (overburden area)	33	7	40	5.01
A310 Marapong Community	24	3	27	8.13
A311 Open cast Coal Mine 3 Sample 1	91	58	150	1.56
A312 Open Cast Coal Mine 2 Sample 2	285	310	596	0.92
A313 Opencast Coal Mine 3 Sample 2 (overburden area)	16	3	19	5.61

The sample oven was then cooled to 525°C and the pure helium eluent was switched to a 2% O<sub>2</sub>/98% He mixture. Peaks were integrated at 580°C (EC1), 740°C (EC2), and 840°C (EC3). The sample oven temperature was then stepped up to 850°C (EC4). During this phase, both the original EC and the EC produced through the pyrolysis of OC during the first phase were oxidized to CO<sub>2</sub> due to the presence of oxygen in the eluent. The CO<sub>2</sub> was then converted to CH<sub>4</sub> and detected by the flame ionisation detector. The darkness of the filter was also continuously monitored throughout all stages of the analysis by reflectance of 633 nm of light from a He–Ne laser. During this phase, original and pyrolyzed black carbon were combusted and the increases in the reflectance were observed. The amount of carbon that was measured after the addition of oxygen until the reflectance achieved its original value was reported as optically detected pyrolyzed carbon (PC).

After the oxidation of all the carbon from each sample, a known volume of methane (Afrox Ltd 99.95%) was injected into the sample oven, resulting in each sample being calibrated to a known quantity of carbon. Based on the Flame Ionisation Detector (FID) response and laser transmission data, the quantities of OC and EC were calculated for each sample. The concentration of OC and EC on each filter punch aliquot was calculated by multiplying reported values by the sample deposit area. The concentrations were reported in µg/cm<sup>2</sup> of deposit area. This approach assumed a homogenous filter deposit. The precision of this technique (Sunset Laboratory method of OC/EC analysis), measured as a relative standard deviation, typically falls into the 4–6% range for samples that are in the afore-mentioned OC and EC concentration ranges. This relative standard deviation range is applicable to the OC/EC speciation values as well as to the total carbon.

## Results and discussion

For this exploratory study, only single samples were taken per location and the conclusions below are preliminary.

### Stable Isotope Analysis

For the mining samples, those representing coal handling and those taken in overburden handling areas (A309 and A313) show different characteristics on the plot of δ<sup>15</sup>N against δ<sup>13</sup>C (Figure 5). As shown in section 3.2, the OC fraction of these samples is also much higher than those of the coal-rich samples, indicating that the carbon in these samples is of a different origin. The mine samples representing mainly coal dust and the residential area samples have distinct characteristic fingerprints, with the community samples having higher δ<sup>15</sup>N values than the coal samples (Table 1 and Figure 5). The high δ<sup>15</sup>N values for the residential areas Marapong (average annual precipitation 437 mm/annum), Clewer (average annual precipitation 693 mm/annum) and Delpark (average annual precipitation 1230 mm/annum) are unexpected. Amundsen et al. (2003) indicate the South African average for soils to be 6.2 to 7.6‰, while they found values to decrease with increased annual precipitation. Savard et al. (2017) give a value of 3.4 to 6.1‰ for coal-fired

power station emissions, while Moroeng et al. (2018) give a value of 2.66‰ for Witbank no 4 seam coal, which is the predominant coal at Opencast Coal Mines 2 and 3. This suggests a contribution by biomass-related particulate for the residential samples. This is confirmed by the δ<sup>13</sup>C value (see below) for the more rural area around Marapong, but not for Clewer and Delpark where biomass is less readily available; the δ<sup>15</sup>N for C<sub>3</sub> and C<sub>4</sub> biomass-related PM<sub>10</sub> is given as 13.7 ± 2.2‰ by Mkombe et al. (2013), while for C<sub>4</sub> biomass-related particulate Bikkina et al. (2016) give a value of 11.5 ± 2.1‰. The δ<sup>15</sup>N isotope ratios for the opencast coal atmospheric PM samples are lower than those for the residential samples, but higher than that given for South African coals by Moroeng et al. (2018) at 2.66‰. This may be due to the extensive use of liquid fuels (diesoline) in opencast coal mining, for which the δ<sup>15</sup>N is given as between 3.9 and 5.4 ± 0.5‰ by Widory (2007), or to the presence of mineral dust in the mine samples.

The carbon isotope fingerprint ratios for the opencast coal mines' atmospheric PM samples were within the δ<sup>13</sup>C ranges measured for coal in various parts of the world (-27.4‰ to -23.7‰) (Suto and Kawashima, 2016; Garbariené et al. 2016). For the coal mined at mines 2 and 3, Moroeng et al. (2018) give a value of -23.27‰. The impact of coal combustion products cannot be distinguished from coal dust itself; values for atmospheric particulate related to coal combustion are given as -23.5 ± 1.3 (Andersson 2015, Fang and Andersson 2017) and -24.5 ± 0.5‰ (Garbariené et al. 2016, Engelbrecht et al. 2002). The lower carbon isotope values for the residential area, especially for the rural area (sample A310) can be attributed to the use of biomass (mainly wood) or the contribution of traffic-derived particulate. The δ<sup>13</sup>C values for wood is given by Garbariené et al. (2016) as -26 to -27‰, with little fractionation with combustion, while Bikkina et al. give a value of -25.8 ± 0.5‰ for C<sub>4</sub> plant-related combustion particulate. For traffic-related particulate, Engelbrecht et al. (2002) provide a δ<sup>13</sup>C value of -28 to -29‰.

### Thermal optical characterisation

The OC, EC and TC concentrations (µg cm<sup>-2</sup>) and the OC/EC ratio obtained from the thermal optical analysis of the opencast coal mines and adjacent communities' atmospheric PM samples are shown in Table 2. Again not taking samples that represent mainly overburden (A309 and A313) into account, OC/EC ratios confirm the observations of the section "Stable Isotope Analysis". Mine samples have a low ratio, commensurate with the ratio between volatile matter and fixed carbon in the coal before combustion. The filters for the samples from mine 2 were both overloaded, and the results are accordingly less accurate. The best range for the deposit concentration is 5–400 µg/cm<sup>2</sup> for OC and 1–15 µg/cm<sup>2</sup> for EC. Concentrations of OC that are greater than this range may result in exceedances of the detection limits of the OC/EC instrument and interference with the EC measurements, particularly when low concentrations of EC are found in the sample (Desert Research Institute, 2019).

Samples from the residential communities have higher values, but source contributions cannot be determined from this ratio

only. Sources that may contribute are coal combustion at OC/EC of 7.0, liquid fuel combustion at 9.7 (Engelbrecht et al. 2002), the combustion of C<sub>3</sub> biomass at 16±5 and the combustion of C<sub>4</sub> biomass (grasses) at 18±4 (Salma et al. 2017). The higher ratio for Marapong would suggest a higher contribution by the latter two sources.

## Conclusion and recommendation

This exploratory work on the use of IRMS and thermal-optical methods for characterising carbon-containing particles near opencast coal mines indicates the possibility of applying the results of these techniques to improve source apportionment for atmospheric PM in such locations. Additional sampling and analysis of the coal itself, with the use of operational data on mine stripping ratios and/or dispersion modelling and the standard source apportionment techniques would be required to allow more exact characteristics to be determined.

## Acknowledgements

Airshed Planning Professionals provided PM<sub>10</sub> monitoring equipment and filter media. Exxaro Resources Ltd allowed sampling on their sites.

## References

Albers, P. N., Wright, C. Y., Voyi, K. V. V. and Mathee, A. (2015) Household fuel use and child respiratory ill health in two towns in Mpumalanga, South Africa, *South African Medical Journal*. South African Medical Association NPC, 105(7), pp. 573–577. doi: 10.7196/SAMJnew.7934.

Amundson, R., Austin, A.T., Schuur, E.A.G., Yoo, K., Matzek, V., Kendall, C., Uebersax, A., Brenner, D. and Baisden, W.T. (2003) Global patterns of the isotopic composition of soil and plant nitrogen. *Global biogeochemical cycles* 17(1) pp1031-1040 doi:10.1029/2002GB001903

Andersson, A., Deng, J., Du, K., Zheng, M., Yan, C., Sköld, M. and Gustafsson, Ö. (2015) Regionally-Varying Combustion Sources of the January 2013 Severe Haze Events over Eastern China. *Environ. Sci. Technol.* 49, 2038–2043 doi:10.1021/es503855e

Bikkina, S., Kawamura, K. and Manmohan S. (2016) Stable carbon and nitrogen isotopic composition of fine mode aerosols (PM<sub>2.5</sub>) over the Bay of Bengal: impact of continental sources. 31 68 pp 31518-31533 doi 10.3402/tellusb.v68.31518

Birch, M. E. and Cary, R. A. (1996) Elemental Carbon-Based Method for Monitoring Occupational Exposures to Particulate Diesel Exhaust, *Aerosol Sci Tech* 25(3), pp. 221–241. doi: 10.1080/02786829608965393.

Chaulya, S. K. (2004) Assessment and management of air quality for an opencast coal mining area, *J Env Man* 70(1), pp. 1–14. doi: 10.1016/j.jenvman.2003.09.018.

Department of Environmental Affairs (DEA) (2017) The Management of Air Quality in South Africa. Available at: [www.saaqis.org.za](http://www.saaqis.org.za) (Accessed: 29 November 2019).

Department of Environmental Affairs (DEA) (2012) Highveld Priority Area Air Quality Management Plan. Government Gazette 35072 of 2 March 2012.

Desert Research Institute (2019) EAF Capabilities- Carbon Analysis (TOR/TOT). Available at: <https://www.dri.edu/eaf-lab> (Accessed: 29 November 2019).

Engelbrecht, J.P., Swanepoel, L., Chow, J.C., Watson, J.G. and Egami, R.T. (2002) The comparison of source contributions from residential coal and low-smoke fuels, using CMB modeling, in South Africa. *Envl Sci & Policy* 5 157–167. doi:10.1016/S1462-9011(02)00029-1.

Fang, W., Andersson, A., Zheng, M., Lee, M., Holmstrand, H., Kim, S., Du, K. and Gustafsson, Ö. (2017) Divergent Evolution of Carbonaceous Aerosols during Dispersal of East Asian Haze. *Scientific Reports* 7 10422-10433 doi:10.1038/s41598-017-10766-4

Garbarienė, I., Šapolaitė, J., Garbaras, A., Ežerinskis, Ž., Pocevičius, M., Krikščikas, L., Plukis, A. and Remeikis, V. (2016) Origin Identification of Carbonaceous Aerosol Particles by Carbon Isotope Ratio Analysis. *Aerosol and Air Quality Res*, 16: 1356–1365 doi: 10.4209/aaqr.2015.07.0443

Hartmann, S., O'Brien, G., Warren, K. and Krahenbuhl, G. (2016) Characterisation of urban dust samples using reflected light microscopy methods, *Air Quality and Climate Change*, 50(3), p. 34.

Huertas, J.I., Huertas, M.E., Izquierdo, S. and González, E.D. (2012) Air quality impact assessment of multiple open pit coal mines in northern Colombia. *J Env Man* 93 pp 121-129 doi: 10.1016/j.jenvman.2011.08.007

Huertas J.I., Huertas, M.E., Cervantes, G. and Díaz, J. (2014) Assessment of the natural sources of particulate matter on the opencast mines air quality. *Sci Total Env* 493 pp 1047-1055 doi: 10.1016/j.scitotenv.2014.05.111

Kunzli, N. and Tager, I. B. (2000) Long-Term Health Effects of Particulate and Other Ambient Air Pollution: Research Can Progress Faster If We Want It to, *Env Health Perspectives* 108(10), p. 915. doi: 10.2307/3435048.

Lim, S.S. et al. (2012) A comparative risk assessment of burden of disease and injury attributable to 67 risk factors and risk factor clusters in 21 regions, 1990–2010: a systematic analysis for the Global Burden of Disease Study 2010 *Lancet* 380 pp 2225-2260

Mannucci, P. and Franchini, M. (2017) Health Effects of Ambient Air Pollution in Developing Countries, *Intl J Envl Res and Public Health* 14(9), p. 1048. doi: 10.3390/ijerph14091048.

Mkoma, S.L., Kawamura, K., Tachibana, E. and Pingqing Fu (2014) Stable carbon and nitrogen isotopic compositions of tropical atmospheric aerosols: sources and contribution from burning of C3 and C4 plants to organic aerosols. *Tellus B* 66(1) pp 20176-20190, doi: 10.3402/tellusb.v66.pp 20176

McGuire, M.L., Jeong, C.-H., Slowik, J.G., Chang, R.Y.-W., Corbin, J.C., Lu, G., Mihele, C., Rehbein, P.J.G., Sills, D.M.L., Abbatt, J.P.D., Brook, J.R. and Evans, G.J.(2011) Elucidating determinants of aerosol composition through particle-type-based receptor modeling. *Atmos. Chem. Phys.*, 11, 8133–8155. doi:10.5194/acp-11-8133-2011.

Moolman, C.J. (2000). *Evaluation of stripping techniques*. Coaltech 2020 report on task 3.14.1.

Mohutsiwa, M. (2015) *Estimation of capital costs for establishing coal mines in South Africa*, MEng thesis, Faculty of Engineering and the Built Environment, University of the Witwatersrand.

Moroeng O.M., Wagner, N.J., Hall, G. and Roberts, R.J. (2018) Using  $\delta^{15}\text{N}$  and  $\delta^{13}\text{C}$  and nitrogen functionalities to support a fire origin for certain inertinite macerals in a No. 4 Seam Upper Witbank coal, South Africa. *Org Geochem* 125 pp 23-32. doi: 10.1016/j.orggeochem.2018.10.007.

Salma, I., Németh, Z., Weidinger, T., Maenhaut, W., Claeys, M., Molnár, M., Major, I., Ajtai, T., Utry, N., and Bozóki, Z. (2017) Source apportionment of carbonaceous chemical species to fossil fuel combustion, biomass burning and biogenic emissions by a coupled radiocarbon–levoglucosan marker method. *Atmos. Chem. Phys.*, 17pp 13767–13781. doi: 10.5194/acp-17-13767-2017.

Savard, M.M., Cole, A., Smirnov, A. and Vet, R (2017)  $\delta^{15}\text{N}$  values of atmospheric N species simultaneously collected using sector-based samplers distant from sources - Isotopic inheritance and fractionation. *Atm Env* 162 pp 11-22. doi: 10.1016/j.atmosenv.2017.05.010.

Suto, N. and Kawashima, H. (2016) Global mapping of carbon isotope ratios in coal. *J Geocheml Expl* 167, pp 12-19. doi: 10.1016/j.gexplo.2016.05.001.

Widory, D. (2007) Nitrogen isotopes: Tracers of origin and processes affecting  $\text{PM}_{10}$  in the atmosphere of Paris. *Atm Env* 41 (2007) 2382–2390 doi:10.1016/j.atmosenv.2006.11.009 Australia, pp. 180-185.